



TECHNISCHE
UNIVERSITÄT
WIEN

Diese Dissertation
haben begutachtet:
Univ.-Prof. Dr. Friedrich Franek
Assoz. Prof. Dr. Andreas Limbeck

Dissertation

A novel approach to characterization of industrial
lubricant additives in boundary surface tribofilms by atmos-
pheric pressure matrix assisted laser desorption/ionization

Ausgeführt zum Zwecke der Erlangung des akademischen Grades eines
Doktors der technischen Wissenschaften
unter der Leitung von

Ao. Univ.-Prof. Dr. Herbert Hutter

E164

Institut für Chemische Technologien und Analytik

eingereicht an der Technischen Universität Wien

Fakultät für Technische Chemie

von

Dipl.-Ing. Dipl.-Ing. Lukas Widder

0026497

Wien, April 2019

Contents

- 1 General Aspects of Tribology and Lubrication 1
 - 1.1 Introduction to tribology 1
 - 1.2 The tribological system 3
 - 1.3 Friction 5
 - 1.3.1 Types of friction 6
 - 1.3.2 Friction regimes 7
 - 1.3.3 Macroscopic friction 8
 - 1.3.4 Microscopic friction 9
 - 1.3.5 Friction mechanisms 11
 - 1.3.6 Stick-Slip phenomena 13
 - 1.4 Principles of wear 14
 - 1.4.1 Wear mechanisms 17
 - 1.5 Lubricant composition and lubrication regimes 21
 - 1.5.1 Principal aspects of lubrication 21
 - 1.5.2 Lubrication and friction regimes 21
 - 1.5.3 Base oils 22
 - 1.5.4 Lubricating greases 23
 - 1.5.5 Solid lubrication 24

- 2 Lubricant additives 25
 - 2.1 Lubrication improvement through additives 25
 - 2.2 General types of additives 26
 - 2.3 Friction modifiers 27

- 3 Boundary lubricant tribofilms 31
 - 3.1 General aspects of boundary lubricant films 31
 - 3.2 Film forming mechanisms and structure 33
 - 3.3 Boundary tribofilm characterization 37

4	Tribotesting	39
4.1	Tribological testing technology.....	39
4.2	Planning and evaluation	41
4.3	Tribological laboratory testing.....	41
4.4	SRV-tribometer	42
5	Mass spectrometry	45
5.1	General principle	45
5.2	Mean free ion path.....	46
5.3	Ion Sources	48
5.4	Mass analyzers.....	49
5.4.1	Ion trap mass analyzers	52
5.4.2	Orbitrap mass analyzer	54
5.4.3	Time-of-Flight mass analyzers	55
6	MALDI.....	57
6.1	Introduction to MALDI mechanisms.....	57
6.2	Analyte molecule incorporation	58
6.3	Laser absorption	58
6.4	Desorption	59
6.5	Ionization	61
6.6	Matrix selection	63
6.7	Sample preparation	64
6.8	Surface Preparation	64
6.9	Atmospheric pressure-MALDI.....	65
6.9.1	Advantages	65
6.9.2	Disadvantages	66
7	ToF-SIMS.....	67
7.1	Introduction	67
7.2	Principles and ion formation	68
7.2.1	General principle.....	68
7.2.2	Basics of ToF-SIMS theory.....	69
7.3	Instrumentation.....	72

7.3.1	Ion generation.....	72
7.3.2	Ion beam sources.....	74
7.4	Time-of-Flight mass analysis.....	75
7.5	Ion detection.....	77
7.6	Analysemethoden.....	78
7.6.1	Static SIMS	78
7.6.2	Dynamic SIMS	79
8	Electrospray Ionization.....	82
8.1	Overview.....	82
8.2	Electrospray ionization process.....	83
8.2.1	The ion evaporation model.....	85
8.2.2	The charged residue model	86
9	Bibliography	87
10	Aim of thesis.....	101
11	Scientific work published.....	103
11.1	Publication A.....	103
	Triboanalysis of hypoid gear components in drive trains	103
11.2	Publication B.....	109
	Atmospheric pressure matrix-assisted laser desorption/ionization mass spectrometry of friction modifier additives analyzed directly from base oil solutions	109
11.3	Publication C.....	117
	Modified-Atmospheric Pressure-Matrix Assisted Laser Desorption/Ionization Identification of Friction Modifier Additives Oleamide and Ethoxylated Tallow Amines on Varied Metal Target Materials and Tribologically Stressed Steel Surfaces	117
12	Conclusions and Outlook	126

Summary

Boundary lubricating films consist of various reaction products from lubrication components and are an important factor in tribological systems. They have drawn increased attention in recent years in the field of tribology and surface science. An important aspect is the determination of the constituents of such tribofilms. As the lubrication additives react with the surface, material properties can change significantly. Thus, the information of the tribofilm composition is eminent for the evaluation of friction behavior of tribo-partners.

As starting point for this study, surfaces and boundary tribofilms on tribologically stressed contact areas were examined and characterized by a combination of various surface analytical methods. Samples of a severely stressed hypoid gearbox system were characterized by means of optical microscopy, confocal white light microscopy, SEM/EDS (scanning electron microscopy / energy dispersive X-ray spectroscopy), XPS (X-ray photoelectron spectroscopy), Nanoindentation, ToF-SIMS (time of flight-secondary ion mass spectrometry), as well as computational simulations. Various material alterations and plastic deformations could be observed on the stressed surfaces and in cross sections. ToF-SIMS revealed grain boundary oxide formations in loaded areas. Additionally, XPS and SEM/EDS analysis detected traces of sulfur and phosphorus from additive residues in contact zones. Results of applied examinations including the combination of several surface analytical methods gave a substantial overview on tribomechanical and tribochemical alterations, whereas identification of originally used additive composition was not readily accessible. Therefore, in a second step, the possibility of direct model additive identification from lubricant solutions without applying additional separation techniques was evaluated via atmospheric pressure matrix-assisted laser desorption/ionization mass spectrometry (AP-MALDI). The method was chosen for its rather simple sample preparation and its soft ionization at atmospheric pressures. Single additive solutions as well as oil blends of two selected organic friction modifier model additives were investigated using ionization tech-

niques ESI (electrospray-ionization) and AP-MALDI. Confirmed by ESI and CID-measurements it could be shown that AP-MALDI was suitable to identify both model additives directly from oils solutions.

The final objective was to establish a method to identify and characterize additive compositions of boundary tribofilms from tribostressed surfaces. Therefore, special target holders for tribotest samples were constructed and applied onto the AP-MALDI ionization chamber. This way, the originally used additives, mentioned above, could be identified directly from tribofilms. Additionally, the ionization behavior of analyte solutions on unstressed surfaces was assessed through material and roughness variations of target samples. Further elucidation using ESI and ToF-SIMS measurements confirmed AP-MALDI results. Moreover, these techniques also revealed degradation fragments of initial additive molecules. This means, the chemical composition of a tribofilm after tribological testing could well be determined by means of AP-MALDI-MS by applying the herein described method, confirmed by supporting methods such as ToF-SIMS and ESI-MS.

Zusammenfassung

Grenzflächenschmierfilme bestehen aus diversen Reaktionsprodukten von verschiedenen Bestandteilen des Schmierstoffes und sind ein wichtiger Faktor in tribologischen Systemen. Sie haben in den letzten Jahren auf dem Gebiet der Tribologie und der Oberflächenwissenschaft vermehrt Beachtung gefunden. Da die Schmierstoffzusätze mit der Oberfläche reagieren und sich die Materialeigenschaften erheblich ändern können, ist die Bestimmung der Bestandteile solcher Tribofilme ein wichtiger Aspekt. Die Information der Tribofilmzusammensetzung ist daher für die Bewertung des Reibungsverhaltens von Tribopartnern von herausragender Bedeutung.

Als Ausgangspunkt für diese Studie wurden Oberflächen und Tribofilme auf tribologisch beanspruchten Kontaktflächen untersucht und durch eine Kombination verschiedener oberflächenanalytischer Methoden charakterisiert. Proben eines stark beanspruchten Hypoidgetriebesystems wurden mittels optischer Mikroskopie, konfokaler Weißlichtmikroskopie, REM / EDS (Rasterelektronenmikroskopie / energiedispersive Röntgenspektroskopie), XPS (Röntgenphotoelektronenspektroskopie), Nanoindentation, ToF-SIMS (Flugzeit-Sekundärionen-Massenspektrometrie) sowie Computersimulationen charakterisiert. An den beanspruchten Oberflächen und im Querschnitt konnten verschiedene Materialveränderungen und plastische Verformungen beobachtet werden. ToF-SIMS zeigte Korngrenzenoxidformationen in belasteten Bereichen. Zusätzlich wurden bei der XPS- und SEM / EDS-Analyse in den Kontaktzonen Spuren von Schwefel und Phosphor aus Additivrückständen nachgewiesen. Die Ergebnisse der angewandten Untersuchungen, einschließlich der Kombination mehrerer oberflächenanalytischer Methoden, ergaben einen umfassenden Überblick über tribomechanische und tribochemische Veränderungen, woingegen die Identifizierung der ursprünglich verwendeten Additivzusammensetzung nicht ohne weiteres möglich war.

Daher wurde in einem zweiten Schritt die Möglichkeit der direkten Identifizierung von Modelladditiven aus Schmierstofflösungen ohne Anwendung zusätzlicher Trenntechni-

ken mittels matrixunterstützter Laserdesorptions- / Ionisations-Massenspektrometrie unter Atmosphärendruck (AP-MALDI) bewertet. Die Methode wurde aufgrund ihrer relativ simplen Probenvorbereitung und ihrer sanften Ionisierung bei atmosphärischem Druck ausgewählt. Einzelne Additivlösungen sowie Ölgemische von zwei ausgewählten organischen Friction Modifier-Additiven wurden mit den Ionisierungstechniken ESI (Elektrospray-Ionisation) und AP-MALDI untersucht. Wie durch ESI- und CID-Messungen bestätigt werden konnte, wurde gezeigt, dass AP-MALDI geeignet ist, beide Modelladditive direkt aus Öl-basierten Mischungen zu identifizieren.

Das Endziel bestand darin, eine Methode zur Identifizierung und Charakterisierung der Additiv-Zusammensetzung von Tribofilmen auf belasteten Oberflächen zu entwickeln. Daher wurden spezielle Probenhalter für Versuchsproben konstruiert und in der AP-MALDI-Ionisationskammer montiert. Die verwendeten Additive konnten so direkt aus den Triboschichten identifiziert werden. Zusätzlich wurde das Ionisationsverhalten der Analytlösung auf nicht beanspruchten Oberflächen durch Material- und Rauheitsvariationen der Proben untersucht. Die weitere Aufklärung mittels ESI- und ToF-SIMS-Messungen bestätigte die AP-MALDI-Ergebnisse. Darüber hinaus konnten diese Methoden auch Abbaufragmente der ursprünglichen Additiv-Moleküle nachweisen. Dies bedeutet, dass die chemische Zusammensetzung eines Tribofilms nach tribologischen Tests mittels AP-MALDI-MS durch Anwendung des hier beschriebenen Verfahrens gut bestimmt werden konnte, was durch unterstützende Verfahren wie ToF-SIMS und ESI-MS bestätigt wurde.

Acknowledgements

Many people have helped me throughout the years and joined me on my journey to complete this project. Without them this would not have been possible and they all contributed to the accomplishment of my PhD thesis.

First of all, I want to thank Dr. Andreas Pauschitz and AC2T research for giving me the chance of performing my PhD program within the scope of internal strategic research and providing me with the necessary infrastructure and scientific equipment. This thesis would not have materialized without the funding provided by the “Austrian COMET Programme” (Competence Centers for Excellent Technologies, Project “XTribology”, Grant No. 849109) carried out at the “Excellence Centre of Tribology” (AC2T research GmbH), as well as funding by the ERDF (European Regional Development Fund), and the province of Lower Austria (“Onlab” project).

I am also very grateful for the proficient guidance of my supervisor Prof. Dr. Herbert Hutter of the TU Wien, who gave me the possibility of joining his research group. He was always available for prolific and worthwhile discussions and his vast knowledge in the field of mass spectrometry and surface analysis was of major importance. At the TU Vienna I also had the privilege to work with Dr. Ernst Pittenauer and benefit from his enormous practical and theoretical knowledge. I am very thankful for his clear explanations and his qualified advices.

At AC²T I want to especially thank Josef Brenner for his years of support and assistance in various matters. Most of all, his counseling for setting up the experiments and planning the experimental approach, as well as his support in interpretation and discussing results were of great importance. I also want to thank my colleagues Dr. Andjelka Ristic and Dr. Alexander Kassler for giving me a helping hand in the lab as well as for providing me with valuable information whenever I had questions about instrument handling or theoretical aspects.

Additionally, I want to thank Prof. Dr. Friedrich Franek for his support and advice concerning the work on my thesis. His vast experience in the field of tribology and the time he spent for revisions and advising truly improved the quality of this result.

This work would also not have been possible without the help of Dr. Markus Varga, who helped to provide resources and room for experiments as well as for publications of the scientific results. Furthermore, I want to say thanks to all my colleagues in the company and from my various offices, for all the little chats and jokes, which made this experience a fun time.

Last but definitely not least I want to thank my family, especially my wife, as well as my parents, for all their patience and support throughout the years. Apart from building a house and having three kids, my wife managed to reserve and free up some time for me to work on this project. But most of all I want to thank my kids Julian, Benjamin and Viktoria for putting a smile on my face in times of despair and lack of motivation.

1 General Aspects of Tribology and Lubrication

1.1 Introduction to tribology

In this work the assessment of tribologically stressed systems and detailed chemical analysis of additive molecules found in surface layers of wear tracks after tribotests were conducted is described. Therefore, a short introduction into the scientific field of tribology and lubrication will be given.

Tribology covers a vast field of knowledge. Many aspects of tribology surround us in our daily lives and its importance is always present. It is a multidisciplinary field of research, which deals with integrated processing of friction and wear considering interdisciplinary collaboration of the scientific fields of physics and chemistry, as well as various material sciences and engineering sciences.

The scientific field of tribology deals with investigations of friction processes, wear behaviors and lubrication mechanisms of interacting surfaces in relative motion. Tribology is a widely interdisciplinary field where various aspects of different scientific fields are involved. These include applied and theoretical physics, chemistry, and material sciences as well as all engineering and computational sciences. Besides the scientific accomplishments, another main objective of research in the field of tribology is the adoption of results for various applications in industrial or production plants.

Implementation of tribological findings and consideration of tribological interdependencies can lead to substantial savings of energy input and material resources, as can be seen in Figure 1-1. Many studies in different industrial countries have shown a significant economic importance of tribology. A substantial amount of cost-saving options could be ob-

tained by reducing damages caused through high friction, wear or corrosion (Franek, 1996; Czichos, 2010; Holmberg, 2012, 2014, 2015, 2017-a, 2017-b). The reduction of friction and wear can also greatly improve production processes and reduce maintenance expenditures for many kinds of mechanical devices and increase the overall life-time of instrument components. Furthermore, the gain of knowledge in tribological mechanisms prove to be beneficial in the prevention of environmental damage and also for advancements in occupational safety and health.

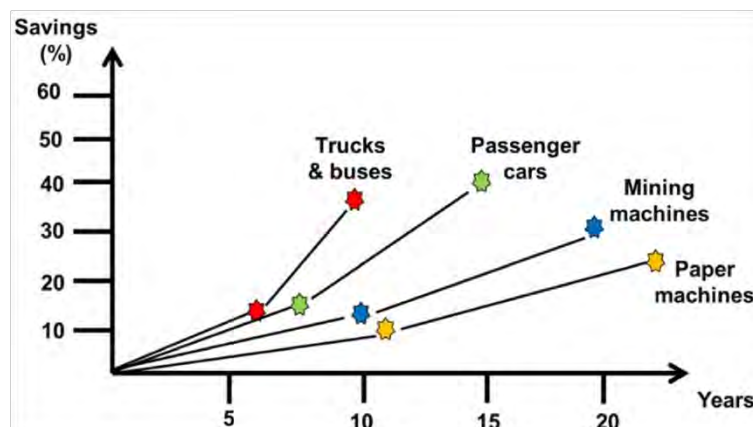


Figure 1-1: Saving potentials in various technological fields after introduction of sophisticated tribological solutions (Holmberg, 2017-b).

Friction and wear always have been subjects of investigations and improvements. All advances and enhancements related to rolling and sliding motions were of utter importance for survival for early human cultures. Real scientific research began with first considerations and drawings of Leonardo da Vinci. Guillaume Amontons, Charles Augustin de Coulomb, and other great thinkers of their times brought the science of friction into the modern age (Dowson, 1979). Contemporary research made its way around the beginning of the 20th century.

The term ‘tribology’ itself derives from the Greek words *tribos* for ‘friction’ or *tribein* for ‘to rub’. Only in the year 1966 in the famous report about the economic relevance of friction and wear the term “Tribology” was coined by Peter Jost (Jost, 1966). There, the first definition of the scientific field of tribology was given as follows: “Tribology is the science

and technology of interacting surfaces in relative motion and of related subjects and practices.“

1.2 The tribological system

To get an overview of the scientific field of tribology it is necessary to look at the description of the tribological system. By definition, in the tribological process two interacting counter bodies are in relative motion to each other. This procedure entails and causes certain friction behavior and possibly wear of affected components. Applied stress and resulting changes of bonding levels on the atomic scale can alter certain properties of materials and surfaces. Friction and wear are no intrinsic material properties and cannot be described directly by simple material parameters (such as hardness or Young's modulus) but are properties of a system composed of various influences. Characterization of friction and wear always requires analysis and consideration of the complete surroundings including all parameters, which could affect the so-called tribological system. Additionally, no simple correlation between friction values and wear volumes can be established (cf. e.g. Czichos, 2010).

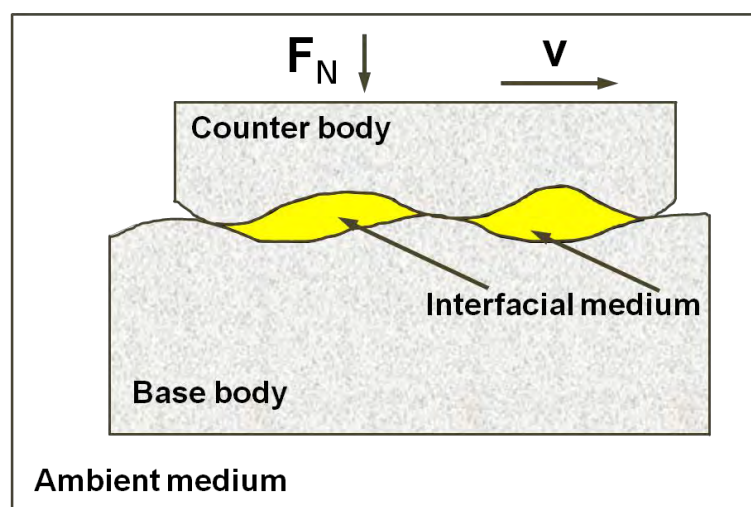


Figure 1-2: Scheme of a tribological system including the basic structural elements.

Tribosystems have to operate input parameters such as energy, material or information into output data. Through interaction of the structural elements of the entire system this transformation is achieved (Czichos, 2014). All physical, chemical, and geometrical processes within this surface contact and the surrounding atmosphere are influenced by various parameters and complex interactions. They only reflect the tribological behavior within the system being analyzed (Axén, 2000; Sommer, 2010). Like all technical systems, tribological systems (Mang, 2014) follow certain rules and consist of structures with four basic structural elements:

1. Base body (main body)
2. Counter body (opposing body)
3. Intermediate or interfacial material
4. Surrounding or ambient medium

A tribological system can in general also be described by its function, the stress collective, including parameters such as load, speed, temperature, the structure and structure-building elements including their material properties and interactions: the four components basic body, counter body, ambient medium and intermediate material including velocity v and normal force F_n (see Figure 1-2) and the friction and wear parameters, which are the output variables of the system (Sommer, 2010).

The function of a tribosystem is defined through its active surfaces. These areas are exposed to tribological stresses through the functional forces and relative movements of both counter bodies. Friction and wear result from dissipation effects in through space and time stochastically distributed micro-contacts within the geometric contact surface. These complicated and multifarious microscopic surface interactions depend on geometrical and topographical material characteristics, the stress collective of forces, speed, exposure time, temperature, atmosphere, contact nature as well as the structure and composition of the entire tribological system (Czichos, 2010; Axén, 2000).

Variables such as the surface geometry, loading parameters, width of lubricant layer are involved in the generation of tribological stresses. The reaction processes of the contacting counter bodies can be either physical, chemical or physico-chemical (Mang, 2007-a). The functional interaction between the active surfaces ensures the conversion of initial state parameters towards functional output. However, tribological effects such as abrasion, chemical reaction of tribopartners, fatigue wear and others, can be affected by both, intermediate and surrounding media, e.g. lubricants, abrasive particles and humidity, gas phase contaminations (Czichos, 2014).

Materials behave differently in different tribological systems. Generally, wear-resistant materials can be prone to corrosion and other detrimental influences. Documentation of friction and wear results is only meaningful for exactly specified test conditions. Carefully documented tribotesting (Axén, 2000) is essential for the development and selection of material pairs in applications involving friction and wear processes, as will be further discussed in section 4.

1.3 Friction

Friction between two counter bodies is, like wear, no material property but a property of the entire surrounding system. It is commonly referred to as the resistance against relative motion of touching counter bodies (Ludema, 2010), either as resistive force not to initiate a relative movement (static friction) or its continuation (kinetic or dynamic friction). These tribological phenomena can be called ‘external friction’, whereas ‘internal friction’ of substances is known as force resisting deformation (motion of atoms) of the internal structure of solids, or also the viscosity of fluids. The friction of a tribological system can be characterized by the Stribeck curve (Stribeck, 1902) (see Figure 1-4 in section 1.3.2). It is described by similar terms, which are used for classification of wear and lubrication.

1.3.1 Types of friction

In general, friction can be divided into *static* friction and *dynamic* (kinetic) friction. Static friction is effective between two bodies at rest, where the applied force or momentum is not sufficient enough to initiate a relative movement of the counter bodies. Contrary to dynamic friction processes, the static friction does not contain an energy conversion process and thus no losses occur. The frictional forces occurring during the relative movement between sliding bodies act against the direction of the movement and try to inhibit the movement (Sommer, 2010). Additional observed variations of frictions include contrasting pairs such as lubricated – dry or internal (hysteretic) – external (viscous) (Ludema, 2010).

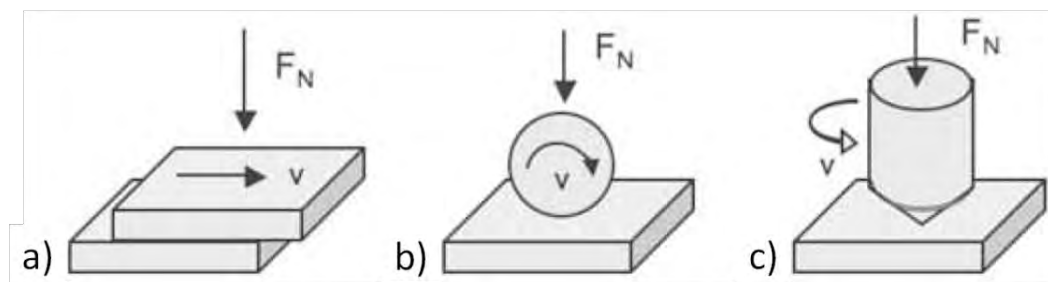


Figure 1-3: Basic forms of relative motion between two bodies: sliding a); rolling b); drilling c) (Czichos, 2010).

Depending on the nature of the relative movement of the contact partners, the following main types of dynamic friction (cf. Figure 1-3) can be distinguished: Sliding friction, rolling friction, drilling friction (Czichos, 2010; Sommer, 2010). *Sliding* is a relative translational motion of two bodies in which their respective individual speeds vary in velocity or direction. Ideal *rolling* would include a rotating body with a rotation axis placed within the contact area and where the direction of movement is perpendicular to the rotation axis. Real rolling usually includes microslip and sliding fractions. For rotating bodies with axis of rotation perpendicular to the contact surface and no additional movements *drilling* friction is present. Additionally, it is characterized by a velocity gradient along the radius.

1.3.2 Friction regimes

Besides the description of different kinematic types of friction, a classification according to aggregate state or contact conditions can also be made. In this way additional distinctions into solid state and fluid friction, or boundary, mixed, and (elasto-) hydrodynamic friction are applied.

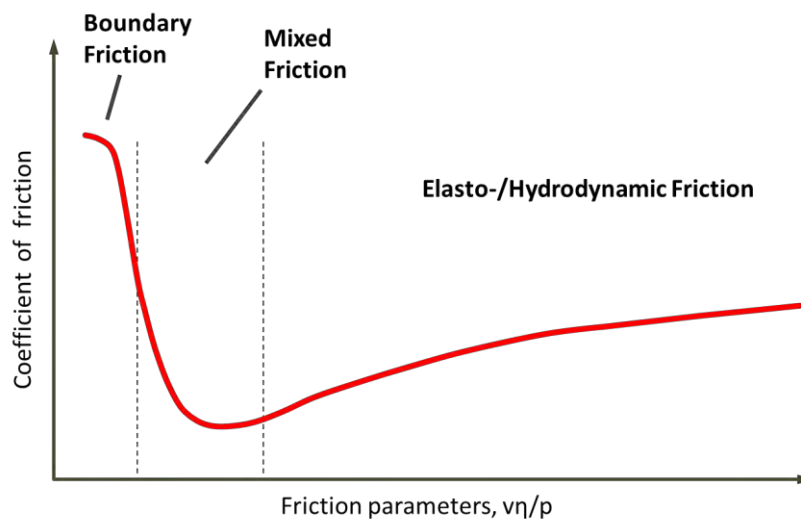


Figure 1-4: Stribeck curve including friction regimes.

The Stribeck-curve (Stribeck, 1902) describes the course of the coefficient of friction as a function of the friction velocity v , the dynamic viscosity η , and load p (see Figure 1-4). The different friction regimes can be described according to parameter value development (cf. e.g. Czichos, 2010; Sommer, 2010). For low velocities and high loads in boundary friction the contacting surfaces are in contact and can be covered by molecular layers of lubricating film and high CoF is found. Increasing the velocity and/or decreasing loads leads to the mixed lubrication regime, with less contacting area and increasing lubricating films, yielding lower friction values. Lowest friction values are found for (elasto-)hydrodynamic friction conditions, where surfaces are completely separated by a stable film of lubricant. A further increase of velocities leads to an approximately degressive increase of the coefficient of friction in the hydrodynamic friction regime. Further descriptions of the regimes are given in section 1.5.2.

1.3.3 Macroscopic friction

Aspects of friction on a macroscopic level have been studied by many great scholars and scientists such as Leonardo da Vinci, Guillaume Amontons, Leonard Euler, Charles Augustin Coulomb, Arthur-Jules Morin, Osborne Reynolds and many others (Dowson, 1979). Their experimental investigations eventually lead to phenomenological descriptions and formulations of Coulomb's law of friction (cf. e.g. Sommer, 2010) which is independent of contact area and velocity.

$$\mu = \frac{F_f}{F_n} \quad (\text{Eq. 1.1})$$

μ = coefficient of friction

F_f = friction force

F_n = normal force

The level of friction can be described through the coefficient of friction μ . It is the ratio of the force F required to sustain or initiate relative tangential motion of the counter bodies and the normal force F_n , which is orthogonal to the contacting surfaces. The coefficient of friction $\mu = F_f/F_n$ in modern technology started to be regarded as a variable, determined by a wide range of operational variables, lubricants, characteristics of the base material, and surface modifications and films (Campbell, 1939; Clark, 1935; Beare, 1935; Dokos, 1946; Boyd, 1945; Ludema, 2010).

The general understanding is that this law is valid only for approximations and holds true only within certain restraints, depending on the difference between nominal geometrical and the real contact areas. This type of macroscopic friction between solids is called external friction. It's mainly based on the mechanical resistances (i.e. physical forces and moments), which compete to impede relative motion (dynamic friction) or completely prevent it (static friction) (cf. e.g. Sommer, 2010).

Various phenomena of friction can be observed (Ludema, 2010). Systems with force transmitting components which are expected to operate without displacement such as drive or traction surfaces and clamped surfaces. In energy absorption-controlling components constant friction without any stick-slip-motion, i.e. microscopic vibrations, is essential. Other components require low friction materials for maximum efficiencies when normal force is applied.

Friction is defined as a process of interaction of contacting bodies or materials. A measured friction variable therefore does not denote the property of a single body or substance, but always refers to a material pairing (Czichos, 2010), i.e. in general the regarding tribological system.

$$\textit{Friction / Wear} = f(\textit{system structure}, \textit{load spectrum}) \quad (\text{Eq. 1.2})$$

The *system structure* is described through the friction bodies and materials directly involved in the friction process as well as their relevant properties. The *load spectrum* is mainly given by the kinematics, the normal force F_N , the velocity v , the temperature T and the exposure time t .

1.3.4 Microscopic friction

The main friction processes occur at surface boundary layers, where physical and chemical interactions take place. The largest portion of the used friction energy is transferred mainly into heat. Physical and chemical interactions taking place within microscopic contact areas can lead to surface and material alterations, whereby the surface boundary layers can have significantly different structure than the main bulk of the tribo-partners. The shape of the surface and the contact conditions within the contact zone play an important role. Compared to the macroscopic geometric contact area even for finely machined sur-

faces and high applied loads the true contact area is relatively small and accounts only for a maximum of a few percent of the "apparent" nominal area of contact (Bowden, 1959; Sommer, 2010).

In a static contact the occurrence of normal forces will lead to elastic-plastic deformations of micro-asperities. Thus, the real contact area increases until it just withstands the load. An increase of the normal force would yield a formation of new contact areas up to a certain load limit, without changing the nominal contact pressure. For constant contact pressure in a first approximation friction conditions stay constant and thus, a constant friction coefficient μ . Hence, Coulomb's law in certain load ranges is very well applicable, whereas upon closer examination, experiments point to a dependence of the friction force of the true asperity contact area. Recent advances of surface analysis on the atomic level contributed significantly to the understanding of friction processes (cf. e.g. Sommer, 2010).

When separating adsorption or reaction boundary layers are ruptured, adhesion bonds between the contacting surfaces can be formed within the contact areas. The reason for this are the same binding forces, which are responsible for the cohesion of the atoms in solids. The bond types in solids depend on the electron structure (metallic, covalent, ionic and van der Waals bonds), which determines the strength of the bond. These bondings are determined by the condition of the surfaces during relative motion and friction processes on an atomic scale. These repeated breaking and bonding can lead to detrimental surface deformations and material transfer that can ultimately yield in various forms of wear appearances on a microscopic scale.

1.3.5 Friction mechanisms

Every friction process requires some kind of energy input, which is achieved through the application of tribological stress (building of contact area, junction growth, delamination, surface bonding). The energy conversion of friction is caused by friction mechanisms, which are movement-inhibiting, energy-dissipating elementary processes of friction (Czichos, 2010). Energy transformation in the contact area is mainly realized through deformation and adhesion processes, which occur in the contact area of a tribological system. Resulting free thermal energy is dissipated through internal absorption or emission to surrounding media. The basic friction mechanisms can be divided into the following four types (see Figure 1-5).

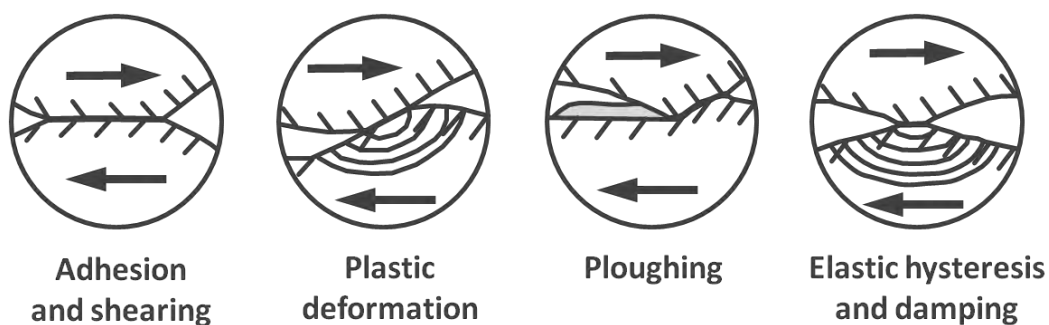


Figure 1-5: Schematic illustrations of the four main friction mechanisms (cf. Czichos, 2010).

1.3.5.1 Adhesion

Adhesion and shearing is based on localized bonding between contacting solid surfaces leading to material transfer or loss from either surface. Adhesion-bonds are built and destroyed and materials can weld together. Rupture of interfacial adhesive bonds will cause fracture and wear.

1.3.5.2 Plastic deformation

Plastic deformation is a stress-induced change of form or shape. At the contact of surfaces and at tangential relative movement of contacting bodies a deformation occurs. Energy losses may occur due to dissipative processes in the plastic contact deformation.

1.3.5.3 Ploughing

Ploughing is the formation of grooves by plastic deformation on the softer of two surfaces in relative motion. Upon contact of two bodies with different hardness, the harder surface roughness elevations may penetrate the soft counter body. In a tangential displacement a frictional component arises as a result of the resistance of the material to the ploughing by the harder counter body (Liang, 2003).

1.3.5.4 Elastic hysteresis

Elastic hysteresis and damping are effects of elastic contact deformations combined with surface roughness, where spatially and temporally stochastically distributed stress and thus vibration fields are built up and dismantled. In this way, lattice defects are generated in the area of plastic contact deformation in the contactless regions and are moved through the lattice (Nicholas, 1959; Landman, 1990), but in general, these effects account for less than 1% (Gane, 1973). Additionally, effects such as frictional electrification (Harper, 1967; Kornfeld, 1976), acoustic emissions (Tolstoi, 1967), photon emission (triboluminescence) (Walton, 1977; Zink, 1978; Heinicke, 1984) and electron- and ion-emission also contribute to energy transmission and dissipations in friction processes (Czichos, 2010; Heinicke, 1984; Wortmann, 1976; Ferrante, 1977).

1.3.6 Stick-Slip phenomena

In sliding friction often stick-slip phenomena can be observed. For macroscopic considerations in tribological sliding contacts, the sliding partners are coupled to the environment by oscillatory systems. Stick-slip phenomena especially occur when static coefficients of friction are high compared to dynamic coefficients. In a simplified way tribological sliding systems can thus often be represented by a model of springs.

In this spring model (cf. Figure 1-6) a sample body is connected to a spring (Ludema, 2010, Czichos, 2010). The driving force F_{Spring} causes the spring to be tensioned until the spring force exceeds the static friction force of the mass of the sample on the base plate. Movements commence as F_{Spring} becomes larger than the static friction ($F_{Spring} \geq F_{STF}$) and drive the counterpart into motion as long as the force F_{Spring} exceeds the dynamic friction (sliding, $F_{Spring} \geq F_{DF}$).

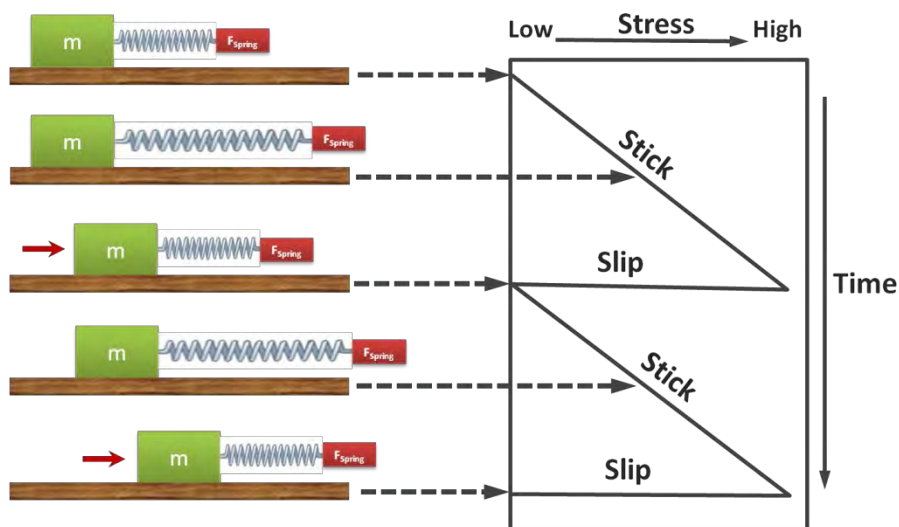


Figure 1-6: Segments of stick-slip motion (cf. Marshak, 2011).

When the driving force F_{Spring} is depleted the spring becomes relaxed and the applied spring force decreases. Due to its inertia, the mass moves a certain distance beyond the point where the spring force F_{Spring} equals the sliding friction force F_{DF} and then slows down (sticking, as soon as $F_{Spring} \leq F_{DF}$). After the velocity is diminished, the driving force

F_{Spring} first picks up this piece and then again increases the spring tension up to the static friction limit F_{STF} (tensing up, as long as $F_{Spring} \leq F_{STF}$). Subsequently, the cycle starts again.

This model can be transposed to real surfaces, which are in relative motion or stick to each other as alternating phenomena. When a certain constant external force is applied on a stationary body, a sudden increase in velocity can occur if the driving force becomes bigger than the static friction, which holds the counterpart in place. Similar to a loaded spring the load will suddenly move, when the static friction is overcome by the force. While the body is moving, the force will decrease, until it is smaller than the friction and will eventually come to a halt. As the force continues to be effective, tension increases until again the force overcomes the static friction followed by a sudden movement of the body and the cycle starts over again.

1.4 Principles of wear

Wear is generally defined as the physical damage to a solid surface's exposed area. This can be the gradual material loss from a surface of a solid body caused by tribological stress with a mating body. The mechanical stress can be applied by contact and relative motion of a solid, fluid or gaseous counter body. As a result separation processes owing to microfractures, chemical dissolutions or high temperatures at contact interfaces appear (Kato, 2000). In general, the control of wear occurrences is of significant importance for instrument reliability in the field of engineering and machine technology.

The spectrum of wear appearances covers a vast variety of wear phenomena. Mild to severe wear can occur depending on the tribological load and friction behavior of the stressed surface materials. Different kinds of wear phenomena are classified depending on localization, structure of the tribological system and the kinematics of the applied tribological load. Generally, wear will result in component damage and the associated failure of

machines and equipment. Depending on the operation parameters and the material composition of the compounds in contact wear rates can vary substantially in a range of around 10^{-15} to 10^{-1} mm³/Nm. (Archard, 1953; Bhansali, 1980; Hokkirigawa, 1997; Hwang, 2016; Kato, 2000; Rabinowicz, 1980). So called wear maps (“Ashby-maps”) for certain operating conditions and selected materials have been proposed for an overview of possible wear appearances (Lim, 1987).

One way to characterize wear appearance is through various indicators either as measured alteration in size, shape, and mass of a body, surface or tribo-partner. Furthermore are changes in surface modifications of tribologically loaded materials or components, such as chemical composition or microstructure, described by different wear manifestations, as well as through the type and form of resulting wear particles. Due to dynamic changes of surface and material properties, as well as tribo-induced temperature increases and tribo-layer formation dominant wear modes might change over the course of the period of tribological stress application (Hwang, 2016). Multiple wear mechanisms may apply during complex tribological processes.

Measurements of wear can be given as wear amounts in different metrological dimensions, such as the wear length, area or volume. In addition to these direct wear measurements, wear is set in relation to a reference quantity for indirect wear measurements which are also referred to as wear rates. These can be measuring the wear rate over time, correlated the covered distance or to the particle throughput. For comparison of wear results the specific wear coefficient is normalized to the load and is defined as the wear volume W_v (mm³) per sliding distance s (m) with regard to the normal force F_n (N) (Archard, 1953; cf. e.g. Czichos, 2010).

$$k = \frac{W_V}{F_n \cdot s} \quad (\text{Eq. 1.3})$$

k = wear coefficient

W_V = wear volume

F_n = normal force

s = sliding distance

A wear rate does not include statements about wear mechanisms and does not constitute a material constant, since wear results of interaction processes between contacting bodies or substances. A determined wear measure therefore does not denote the property of a single body or substance, but must always be based on the material pairing and the appropriate tribological system. Due to the complexity of wear behavior, it is generally not exactly possible to calculate theoretically wear characteristics. These must be determined experimentally with suitable measuring and testing techniques (Czichos, 2010).

A number of processes occur during interaction of engineering counterparts when loaded and sliding or rolling motion is applied. Wear is, like friction and lubrication, an integral part of tribology. In tribological terms, all engineering surfaces have a certain roughness. This means, only a small amount of their apparent surfaces is in real contact when surfaces are loaded against each other. These surfaces asperities have very small radii on the top, so the contact stresses are high. These small impacts on the surface have major impact on processes of friction and wear. Additionally, it can be assumed that all engineering surfaces in atmospheric environment are contaminated. This can be a naturally occurring contaminant film like a single layer of adsorbed molecules deriving from the surrounding atmosphere or thicker oxide or other films formed by chemical reactions between the surface and adjacent substances (Archard, 1980).

1.4.1 Wear mechanisms

Physical and chemical interactions occurring in the contact area of a tribological system are commonly referred to as wear mechanisms. The types of material interaction in the contact zone are manifold. All variations of contact configurations are included, as well as detached solid particles within the contacting surfaces (Kato, 2000). These interactions set off elementary processes and eventually lead to changes of composition and shape of the contact partners as they contribute to wear processes. They emanate from micro-contacts in the contact area stochastically distributed over position and time. Their contribution to the wear is dependent on both the structure of the tribological system as well as the set of stress factors. The true contact area typically increases through the growing number of micro-contacts proportional to normal force F_N or sliding distance s .

In general, mechanisms leading to wear appearances can be divided into the two groups (Czichos, 2010) of *mechanical interactions* (force-, stress-, energy-related interactions) leading to cracks and material removal and *atomic and molecular interactions*, which are related to occurrence of chemical bonding between contacting surfaces in the contact area. The wear of materials resulting in material damage and can lead to a failure of the entire technical system in tribological systems due to wear-related substance -and- shape changes of components, if certain component or feature tolerances are exceeded (Czichos, 2010). Thus, in engineering applications, the wear is an important factor influencing the reliability of technical systems.

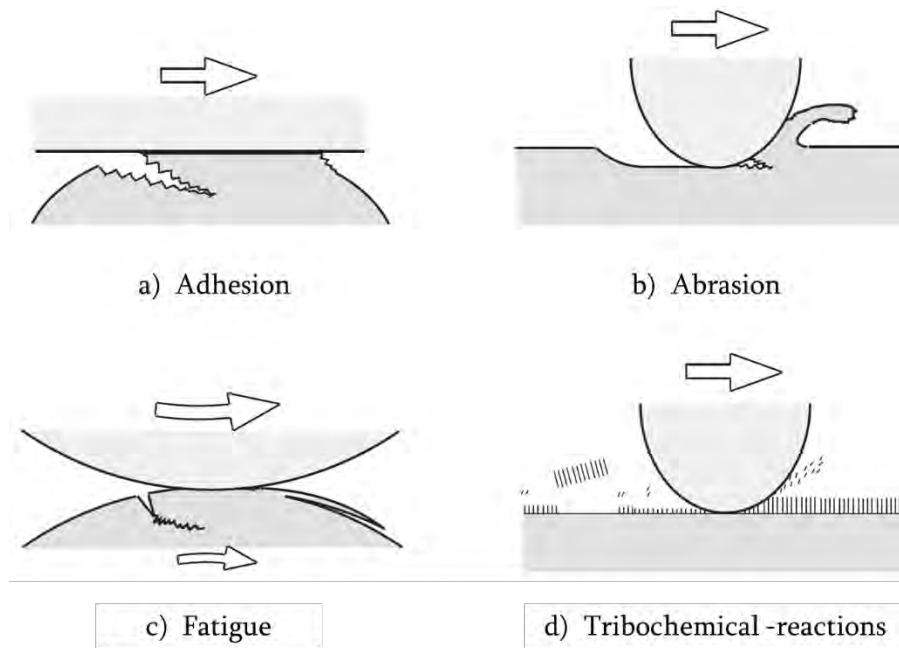


Figure 1-7: Overview of the four wear processes (cf. e.g. Kato, 2000).

The following four wear processes (see Figure 1-7) are mainly considered the major types and will be discussed shortly (Burwell, 1957; Zum Gahr, 1987; Czichos, 2010; Varenberg, 2013). Additional types can include fretting wear, erosive wear, corrosive wear, cavitative, diffusive wear.

1.4.1.1 Adhesion

In adhesion the material interactions on the atomic and molecular level play a decisive role (Holm, 1967). Adhesion is a phenomenon, where tribological stress caused by high local pressures on single surface asperities in plastic contact break up protective surface layers and local interface bonds are generated (de Gee, 1982). These interfacial bonds can have a higher strength than the original material of the contact partners. Therefore, in the case of a relative movement of the contact partners, a separation or displacement of the contacting material regions may not take place in the original contact interface but in the adjacent volume of one of the partners. In this way, holes and scale-like particles of material that often adhere to the sliding surface of the counter body with higher hardness can be generated.

1.4.1.2 Abrasion

Abrasion occurs in tribological contacts when the counter body is considerably harder and rougher than the tribologically stressed body or when hard particles are pressed into a tribologically stressed material. This way interlocking processes with the indented material take place (Kato, 2000). During a relative movement of the counter bodies, abrasive wear can be produced from the soft base body by various material separation processes, such as scratching or micromachining.

1.4.1.3 Surface disruption (Fatigue)

In every tribological system, the contacting surface areas must absorb forces which cause a material strain in correlation with the relative movement of the contact partners. In the case of fluid friction, the force transmission takes place via a separating lubricating film. For mixed, boundary and solid friction, the micro-contacts partially or completely absorb the normal and tangential forces acting on them. This wear mechanism is generally, caused by alternating or swelling mechanical stresses induced by repeated friction cycles (cf. e.g. Kato, 2000; Czichos, 2010). The result is a disruption of the surface, which means micro-cracks arise and grow in the near-surface layers of material. When the stress in the micro-contacts of the base and counter body is applied periodically, there might occur an accumulation of damage in terms of material fatigue in affected areas. This way small pits may be created on the surface. Since tensile stresses in the surface promote surface dislocation, compressive stresses can be introduced into the surface as a countermeasure. Suitable methods are nitriding, oxidizing or shot peening the surfaces.

1.4.1.4 Tribochemical reactions

Tribochemical reactions are chemical reactions between the base or counter body of a tribological system and the constituents of the intermediate or surrounding medium. An overview of possible tribochemical activities is given in Figure 1-8. They are caused by tribological stresses or at least reinforced by them. The tribologically stressed surfaces re-

act with the ambient medium in such a way, that in a relative motion constantly new reaction products are generated and abraded again (Fink, 1932).

The tribochemical reactions promoted by friction-induced temperature increases and resulting lattice defects change the mechanical properties of the surface regions. As a result of thermal and mechanical activation, the surface areas adjacent to the micro-contact sites have an increased chemical reactivity. Therefore, chemical reactions preferably take place in these regions and, for example, oxide islands can grow in the case of metallic contact partners. These oxide islands, formed especially with metallic contact partners, can only reduce mechanical stresses to a limited extent by plastic deformation. They rather tend to brittle spalling and generation of wear particles when reaching a critical thickness (Czichos, 2014; Hwang, 2016).

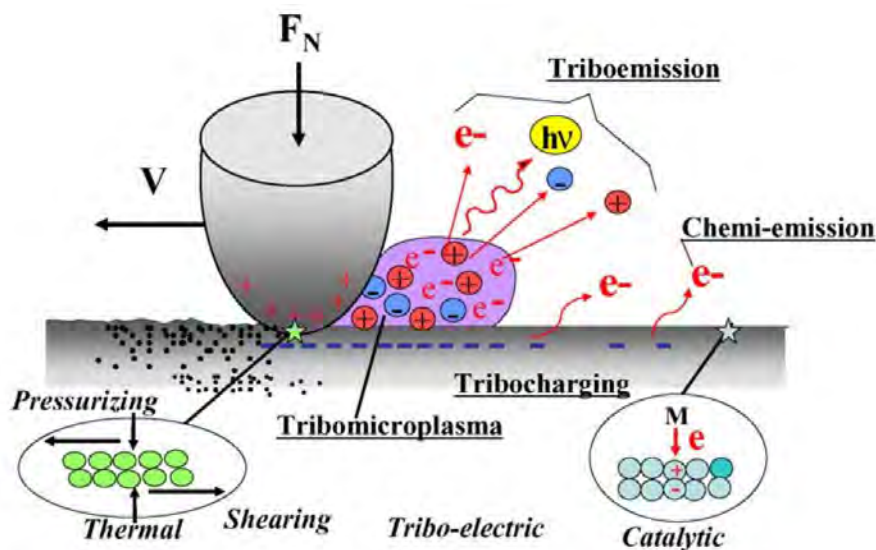


Figure 1-8: Overview of possible tribochemical activities in a tribological contact zone (Nakayama, 2006).

1.5 Lubricant composition and lubrication regimes

1.5.1 Principal aspects of lubrication

Generally, lubricants are used to reduce friction and wear occurrences in tribological systems. They can be applied in various aggregate states as lubricating oils, greases or solid lubricants. Occasionally, water, liquid metals or gases are used as lubricants. Depending on the operating conditions and the surface properties an application of lubricants in tribological systems possibly allows for the formation of a hydrodynamically generated lubricating film separating the contact partners according to the Stribeck-curve (see section 1.3.2) (Czichos, 2010). Through the application of lubricants friction and wear can be greatly reduced due to the reduction of direct contact of the surfaces of the base and counter bodies. Depending on the geometry and arrangement of the tribopartners as well as their surface roughness, lubrication viscosity, velocity and applied load various lubrication conditions can be described through the Stribeck-curve. This curve shows the friction coefficient plotted against viscosity, speed and load. In principal, lubricants can be based on either solids, liquids, any dispersions, as well as gases. The different lubrication mechanisms can also be differentiated by various lubrication regimes (Czichos, 2010), as will be shown subsequently.

1.5.2 Lubrication and friction regimes

In *boundary friction* (cf. Figure 1-4) the tribologically loaded surfaces are covered with an adsorption layer of lubricant molecules. The load is absorbed by the contacting surface asperities of the contact partners with no fluid lubricant present. During relative motion, shearing takes place predominantly on and is primarily influenced by the adsorbed lubricant additive molecules on the surface.

In *mixed friction* a part of the load is absorbed by the lubricating film, that can be established either hydrostatically or also in an elastohydrodynamic or hydrodynamic way. The remaining amount of applied load is again transmitted through surface asperity contacts. The separation of the contact surfaces in *hydrostatic friction* allowing for a consistent film of liquid lubricant is achieved through externally applied pressures. In *hydrodynamic lubrication* the relative motion of the counter bodies towards a narrowing lubrication gap leads to intake of the lubricant. The lubricant pressure increases and the contacting surfaces become separated (cf. Figure 1-9). The *elastohydrodynamic lubrication* is a result of elastic deformation of the contact partners and the increase in oil viscosity with increasing pressure. As the pressure increases, the tribopartners experience elastic strain and deformation. In this load-bearing section a close to parallel gap develops, which allows for the liquid to pass through. In full film *hydrodynamic lubrication* the surfaces are completely separated.

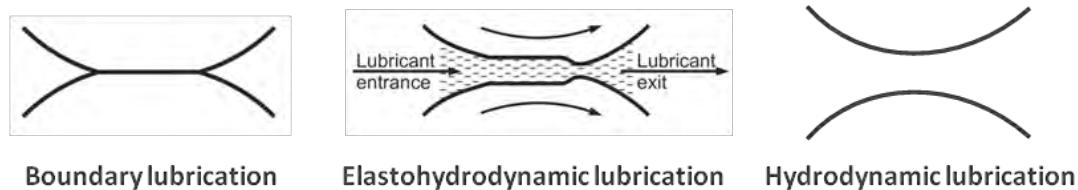


Figure 1-9: Development of lubrication clearance (cf. Mang, 2007-a).

1.5.3 Base oils

Oils used as lubricants in technical systems mainly have the goal to influence friction and wear, transport heat away from the contact area, as well as to transmit power. One way to classify lubrication oils is to separate them after their origin: mineral oils, animal or vegetable oils, synthetic oils, other fluids like water or liquid metals. In general, hydrocarbon base fluids are used for formulations of industrial engine oils, greases, or other lubricants. Present-day methods and technologies helped to understand chemical and physical properties of liquid lubricants and made it possible to produce specific fluids for certain appli-

cations. The properties of the base oil play a key role in the performance of the formulated lubricant. Since they are a blend of various molecules, the combination of the individual properties define the performance of the final lubricant (Stipanovic, 2003). In different applications many different types of hydrocarbon lubricants, such as engine oils, gear oils, hydraulic oils, turbine oils and many others are used (Czichos, 2010).

In general, a lubricant is composed of the base oil and chemical additives. As an average, around 95 % of the lubricant volume is the base oil component. Special lubricants can contain as low as 1 % (hydraulic oils, compressor oils) or even up to 30 % additives (greases, gear lubricants, metalworking lubricants) (Mang, 2007-b). Additional to mineral base oils also synthetic base oils are available on the market today. Mainly, the synthetic oils have considerably higher prices and are used in special applications such as extreme terrestrial conditions at high temperatures and pressures or space applications at low temperatures and pressures. The most common synthetic base oils are polyalphaolefines (PAO) (Dresel, 2007-a).

1.5.4 Lubricating greases

Greases consist of a lubricating oil without or with additives and a soap, or other substances like micropowders, as a thickening substance. As a rule, the soap is fibrous as a framework in which the lubricating oil is fixed. According to the type of soap, one differentiates between sodium fats, lithium fats, calcium fats, aluminum fats, barium fats and complex fats. In the case of the complex fats, the soaps are formed by co-crystallization of two or more compounds. In addition, greases containing organic, ash-containing thickeners (organic bentonites) and ashless polyureas are used for special applications.

The rheological behavior of greases is initially characterized by a flow limit, that is, no flow occurs below a certain shearing stress. The viscosity of the structure-viscous lubricating grease depends not only on the temperature and the pressure but also on the pre-treatment and on the shear gradient. In general, the viscosity of grease with shear duration and shear drop decreases. In the lubrication technology lubrication greases can fulfill tasks such as dispensing a suitable amount of liquid lubricant by slow separation to reduce friction and wear over wide temperature ranges and long periods, as well as sealing against water and foreign particles (Czichos, 2010; Dresel, 2007-b).

1.5.5 Solid lubrication

Lubricants are often used for lubrication under extreme conditions, such as at very high or very low temperatures, in aggressive media, in vacuum or under conditions where lubrication with oils or greases for maintenance, safety, environmental or health reasons is not applicable. In general, solid lubricants can be divided into the various groups (Busch, 2007): most widely used are compounds with layer lattice structure, these include the dichalcogenides of the transition metals such as molybdenum disulfide, graphite, graphite fluoride, hexagonal Boron nitride and a series of metal halides. Others include oxidic (lead oxide, molybdenum oxide, tungsten oxide, zinc oxide, cadmium oxide, copper oxide, titanium dioxide) and fluoride (calcium fluoride, barium fluoride, strontium fluoride, cerium fluoride, antimony trioxide, lithium fluoride, sodium fluoride) compounds of the transition and alkaline earth metals. Also, soft metals such as lead, indium silver, or tin or polymers like PTFE, or polyimide are used (Czichos, 2010).

2 Lubricant additives

2.1 Lubrication improvement through additives

The demands on lubricants have increased substantially due to the challenging requirements of modern machines and industrial plants. Pure unalloyed base oils, mineral base oils as well as synthetic oils, would not be able to fulfill these high performance demands anymore for a long time. Using the advantages of modern oil-soluble active substances or additives and their chemical and / or physical effects, the positive properties of the synthetic or mineral base oil could be improved, negative properties could be suppressed, or additional properties initiated. In general, most modern industrial equipment must be lubricated in order to prolong its lifetime (Braun, 2007).

Lubricants perform a number of critical functions for the specified system, such as lubrication, cooling, cleaning, suspending, protection of metal surfaces against corrosive damage and others. Lubricants are usually comprised of a base oil and a customized additive package. The primary function of the base fluids are to lubricate the tribocontact, heat transfer, and to act as a carrier for the contained additives. The overall function of additives is to enhance an already existing property of the base fluid, such as viscosity, viscosity index, pour point, oxidation resistance or to add a new property like cleaning/suspending abilities, anti-wear/extreme-pressure performance or corrosion inhibition. Typical lubricants contain around 90 % base oil and less than 10 % of additives. The lubricant base is most often comprised of petroleum fractions (mineral oils), or synthetic liquids such as hydrogenated polyolefins, esters, silicones, or fluorocarbons.

The lube oil base is the substrate where appropriate additives are selected and properly blended together to achieve a balance in performance characteristics of the finished lubricant. To achieve the highest levels of performance in finished lubricants it is utterly important to understand the interactions of base oil and additives to match them to the requirements of the machinery and the operating conditions.

2.2 General types of additives

Several types of additives are existent. Some additives impart new and useful properties to the lubricant, others enhance properties which are already present. Further additives act to reduce the rate at which undesirable changes take place in the product during its service life. A main reason to add additives to lubricants is to protect the lubricant in service by limiting the chemical change and deterioration as well as to improve existing physical properties and to create new beneficial characteristics.

Chemical effects	Physical effects
Extreme pressure additives	Pour point depressants
Anti-wear additives	Anti-foam agents
Detergents	Viscosity index improvers
Dispersants	De- and Emulsifiers
Corrosion inhibitors	Seal swell agents
Antioxidants	
Friction modifiers	

Table 2-1: Overview of common types of lubricating additives.

Many different additives for various purposes are available on the market. Table 2-1 gives a short overview over the most common types of additives in liquid lubricants. For the present work only friction modifiers as type of surface active model additives are used in the tribolayer generation process for the additive identification method development. Therefore, the additive type of organic friction modifiers (OFM) will be discussed in more detail in the following section.

2.3 Friction modifiers

The general type of friction modifier additives has been around for a long time. Their main purpose is to reduce the friction in industrial machinery and decrease wear appearances. Especially in the boundary friction regime they come into play, where the prevention of solid surface contacts is utterly important to significantly reduce friction and wear. The most common types of organic friction modifiers and their mode of action are given in Table 2-2.

Type of action	Commonly used products
Formation of reacted layers	Saturated fatty acids, phosphoric and thiophosphoric acids, sulfur-containing fatty acids
Formation of absorbed layers	Long-chain carboxylic acids, esters, ethers, amines, amides, imides
Formation of polymers	Partial complex esters, methacrylates, unsaturated fatty acids, sulfurized olefins
Mechanical types	Organic polymers

Table 2-2: Various types of organic friction modifiers and their mode of action (cf. Kenbeck, 2009).

Friction modifiers, like other additives, such as anti-wear (AW) or extreme pressure (EP) additives, are film forming additives. Contrary to AW and EP additives, which can build strong boundary layers to prevent damage generation from counter body asperities under severe stress conditions, organic friction modifiers consist of multi-molecular layers of tightly packed long-chain molecules. Polar heads are loosely bound to the metal surface, whereas the long carbon chains are directed towards the counter surface. Films of AW/EP-additives are designed to prevent metal-to-metal contact by chemical bonding and formation of strong films, by formation of monolayers films for reduction of local shear stresses or by general support of hydrodynamic films. While these additives usually contribute little to reduce overall friction and shearing off of strongly bound layers commonly comes with moderate to high friction coefficients, organic friction modifiers tend to be more loosely bound. Therefore, shearing off is performed more easily and lower coefficients of friction are achieved.

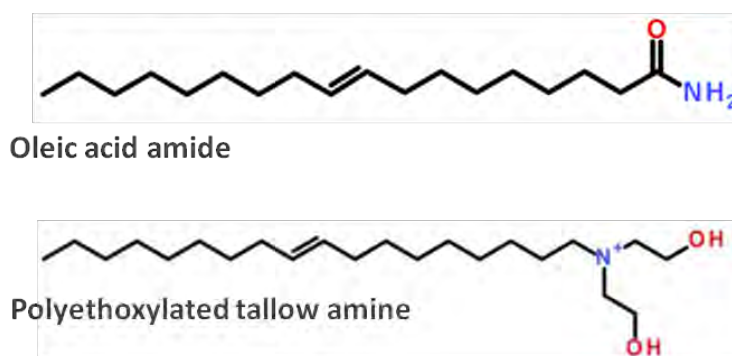


Figure 2-1: Chemical structure of frequently used organic friction modifiers (Widder, 2015).

In general, OFM molecules consist of long hydrocarbon chains and a polar head group. Their structure can derive from various origins, such as carboxylic acids, amines / amides / imides, phosphoric / phosphonic acids, organic polymers and many of their derivatives. Mechanisms of friction reduction can vary depending on the molecular structure. The polarity of the head groups leads to absorption of the molecules onto the surface. Oxidized or hydroxylated metal surfaces apply strong absorption forces on the OFMs. Polar heads

are bound to the metal surface. The tails of the friction modifier persist of long hydrocarbon chains, which are attracted to the apolar lubricant. The structure of two common organic friction modifiers oleic acid amid (oleylamide) and an example of polyethoxylated tallow amines is given in Figure 2-1. These additives have also been used within the scope of the scientific work for this thesis.

Hydrogen bonding and dipole-dipole interaction lead to parallel orientation of the head groups, while van-der-Waal forces yield aligned hydrocarbon chains. This means head groups of two layers are attracted to each other and terminal methyl groups of the hydrocarbon tails absorb apolar methyl groups of a next additive layer. Subsequent layers of friction modifier additive molecules will align in a regular, homogeneously distributed and perpendicular way and form multilayer matrices of FM molecules between the metal surface and the lubricant.

The main purpose of friction modifiers is reduction of the coefficient of friction. This is achieved by easy shearing of the individual FM layers due to low energy bonding of the van-der-Waals forces of the hydrocarbon chain interactions (see Figure 2-2). Realignment of the molecules after disturbance of the structure and shearing off is a fast process due to high attraction forces within one molecule monolayer. Reaction layers of organic friction modifiers derive from chemical bonding of additive molecules to the metal surface, usually under moderate loading conditions. Therefore, a relatively high chemical activity is required for proper surface bonding.

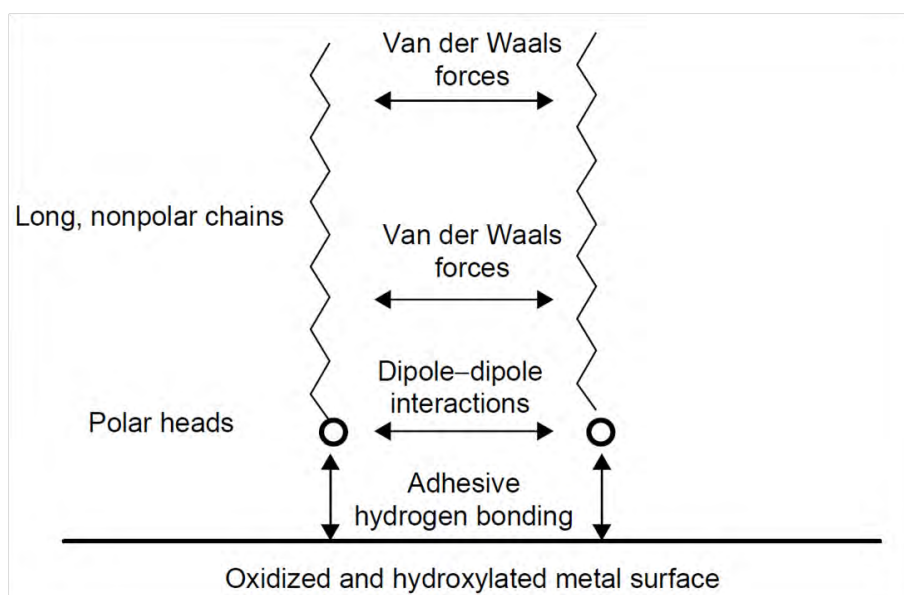


Figure 2-2: Formation of adsorbed layers of friction modifiers (Kenbeck, 2009).

Several main parameters have significant influence on the layer build-up and the performance efficiency of adsorbed layers of organic friction modifiers. The polarity of the head group (for dipole-dipole-interactions) combined with the possibility of hydrogen bonding play a major role in development of the layer structure. Additionally, the chain length influences the layer thickness as well as the interlayer attraction forces. The structure of molecules and the hydrocarbon chains also influences the close packing efficiency, therefore, molecules with tighter structure yield stronger films and increased attraction between neighboring chains. FM additives usually adsorb to the metal surfaces at lower temperatures as for example AW additives (higher temperatures needed for chemical reactions). Therefore, increased temperature can influence the thickness and toughness through adsorption/desorption phenomena since desorption of FM molecules can be promoted for increased input levels of thermal energy. Additionally, the presence of other additives competing for adsorption onto the metal surface as well as possible contaminants in the lubricant influences friction reducing properties. Also, the chemical structure of the metal alloy and the affinity of FM molecules as well as the concentration of the additive in the lubricant play a substantial role for friction reduction of the affected tribological system. (Kenbeck, 2009).

3 Boundary lubricant tribofilms

3.1 General aspects of boundary lubricant films

Material instabilities and surface deteriorations in highly loaded systems, operating mainly in boundary or mixed lubrication regime generally occur due to high abrasive and adhesive stress. Lubricants with suitable friction lowering and wear preventing additives are applied in order to avoid complications and reduce detrimental wear appearances. Chemical and physical reactions in the contact zone lead to interaction and deposition of additive components onto the surface of the counter bodies. Subsequently, tribofilms are generated within the area of the contacting surfaces. They mainly derive from the lubrication additives and their reaction products and can have significant influence on friction and wear of the tribosystems (Stratmann, 2017). The initiation of tribofilm growth can have several influencing factors, such as high stresses, additive concentration, temperatures and others.

These boundary lubrication films are based on the principle that additives contained in the lubricant can provide a sufficient interface layer to prevent direct contact of the counter bodies. Through complex chemical phenomena in the contact zone of the tribosystem the additives are consumed onto the material surface. Kapsa and Martin describe two kinds of tribochemical reaction films based on the chemical composition of the wear preventing additives (Kapsa, 1982). The first kind, tribochemical reaction films, are compiled of all films that are based on reactions with the friction surface and also rely on environmental conditions. These tribolayers are in dynamic equilibrium with film formation through reactions of the material substrate and the additives contained in the lubricant as well as the removal through mechanical forces effective in the relative motion of the friction partners. The second kind of tribochemical reaction films is described as polymerization processes that yield higher molecular weight substances, mainly independent of the

substrate material properties, as proposed by Hermance and Egan in 1958 (Hermance, 1958).

Organic tribofilms have been studied extensively over the years in regard of their chemical composition, their physical properties and the reaction mechanisms (Kapsa, 1982). Generally, these layers of reaction products are merely micrometer sized particles of substrate material and oxides in combination with high molecular weight organometallic reaction products. They can contribute to the friction conditions in several ways such as to be sacrificial layers, low shear or shear resistant layers, to act as solid particles or to vary the frictional behavior of the system. The basis for the friction varying mechanism is the generation of an ordered substructure of weakly bonded additive molecules at the counter body surface where interaction during relative motion takes place (Hsu, 2005).

One of the most commonly studied tribofilms of organic additives are from the family of zinc dialkyldithiophosphates (ZDDPs) anti-wear additives. These tribofilms have been the subject of extensive research over the last decades. Much effort has been put into the elucidation of reaction kinetics, film structure and behavior as well as film forming mechanisms of ZDDP tribofilms (Morina, 2007-a; Barnes, 2001; Nicholls, 2005; Spikes, 2004; Zhang, 2016).

But also organic reaction layers from friction modifier lubrication additives, which were used for scientific experiments herein, have been thoroughly investigated in recent years and will be discussed in more detail below (Morina, 2006; Morina, 2007-a; Grossiord, 1998; Martin, 2000; Morina, 2007-b; Spikes, 1993; Fox, 2004). To achieve optimal performance of tribosystems it is utterly important to reduce friction and wear in boundary lubrication contact situations. In this friction regime the chemical composition of the used additive conglomerate becomes much more effective than physical parameters of the base oil. In the boundary lubrication regime tribofilms formed on the surfaces help to protect the contact area from severe wear occurrences and also reduce friction values. Thus, it is of paramount importance to gain knowledge on the film forming mechanisms and their properties as well as the dynamic processes of formation and removal (Morina, 2007-b).

3.2 Film forming mechanisms and structure

In the following section a closer look will be taken at the film forming mechanisms and the resulting microstructure of boundary lubrication films derived from the use of organic friction modifier additives. There are also other classes of friction modifiers such as the organo-molybdenum compounds, functionalized polymers or recently developed nanoparticles, but focus will be placed on OFMs. In general, boundary lubrication occurs for low velocities and high loads. Wear and friction properties are influenced by layers of additives bound to the surface. Essentially, the three processes of physisorption, chemisorptions, and tribochemical reactions are the reason for additive layer build-up.

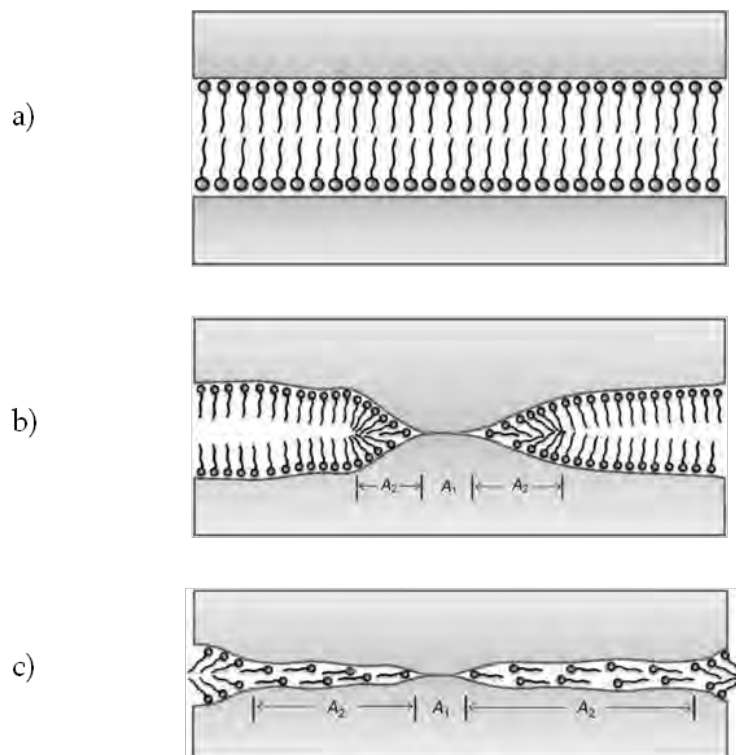


Figure 3-1: Schematic depiction of the boundary lubrication models of Hardy (a), Bowden (b) and Adamson (cf. Spikes, 1993; Zhang, 2015).

In physisorption the surface allocation depends on local temperature and additive concentrations. Adsorbed long-chain molecules such as friction modifiers with polar head groups and long apolar carbon chains tend to align in ordered structures on the substrate surface. Friction reduction also depends on the polar behavior of the material's surface. Metal surfaces with polar oxide layers support the formation of van-der-Waals bonds, whereas on some ceramics surfaces less or no adsorption occurs.

More stable bonds are created through chemisorption of molecules due to higher binding forces. Chemisorbed layers and reaction products can have properties that are significantly different from the starting material. Tribochemical reactions between lubricant additives and the metallic surface yield layers that are generally more stable than physisorbed or chemisorbed additive films under high mechanical and thermal stresses (Czichos, 2010). Tribochemical reaction layers very much depend on the adsorption properties of the lubricant additive as well as activation energies and reaction temperatures present in the contact area.

Mechanisms and structures of organic friction modifier additive films and layers have been subject of research for the last one hundred years. Boundary lubricant films are generated through physical or chemical processes during relative motion of the sliding partners and exhibit structures and properties that are distinguishable to the original lubricants and solid surfaces. In the early days of lubrication research the property of friction reduction was called 'oiliness' (Stanton, 1923). Already in the 1920s Hardy described the oiliness as a matter of adsorbed monolayers settled on the opposite sides of the sliding surfaces (Hardy, 1925). The chain length of the adsorbed molecules was shown to be crucial for the reduction of friction values, as long-chain friction modifiers proved to be more effective (Hardy, 1922). For excess amounts of additives the friction is not reduced more than monolayers would do, but the durability of the layer increases significantly, thus the ability to re-organize is a major property of effective friction reduction (Bowden, 1940). The structure of the additive films is almost vertically oriented due to the self-aligning

long non-polar chains (Bailey, 1955). For high pressures these monomolecular layers may also be compressed to flat boundary films (Adamson, 1967). In Figure 3-1 a comparison of the various models of the generation of boundary lubrication films of OFMs is given.

Already early investigations of boundary films deriving from additive containing lubricants lead to three-dimensional structures which could exhibit several molecule-layers of thickness (Hardy, 1931; Trillat, 1931). Additionally, stearic acid has shown to react with metal oxides on the surface to form thick films of chemically bonded soap-like ferrous stearates (Ratoi, 2000). Another very important property of friction modifiers is the ability to replenish adsorbed layers during sliding operations, as they are ablated and worn away.

In 2015 Spikes impeccably outlined the current state of the general knowledge about organic friction modifier boundary layers and structures as follows:

“The classical mechanism proposed to explain the friction-reducing properties of OFMs is that their amphiphilic molecules self-assemble on polar solid surfaces to form vertically oriented, close-packed mono-layers. These reduce friction since there is easy slip between the resultant, opposing methyl end groups. The films are strong and able to withstand high applied pressure because of cumulative van der Waals forces between the methylene groups on the closely packed alkyl chains. The polar group serves to locate the molecules of the solid surfaces, and its bonding can be reversible or, especially with carboxylic acids, involve soap formation and is thus irreversible.” (Spikes, 2015)

The property of friction reduction is attributed to three main mechanisms that are based on monolayer adsorption, viscosity modification in the range of several molecular layers, as well as the generation of viscous or sticky layers (Spikes, 1993). Despite vast research in the field of OFMs still some questions about the actual layer structure in the tribocontact, or the solvent composition during generation of tribolayers remain. Additionally, the film formation using OFMs that contain unsaturated carbohydrate chains, as well as whether

the actual friction reduction property derives from the starting material or foremost from reaction products are still subjects or recent investigations (Spikes, 2015).

The generation and analysis of tribofilms was subject of detailed investigations since the 1950's (Davey, 1950; Furey, 1959; Russel, 1965; Allen, 1969; Drauglis, 1970). One single additive of very high interest is zinc dialkyldithiophosphate (ZDDP). It is an often used anti-wear and extreme-pressure additive which has been applied for several decades. The structure of the molecules can vary and therefore influence the performance during operation. The tribofilm structure and mechanisms of ZDDP film formation are based on deposition and formation of sulfides, phosphate and oxides on the surface and have been comprehensively investigated in multiple publications (de Barros-Bouchet, 2005; Fujita, 2004; Morina, 2006).

Originally, tribofilms on steel were of main interest (Sakurei, 1962; Fein, 1965), whereas in recent years the number of investigations in the field of tribofilm characterization on diamond-like carbon (DLC) surfaces has increased significantly (Topolovec-Miklozic, 2008; Kubo, 2008). In general, research in the field of tribofilms has increased significantly over the last decades (Percipio.com, 2019), as can be seen in Figure 3-2.

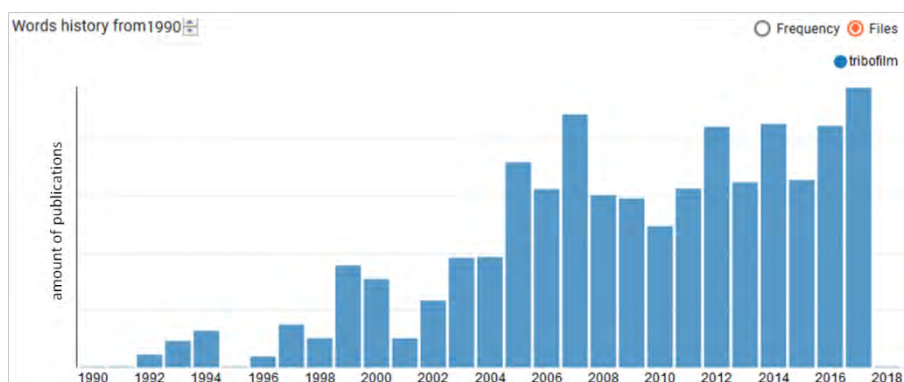


Figure 3-2: Publications history using “tribofilm” as search term (Percipio, 2018).

3.3 Boundary tribofilm characterization

For general tribofilm characterization many different analysis techniques have been applied. SEM and EDX analysis can be carried out for characterization of chemical composition. Additional to the topographic information of the SEM analysis, EDX-spectra yield facts about the elemental composition and can allow conclusions about the residues from applied lubricants and additivation, or surface modifications. Additionally, the use of the XPS analysis method is very common to characterize additive layers from tribocontacts (Yamaguchi, 1998; Gabler, 2014; Sharma, 2015).

Typically, the analysis of the X-ray absorption near-edge structure (XANES) is applied for information on the chemical environment. XANES measurements do not cause significant damage induced through the irradiation of the sample surface. Therefore, on the same surfaces analysis using other methods (for example XPS) can be executed (de Barros, 2003). The high resolution of XANES allows for characterization of the chemical nature of the developed tribolayers (Yin, 1997; Yu, 2007). Expecially ToF-SIMS investigations can lead to information of the molecular structure of boundary tribofilms from the lubricated surfaces (Minfray, 2004; Kubo, 2006). Additionally, other characterization methods such as Raman-spectroscopy (Joly-Pottuz, 2005), TEM (Evans, 2005), EELS (Varlof, 1999), EX-AFS (Martin, 2005) have been applied occasionally on boundary tribofilms and additive reaction layers from tribocontacts.

Only recently, based on findings of the scientific work carried out in the process of this thesis, LDI has been applied to analyze tribolayers and boundary lubricant tribofilms of ionic liquids (Gabler, 2012; Repka, 2017).

Tribofilms and boundary layers of organic friction modifiers have been studied since the early 1920's. The main investigation methods in the early days were based on adsorption analysis solution concentration measurements (Daniel, 1951), radiotracer (Gaines, 1960) or contact potential methods were used (Haydon, 1963). Later on analytical techniques

such as infrared (IR) and x-ray fluorescence (XRF) spectroscopy followed by X-ray photoelectron spectroscopy (XPS), Auger electron spectroscopy (AES), as well as secondary-ion mass spectrometry (SIMS) become readily available and were applied for in-depth and comprehensive investigations of boundary films of anti-wear and extreme-pressure additives. Usually, boundary films of OFMs were too thin for this kind of analysis, therefore microcalorimetry was applied for adsorption measurements (Groszek, 1970). In the last few decades much more advances were achieved with the development and application of the force balance apparatus (Isrealachvili, 1981), scanning tunneling (Smith, 1989) and atomic force microscopy (Campen, 2015), ultrathin film interferometry (Johnston, 1991), in-track ellipsometry (Çavdar, 1991), in-contact visualization (Sheasby, 1991) and film freezing techniques (Bell, 1990). Recent developments for investigations of OFM tribolayers additionally include the surface force apparatus (SFA) (Georges, 1994), quartz crystal microbalance (Lundgren, 2006), neutron reflectometry (Hirayama, 2012), as well as surface-specific spectroscopic methods such as IR (Allara, 1985), second harmonic generation (Marucci, 2002), and structure-property relationships combined with sum frequency generation spectroscopy (Koshima, 2010).

4 Tribotesting

4.1 Tribological testing technology

For surfaces in sliding or rolling motion, the real contact area is significantly less than expected from the nominal contact area. Only a relatively small amount of local asperities perform real contact between the two counter bodies. All macroscopic friction and wear results derive from these asperity contacts. Locally high pressures and stress as well as high flash temperatures may appear and cause local plastic deformation of the material. For these small locally concentrated contact points the mechanical properties of the materials can vary substantially from bulk values. Additionally, also influences from small amounts of oxide layers, contaminations, or phase transformations can increase significantly. Therefore, tested properties can vary from measured parameters of macroscopic material testing and correlations of wear and friction to physical material parameters can be vague and unconstrained (Axén, 2000).

The entire field of measurement and test engineering for tribological challenges can in short also be summoned as tribometry. It reaches from laboratory model tests using simple sample geometries to investigations of technical system under real operating conditions. The broad scope of activities in tribometry can be subdivided into several specific aspects (Czichos, 2010). One goal is the determination of wear-related influences on the overall function of tribological systems as well as the monitoring of the wear-dependent operational capability and the constant diagnosis of operating conditions.

On the other hand, a main objective is general wear research and mechanism-oriented wear testing for the optimization of components or tribotechnical systems to achieve a given wear-related service life including the preselection of materials and lubricants for practical application. Very important are the quality control of used materials and lubri-

cants and the collection of data sets for optimization of maintenance routines. Considering these aspects as well as function and structure of tribological systems and components tribotechnical testing technology can roughly be categorized into six different categories (Heinke, 1975; Uetz, 1979; Zum Gahr, 1987; Axén, 2000).

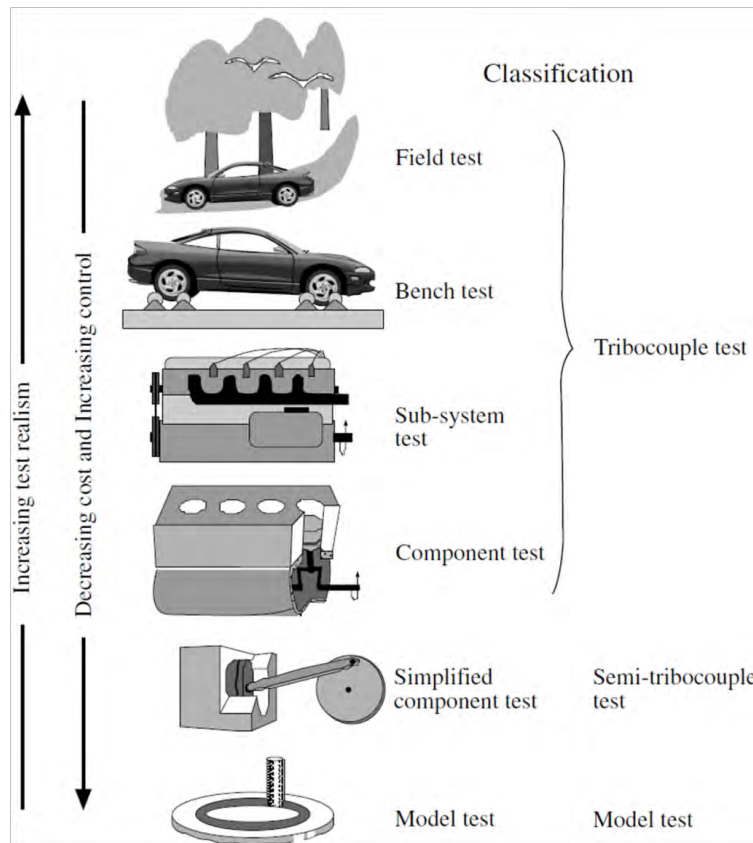


Figure 4-1: Classification of tribotests, as shown in (Axén, 2000).

In general, testing conditions and operating parameters will become increasingly more realistic going from model tests towards real field tests (cf. Figure 4-1). On the contrary, the monetary expenses will significantly increase, whereas the entire tribological system tested becomes less controllable as more and more components and surroundings interact and have possible effects on testing results. In laboratory model tests with more simple test geometries the main influences are substantially easier to control. Furthermore, tests will be more reproducible. Lower costs and less testing time as well as a better accessible tribocontact are additional parameters of model testing in lab surroundings.

4.2 Planning and evaluation

Due to the numerous influencing factors to be considered in tribological tests, careful planning and evaluation of tribological investigations is required. Commonly, in the conventional approach of laboratory testing, a particular tribological measure as a function of an independent variable is selected from the general influence factors test duration (i), a stress parameter, such as normal force or pressure (ii) and a parameter of the system structure, for example hardness (iii) (Czichos, 2010). All other parameters and conditions are kept constant in laboratory testing. Thus, a dependence of detrimental effects of certain factors can be evaluated. Through series of testing and variation of independent variables, the specific influence of several parameters can be elucidated. Very important is the number of tests carried out. Only a sufficient amount of results yields significant relevance and validity (Mücke, 1980; John, 1998).

In general, it is advisable to evaluate the measurement uncertainty of the test results for coincidental or systematic deviations of certain values (Czichos, 2010). Additionally, the precision and accuracy of the measurements is a key factor as well as the determination of relevant limits for material parameters. Moreover, a system for quality management of the test procedures and systems as well as regular reference measurements need to be taken into consideration.

4.3 Tribological laboratory testing

The main objectives of tribological laboratory testing technology are the investigation of friction and wear processes, the mechanism-oriented wear test as well as the evaluation and pre-selection of materials and lubricants for practical applications. To carry out tribological laboratory tests, various kinds of tribometers have been developed. These measuring and testing devices usually are applied for geometrically simple test specimens, which

are based on the basic forms of technical contact geometries and effective surface configurations. The tribological stresses in each of the various systems are vastly different and must be precisely analyzed and taken into account with respect to contact geometry (point, line, area), contact mechanics, kinematics and the friction-induced thermal processes (Czichos, 2010).

4.4 SRV-tribometer

In this work the technique of a SRV-tribotesting device was utilized and an overview will be given to describe this method representatively as one type of tribological laboratory testing systems. The SRV-device was only used herein to generate tribolayers of additives and reaction/degradation products containing in the lubricant. Therefore, the detailed description of friction and wear data evaluation will not be considered herein.

The SRV[®] tribometer (German for „Schwing-Reib-Verschleiß“ – oscillating friction wear, Optimol Instruments Prüftechnik GmbH: DIN 51834-1, 2010) is a high frequency oscillation test device. It has a multifunctional modular design, which enables the determination of friction and wear behavior of lubricants and sample specimens. Commonly, it is used for dynamic mechanical testing in lubricated mixed friction conditions. Its design with optional selection of the tribocontact kinetics is able to perform tribological test in close to real conditions (Rigo, 2014).

Generally, the SRV tribometer can determine friction and wear parameters of the surface interactions of two counter bodies/specimens and an intermediate lubricant. Additionally, also the wear loss volume, or electrical resistances could be measured. An interchangeable sample holder for various shapes of the counter body is applied. Common shapes include balls or cylinders, as well as ring designs. Possible counter body sliding directions include translation and oscillation motion as well as rotary movements. A general overview of

most common test modifications is given in Figure 4-2. The pressure load and rotary or linear movements, the frequency, stroke lengths, or testing temperatures and the testing duration can be set up individually for each test.

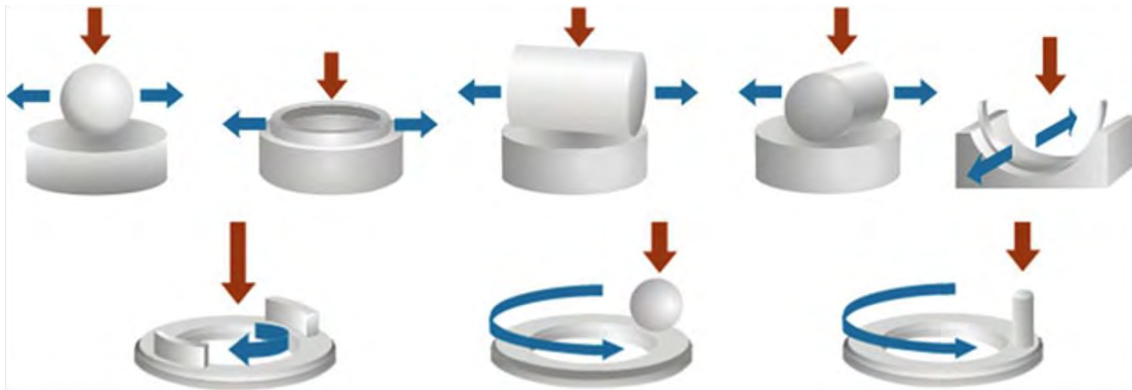


Figure 4-2: Overview on specimen types and SRV-test modifications (Rigo, 2014).

The assembly of all relevant components is set into one testing chamber and the main components are depicted in Figure 4-3. This machine frame can also be flooded with different gases or humidity to vary defined atmospheric conditions. The basic sample is commonly a standard SRV-disc and is mounted at the bottom. The normal force is applied through the top counter sample holder. The top sample holder is powered by the adjacent power trains on both sides, which define the kind of relative movement in the applied testing setup.

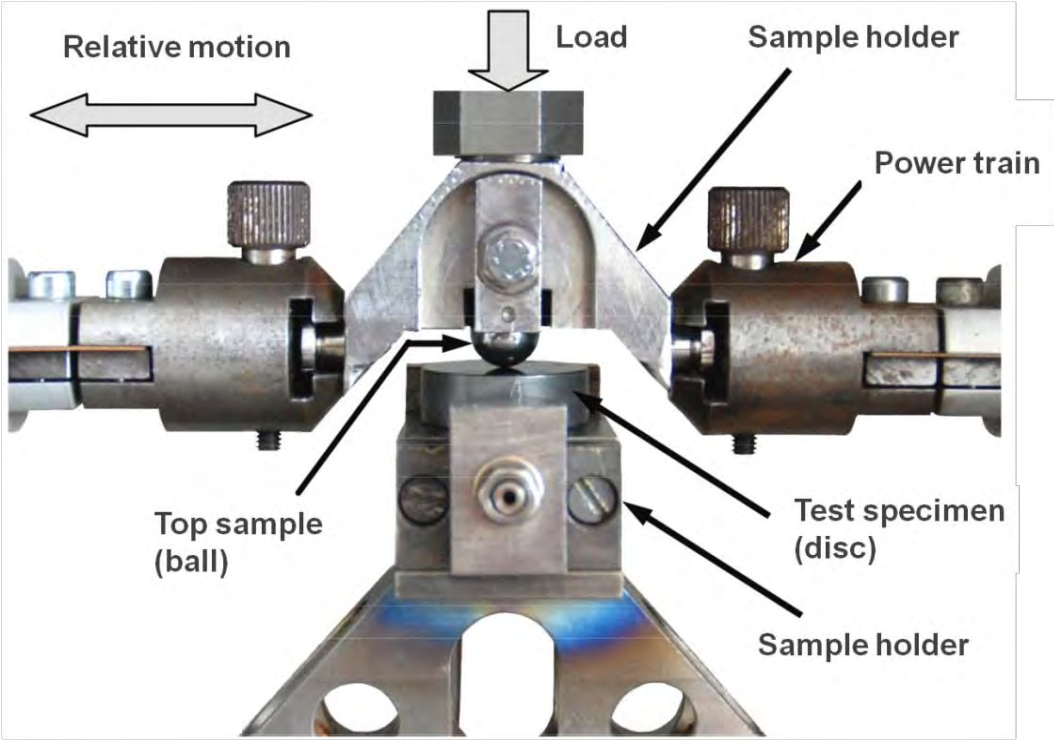


Figure 4-3: General view of a SRV-test setup (cf. Durst, 2008).

5 Mass spectrometry

5.1 General principle

The main characteristics and properties of the method of mass spectrometry make it a powerful analytical tool. This technique can be used to qualitatively identify and quantify target sample molecules and also to elucidate the chemical structure and properties of probed substances. Its low detection limits, extreme sensitivity and the speed of data generation made it a very widely used analysis method and a key technique in the scientific field of chemical analysis. It is superior to other chemical analysis methods due to the features of its high sensitivity and selectivity, the possibility to obtain compound masses and formulas and especially the possibility of the couple the mass spectrometry device with chromatography instruments for substance separation (de Hoffmann, 2007; Premierbio-soft, 2019).

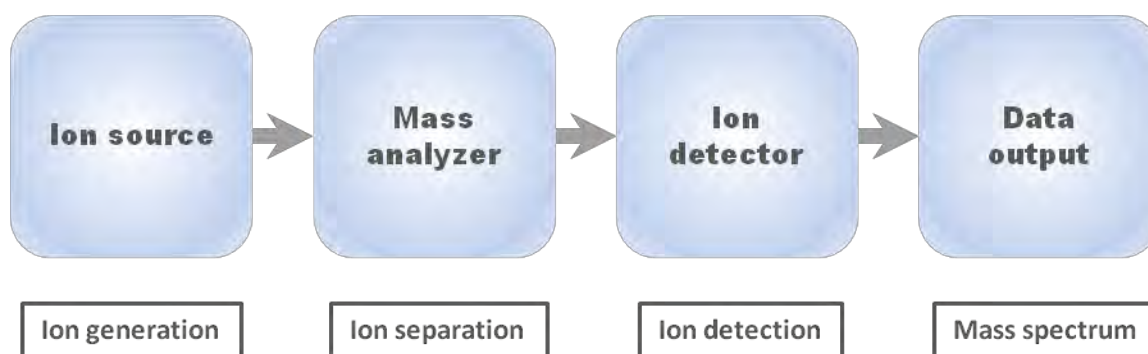


Figure 5-1: Principle assembly of a mass spectrometry system.

In the first step of the mass spectrometry process charged gaseous ions are generated from analyte molecules from the sample target under investigation and transferred into the vacuum of the mass spectrometer device. The generated molecular ions are then separated and analyzed using their specific mass to charge ratio (m/z) and the relative proportion of

the abundance (ion count) of each ion species. Additional structural information can be derived from fragmentation of the molecular mother ions and subsequent analysis of fragment ions (Premierbiosoft, 2019). Each molecular ion and their primary product ions can be fragmented and thus, after separation of the ions the structure of the precursor molecule can be derived.

In Figure 5-1 the general components of a mass spectrometer are given. The major components of the instrument are the ion source, the mass analyzer and the detector. For each system a variety of techniques are available. Several ion sources for the production of gaseous molecular ions from the sample substance such as electrospray ionization (ESI), (atmospheric pressure-) matrix-assisted laser desorption/ionization ((AP-) MALDI) and many others. In the analyzer device the ions and fragments are separated into their characteristic mass components according to their mass-to-charge ratio. Multiple techniques such as quadrupole, ion trap, Orbitrap, or time-of-flight (ToF) analyzers are available for a wide variety of applications. Detection systems record the relative abundance for each single ionic species resolved in the analyzer devices and become converted into electrical signals.

5.2 Mean free ion path

One main criterion for good mass resolution is the mean free ion path of the ionized analyte molecules since mass spectrometers are based on mass detection under vacuum conditions. Low pressure atmospheres are necessary for ions to travel to the mass analyzer without contacting other surrounding gas-phase molecules. A schematic image of the molecule random-walk process in the gas phase during continuous collision events is given in Figure 5-2. One problem would be the deviation of the tractor after and subsequent collisions with the instrument's inner walls and loss of the charged state. In addition, reactions or fragmentations of analyte ions after unwanted collisions with gas-phase molecules

could further reduce the ion yield and make peak detection in the mass spectrum more complex (Gross, 2012). Nevertheless, controlled collisions are a useful instrument for analysis of unknown molecule structures. The mean free path L (de Hoffmann, 2007) of molecules in gaseous atmospheres is given by the formula

$$L = \frac{k \cdot T}{\sqrt{2} \cdot p \cdot \sigma} \quad (\text{Eq. 5.1})$$

L	=	mean free path
k	=	Boltzmann constant
T	=	Temperature
p	=	pressure
σ	=	effective collision cross-sectional area

Efficient pumping devices such as mechanical pumps in combination with turbomolecular and diffusion pumps control and regulate the pressures within the mass spectrometer. Commonly the mean free path of ions inside should be around 1 m but for the generation of fragments under controlled collision the mean free path must be reduced to around 0.1 mm.

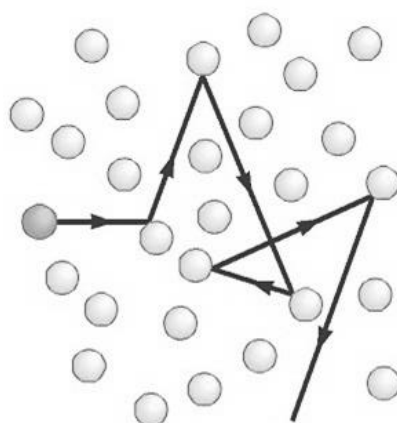


Figure 5-2: Schematic of molecule random-walk process and collisions in gas phase, showing several free molecule paths followed by consecutive collision events.

As the analyte molecules need to be introduced into the vacuum of the mass spectrometer the vacuum itself needs to be unchanged. Usually, the ionization chamber as the source for gas-phase ions is held under vacuum conditions. The samples can be inserted through a vacuum interlock. For *atmospheric pressure ionization* sources samples are kept at atmospheric pressure and only ionized molecules are lead into the vacuum system through interlock systems.

5.3 Ion Sources

A vast variety of different ionization techniques are available on the market and are used in mass spectrometry. In general, the ion source ionizes the analyte molecules from the targeted sample for subsequent analysis in the mass spectrometer instrument. Important considerations have to be made about the energy transfer onto the analyte molecules during the process of ionization. Also, the physical and chemical properties of the target molecules can have major influence on the overall ionization behavior. More energetic ionization techniques lead to increased amounts of fragmented ions. Other methods use softer energy transfer and are able to mainly generate molecular ion species of the intact analyte molecules. Some ionization methods are only suitable for gas-phase ionization, such as electron, chemical or field ionization. Their application is limited to thermally stable and volatile substances. Many other compounds are less stable at higher temperatures or are non-volatile, i.e. don't have enough vapor pressure to escape to the gas-phase. Thus, these molecules are transferred from the condensed (liquid or solid) phase to the gas-phase prior to the ionization process (de Hoffmann, 2007; Gross, 2012).

These type of ion sources can be divided into two groups of mechanisms, a liquid-phase and a solid-state ion source. In liquid-phase ion sources the analyte molecules are dissolved in solutions. The solution will be finely dispersed into small droplets and at atmos-

pheric pressure molecular ions are produced in the ion source. Examples thereof can be electrospray ionization, chemical ionization and photoionization mechanisms. For solid state ion sources the analyte sample is prepared into a solid deposit. After irradiation by means of highly energetic particle or photon beams the analyte molecules become ionized and desorb from the solid into an extraction field. This type of ionization sources are for example MALI (matrix-assisted laser desorption ionization), SIMS (secondary ion mass spectrometry), plasma desorption and field desorption techniques. General ion formation reaction into the gas phase include protonation, deprotonation, adduct formation, electron capture and ejection, or transfer of charged particles into the gas phase. An overview of ion sources used within the frame of this work (MALDI, Secondary ion mass spectrometry, Electrospray) is found in sections 6, 7 and 8.

5.4 Mass analyzers

For the determination of the mass of the ionized analyte ions mass analyzers are used. The gas-phase ions are separated according to their m/z ratio. Different separation principles are used since also a great variety of ion sources exist. An overview of different mass analyzers including their separation principles is given in Table 5-1. In general, static and dynamic magnetic or electric fields are applied to reach ion separation, whereas the difference of mass analyzers lies in the application of the fields onto the passing molecular ions. Depending on the separation technique mass analyzers either only single ion masses are transmitted through the analyzer or all ions simultaneously pass through. One way of categorizing mass analyzers is to observe the ion collection mode. One class will transmit ions with only specified m/z -ratio at a given time (scanning analyzers, e.g. quadrupole instruments), whereas others can allow simultaneous transmission on the entire bulk of ion molecules (e.g. ToF, ion trap, cyclootron, Orbitrap). Other categorization by means of mass analyzers properties can include ion beam/ion trapping, continuous/pulsed, low/high

kinetic energy. The Orbitrap mass analyzer is a relatively new type of analyzer with performance of high masses and resolution similar to Fourier transform ion cyclotron resonance (FT-ICR) mass analyzers, but with smaller dimensions and lesser complex settings and costs.

Type of analyzer	Principle of separation
Electric sector	Kinetic energy
Magnetic sector	Momentum
Quadrupole	<i>trajectory stability</i>
Ion trap	Resonance frequency
Time-of-flight	Velocity (Flight time)
Ion cyclotron resonance	Resonance frequency
Orbitrap	Resonance frequency

Table 5-1: Various types of mass analyzers used in mass spectrometry (de Hoffmann, 2007).

The main parameters (de Hoffmann, 2007) for characterization of a mass analyzer device and its output are commonly the limit of the mass range (1), the speed for ion analysis (2), the transmission (3), and of course the mass accuracy (4) and the mass resolution (5).

1) Mass range limit

The mass range defines the upper and lower limits within which the mass analyzer can determine the m/z -ratio of analyte ions in atomic units u. Small molecules exhibit lower mass up to around 1000 u, whereas polymers and biomolecules can show molecular masses of several order of magnitudes higher.

2) Speed of ion analysis

The speed of ion analysis determines the time period through which a specified mass range is scanned. The scan speed shows how quickly the mass analyzer can measure a given mass range.

3) Transmission

Not all particles entering the mass spectrometer device pass through the mass analyzer to reach the detector. Ions are lost as they hit the instrument's wall and become uncharged. The transmission factor is the ratio of the amount of ions which pass entirely through the mass analyzer to reach the detector and the amount of incoming ions at the front of the mass analyzer.

4) Mass accuracy

The mass accuracy of a mass analyzer determines how well the actually measured m/z -values fit the theoretical m/z -values of the analyte ion. This factor indicates the difference of the mass-to-charge ratios. In general, it is expressed in parts per million (ppm). High mass accuracy is essential for tasks such as identification of elemental composition. It is also strongly connected to the stability and the resolution of an instrument.

5) Mass resolution

The mass resolution in mass spectrometry is the ability to distinguish two distinct signals of incoming ions with only minor difference in m/z -ratio in such way, that two separate peaks appear. For ions with small m/z difference a mass analyzer with high resolving power can yield two distinguishable signals. For two peaks the resolution is based on the height of the valley between the two signals. The peaks can be considered separated (resolved) when the valley has 10 % (for FT-ICR, Orbitrap) or 50 % (quadrupoles, time-of-flight, ion trap) of the intensity of the small-

er peak. For two peaks with masses m and $m + \Delta m$ the resolving power R is defined as $R = m / \Delta m$. Thus, high mass resolution allows for distinct separation of ions with small mass differences.

For single peaks the resolving power also defined in a similar way. It is described by the peak width Δm at a certain height x of the peak. Usually, the median height at $x = 50\%$ is used, leading to a definition of the peak resolution as full width at half maximum (FWHM). In general, resolving powers above around 10,000 (FWHM) are termed high resolution mass analyzer.

Subsequently, the mass analyzers used for the work within the scope of this publication will be discussed in more detail. These include the ion trap, the Orbitrap and time-of-flight analyzers.

5.4.1 Ion trap mass analyzers

In general, ion traps use oscillating electric fields to keep the ionized molecules contained in a specified location. By utilizing radio frequency (RF) fields of quadrupolar electrodes ions are trapped. Originally, the first ion traps were composed of a circular ring electrode with two ellipsoid caps applied on both sides. This set up would create a sort of three dimensional field. Therefore, they are called 3D-, quadrupole (QIT), or also Paul ion trap after their inventor (Paul, 1953; Paul, 1960).

Contrary, in linear ion traps (LIT) or 2D-ion trap mass analyzers the sample ions are trapped in a quadrupolar field in radial direction repelling the ions within the four rods, whereas an electric field at the end of the linear rods constrains them in the axial direction (Douglas, 2005). In Figure 5-3 an image of a linear ion trap is shown. In this work a linear ion trap system was used. Positive potentials are used for positive analyte ions and vice versa negative voltage for negative ions. Inside the linear trap ions cool down

through collision with inert gas. The ions travel back and forth along the z-axis between the confining electrodes. At the same time they oscillate according to the RF-potential applied at the linear rods. Ions are repelled from the voltage of the end electrodes towards the center. In this way, the ions can be trapped inside.

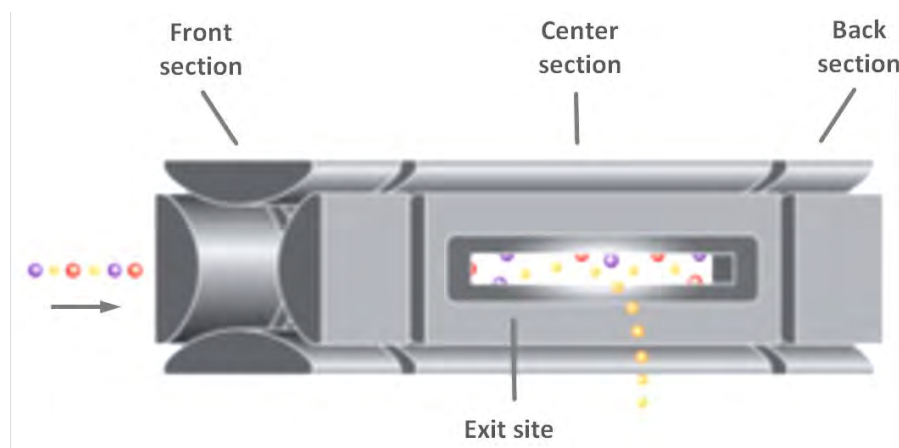


Figure 5-3: Schematic view of a linear ion trap (MS-Museum, 2019).

Compared to 3D-Paul ion traps a much lesser space charge effect is seen. This effect describes from repulsive forces of the ions when too many ion molecules are stored within the ion trap above the space charge limit. This repulsive charges cause excess ions to be ejected and can lead to poor performance in the mass detection. Additionally, the linear ion traps exhibit significantly higher ion trapping capacities of more than ten times of Paul traps. From the incoming ions more than 50 % can be stored within the LIT, whereas the trapping efficiency of 3D-traps with only around 5 % is substantially lower (de Hoffmann, 2007). These advantages can truly increase the mass analyzer's sensitivity and the mass range. By application of proper voltages ions can be ejected from the ion trap towards the detector selectively by their masses.

5.4.2 Orbitrap mass analyzer

Orbitrap mass analyzers make use of Fourier transformation to generate mass spectra out of incoming signals. Instead of using magnetic fields, the orbitrap is an electrostatic ion trap with quadrupole fields (Makarov, 1999; Makarov, 2000; Hu, 2005). The orbitrap is composed of three electrodes. The external electrodes consists of two cup-shaped parts including a small interstice. The central electrode is spindle-like formed. An image of the assembly of an Orbitrap is given in Figure 5-4. Together they produce the linear and radial electrical fields necessary for analysis of the ion mass. Some kilovolts are applied to the inner electrode, negative for positive target sample ions. Analyte ions are tangentially injected through the interval between the separated outer electrodes. Their tangential velocity force (several kiloelectronvolts of kinetic energy) them to oscillate in a spiral orbit motion around the inner electrode. The motion of the ions relies purely on electrostatic fields with quadro-logarithmic potential distribution originating in the DC voltage of the trap (de Hoffmann, 2007).

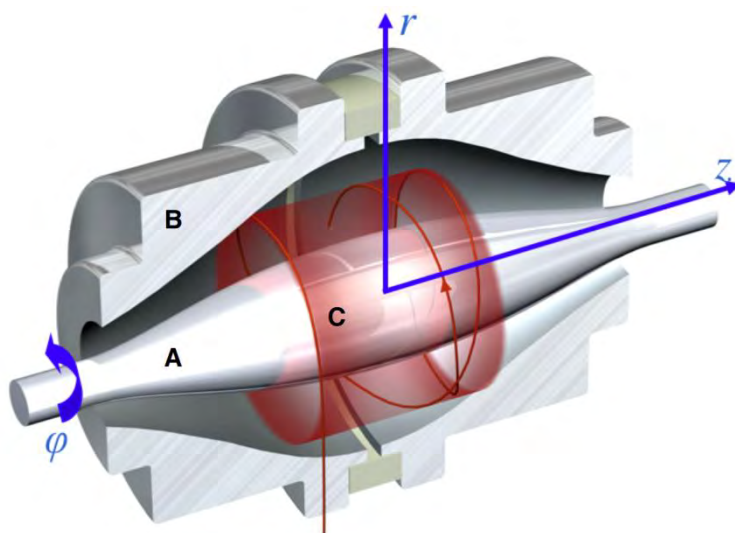


Figure 5-4: Model of an Orbitrap mass analyzer. Inner electrode (A); two outer electrodes, split by an insulating ceramic ring (B); orbital path of incoming ions (C). (Snow, 2014).

The frequency of the rotating ions is directly related to the m/z ratio, as can be seen in equation 5.2 (Makarov, 2000). Most importantly, this property is independent of any influence of the kinetic energy of the inserted analyte ions. The ions oscillating around the inner spindle-electrode induce a broadband current. This current is converted through Fourier transformation into specific intensities and frequencies for each individual m/z ratio, resulting in the final mass spectrum. Ions are injected one m/z at a time due to distance adjustment to the focus plane. This grouping of similar ions as well as the coherent axial transition leads to efficient mass resolution. Additionally, the slight temporal separation of ions with different masses, decreases space charge influences.

$$\omega_z = \sqrt{k \left(\frac{z}{m_i} \right)} \quad (\text{Eq. 5.2})$$

ω_z = frequency of axial oscillations

k = electric field curvature in Orbitrap

m_i/z = mass-to-charge ratio of ions

Compared to FT-ICR instruments the mass resolution of the orbitrap at low masses is significantly lower but decreases much slower towards higher masses. However, in relation to Q-TOF instruments the resolution as well as the dynamic range are substantially increased (Gross, 2012).

5.4.3 Time-of-Flight mass analyzers

Already in 1946 the basic principles of time-of-flight mass analysis were published (Stephens, 1946). The general design of this method is well adaptable to pulsed ionization methods like ion bombardments or laser desorption. When ions are extracted by the used ion source and accelerated towards the mass analyzer system using a certain electric po-

tential between the inlet and an opposing electrode, in time-of-flight designs a field-free flight tube acts as mass separator. Since all the ions bear the same kinetic energy, only the m/z -ratio determines the velocity and thus, the distribution in time-of-flight of the acquired ion bundles. ToF-instruments have high mass ranges and their high transmission efficiency allows for detection of very small amounts of analyte ions and high sensitivity (Mamyryn, 2001; de Hoffmann, 2007; Schlag, 2012).

Alas, a major disadvantage was the minor mass resolution, deriving from the ion pulse time distribution, the spatial distribution of the ion ablation, as well as the kinetic energy distributions of the ions. For correction of the energy dispersion two approaches have been applied for higher mass resolution. First, the delayed pulsed ion extraction (Wiley, 1955) allows for reduction of the kinetic energy deviations through concentration of equal m/z -ion bundles via a separate electric extraction pulse. Secondly, the use of “ion mirrors” is used to enhance mass resolution (Mamyryn, 1973). These mirrors, called reflectrons, are electrostatic reflectors, where the ions are attenuated in a deflecting field and forced into an additional flight channel. Again, ion bundles of same m/z ratios but slight energy distributions are more concentrated and hence, peak broadening is reduced (de Hoffmann, 2007; Gross, 2012). A more detailed description of time-of-flight mass analysis is given section 7.4, focused on the ToF-SIMS method.

6 MALDI

6.1 Introduction to MALDI mechanisms

The principles of matrix assisted laser desorption/ionization (MALDI) were introduced in 1988 by Hillenkamp and Karas (Karas, 1987; Karas, 1988; Hillenkamp, 1990). This method is based on the use of a so called matrix, which is essential for both desorption and ionization reactions of the analyte. Generally, the use of MALDI benefits from simple sample preparation and quite substantial tolerance for contaminations of the sample under investigation (Stump, 2002). Since its introduction MALDI has become commonly used source for gas-phase ions for many different scientific applications (de Hoffmann, 2007).

MALDI and ESI are two soft ionization techniques used in mass spectrometry which allow the detection of nonvolatile and labile compounds over a broad range of molecular mass. MALDI principles were discovered in 1984 when Karas and Hillenkamp used organic polymers to embed the tissue sections using laser micropulse mass analyzer (LAMMA) investigating large biomolecules. LAMMA reached submicron resolution of analytes in organic resin-based matrices via laser desorption but significant background of the organic resins was observed (Hillenkamp, 2013). Therefore, they investigated desorption behavior of amino acids with Nd:YAG laser observing simultaneous desorption of organic molecules (Karas, 1985). First, MALDI was limited to small organic molecules but soon the mass range was extended to larger peptides and proteins. MALDI-spectra of proteins with masses exceeding 10 kDa and 100 kDa were reported in 1988 (Karas, 1988; Tanaka, 1988). One large benefit of the MALDI-technique was the large sensitivity, which nowadays is down in the low attomole range.

6.2 Analyte molecule incorporation

The core of the MALDI technique is the use of an organic laser-absorbing matrix used in large excess compared to analyte quantities. The way in which matrix and analyte molecules interact is one important feature. Commonly the matrix is prepared as near-saturated 0.01-0.1 M solution and mixed with a $10^{-6} - 10^{-9}$ M solvent solution of the analyte. Matrices need to be soluble in the same solvent as the analyte. Important matrix properties for analyte incorporation are the ability to embed and isolate analyte molecules for example through co-crystallization. The solvent is then evaporated upon which the matrix crystallizes and forms crystals of up to a few hundred micrometers. The matrix homogeneously incorporates analyte molecules in its crystal structure. Morphology of the matrix crystallization is very much depending on the matrix, the solvent, the surface parameters and influence of sample treatment during preparation (Hillenkamp, 2013).

6.3 Laser absorption

Optical absorption of the laser radiation energy transfers the laser beam energy to the analyte sample and is regulated by Beer's law (Karas, 1985)

$$H = H_0 \cdot e^{-\alpha z} \quad (\text{Eq. 6.1})$$

H = laser fluence at depth z

H_0 = laser fluence at the surface

α = absorption coefficient

The absorption coefficient α is dependent on the wavelength-dependent molar absorption coefficient α_n of the matrix and the concentration c_n of absorbing matrix molecules. Highest molar absorption coefficients are provided by systems with aromatic electron structures. Therefore, matrix compounds commonly consist of phenyl or styryl derivatives supported by other electron-donating groups. The absorbed energy per unit volume E_{ab}/V (energy density)

$$\frac{E_a}{V} = \alpha \cdot H \quad (\text{Eq. 6.2})$$

$$\frac{E_a}{V} = \text{energy absorbed per unit volume}$$

$$H = \text{laser fluence}$$

$$\alpha = \text{absorption coefficient}$$

is the determining factor of the MALDI-process. Matrices with sufficiently high absorption coefficients α allow lower laser fluences H_0 to initialize ablation of embedded analyte molecules for ionization. The electronic excitation energy is converted into lattice energy and the vast amount of deposited energy leads to an explosive ablation reaction of the excited sample volume (Hillenkamp, 2013).

6.4 Desorption

Since the majority of the ablated material is removed in neutral state the ablation and ionization processes can be treated separately. The energy of the laser pulse onto the sample leads to the removal of a sample volume consisting of many monolayers of matrix and analyte molecules (Hillenkamp, 2013). The processes of material ablation and the ionization of a minor fraction of the matrix and analyte molecules occur on a geometric micro- and a time nano-scale. Some commonly used types of laser for MALDI experiments are given in Table 6-1.

Matrix molecules play a key role in releasing intact large analyte molecules into the gas phase. The matrix crystals disintegrate during irradiation with UV-laser light releasing cocrystallized analyte molecules into the gas phase. After laser irradiation the matrix undergoes rapid molecular dissociation, while high pressure at the surface creates supersonic expansion (Li, 2009).

Laser	Wavelength	Energy	Pulse width
<i>Nitrogen</i>	337 nm	3.68 eV	< 1 ns to a few ns
<i>Nd : YAG μ3</i>	355 nm	3.49 eV	5 ns
<i>Nd : YAG μ4</i>	266 nm	4.66 eV	5 ns
<i>Er : YAG</i>	2.94 μ m	0.42 eV	85 ns
<i>CO2</i>	10.6 μ m	0.12 eV	100 ns + 1 μ stail

Table 6-1: Frequently used laser types for MALDI experiments. (de Hoffmann, 2007)

The exact underlying mechanisms are currently still a matter of ongoing scientific investigations. Many different parameters can have influence on the desorption behavior of matrix and analyte molecules. Main focus lies in the role of irradiation parameters, as well as preparation and matrix parameters. For laser parameters this include for example the laser pulse duration, the laser wavelength and the laser energy per pulse and unit area (laser fluence). Important are also the different types of cocrystallization and incorporation of analyte molecules into the solidified matrix structure. Furthermore, kinetic energies and energy distributions of the expanding particle plume as well as the general composition of the initially ejected molecules and ions (Dreisewerd, 2003). For the plume important parameters are the ratio of ions to neutral material, along with desorption of particles and clusters compared to the discharge of molecules.

As mentioned above, the exact process and fine details of desorption and ablation is still under investigation. Yet, the main influences are accepted to be stress generation through thermoelastic waves, as well as the rapid heating process where very high pressures build up within the excited sample volume causing microcracks, entailed by ejection of large material particles and clusters, besides gaseous components (Hillenkamp, 2013).

6.5 Ionization

Two general processes are present for analyte ionization. MALDI ionization starts with matrix ionization followed by subsequent charge transfer to yield analyte ions with intensification in favor of the analyte molecules (Hillenkamp, 2013). More than two photons are needed for photoionization of the matrix molecules. Ionization energy is lowered for larger matrix aggregates. Since the majority of the absorbed energy is converted into lattice energy additional thermal energy is present to aid photoionization (Lüdermann, 2002). Photon fluxes of MALDI-lasers are too low for two-photon absorption, but since the excited energy is highly mobile in matrix aggregates with aromatic π -electrons two excitons (excited molecules) can interact electronically and yield matrix molecules with higher excited state (Setz, 2005).

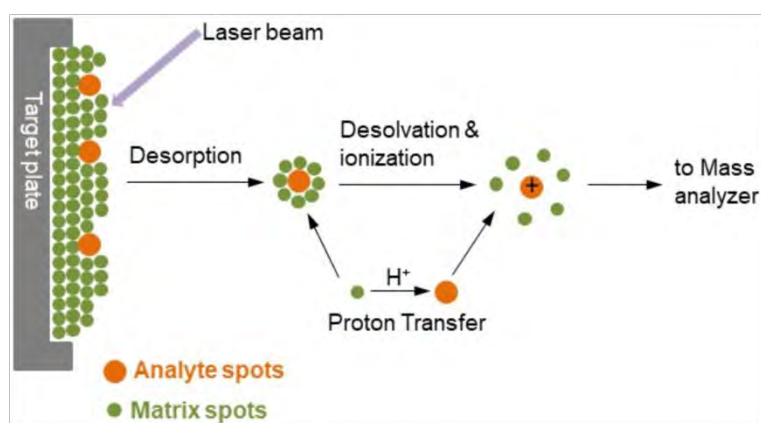


Figure 6-1: Schematic representation of the ionization process of analyte molecules in MALDI (cf. Proteomics, 2019).

A schematic of basic ionization processes is given in Figure 6-1. For analyte ionization two different models have been proposed (Hillenkamp, 2013): First, the *Coupled Physical and Chemical Dynamics (CPCD)* model, where neutral analyte molecules are protonated [analyte + H]⁺ and deprotonated [analyte - H]⁻ through charge transfer from matrix molecules after secondary intermolecular matrix reactions following their photoionization.

The second model is the “*lucky survivor*” model. Herein, as a first step analyte molecules are assumed to be precharged within the matrix crystals corresponding to charges in the

solution previous to matrix/analyte crystallization. As a second step, in the model the crystal lattice is broken up into clusters of various size. Statistically these analyte-containing clusters carry some excess protonated or deprotonated matrix ions. During cluster dissociation these excess charges can yield generation of protonated and deprotonated analyte ions, ‘surviving’ simultaneous neutralization processes. This model can well be applied to the formation of negative and positive ions from both, basic and acidic analytes.

Analyte type	Matrix	Abbreviation
Peptides/proteins	α -Cyano-4-hydroxycinnamic acid	CHCA
	2,5-Dihydroxybenzoic acid	DHB
	3,5-Dimethoxy-4-hydroxycinnamic acid	SA
Oligonucleotides	Trihydroxyacetophenone	THAP
	3-Hydroxypicolinic acid	HPA
Carbohydrates	2,5-Dihydroxybenzoic acid	DHB
	α -Cyano-4-hydroxycinnamic acid	CHCA
	Trihydroxyacetophenone	THAP
Synthetic polymers	Trans-3-indoleacrylic acid	IAA
	Dithranol	DIT
	2,5-Dihydroxybenzoic acid	DHB
Organic molecules	2,5-Dihydroxybenzoic acid	DHB
Inorganic molecules	<i>Trans</i> -2-(3-(4- <i>tert</i> -Butylphenyl)-2-methyl-2-propenylidene)malononitrile	DCTB
	Dithranol	DIT

Table 6-2: Frequently used matrix molecules for MALDI-experiments (Gabler, 2014).

6.6 Matrix selection

To analyze different classes of analyte molecules in AP-MALDI-MS various MALDI matrices have to be taken under consideration. No single matrix and preparation method is suitable for all analytical problems. Many different matrices are available for different classes of analytical problems and molecules to be investigated.

Most commonly used are the matrices CHCA (α -cyano-4-hydroxycinnamic acid) and DHB (2,5-dihydroxybenzoic acid, gentisic acid). CHCA is mainly used in a majority of proteomics applications for the analysis of peptide-mass-fingerprints as well as for fragmentation experiments in tandem mass spectrometry. DHBs solidify into large crystals and are mainly used for protein analysis. Additionally, a large variety of matrices is available and is being used for various MALDI analyses. Comprehensive lists of commonly used matrices and their main applications are already given in several references (cf. Li, 2009; Navare, 2010; Gross, 2012; Hillenkamp, 2013). A few frequently used matrices including mostly applied analyte molecule types are shown in Table 6-2.

The general demands on matrix requirements include the following important aspects of matrix selection, depending on the targeted analyte ions:

1. The ability to embed and isolate analyte molecules through co-crystallization.
2. These matrices need to be soluble in solvents that are compatible with the desired analytes and ensure stable analyte molecules.
3. Effectively absorb the applied laser wavelengths.
4. Co-desorption of the analyte molecules after laser irradiation and the promotion of analyte ionization.

6.7 Sample preparation

A standard method for sample preparation is the so called dried-droplet-method. In this simple method the analyte sample is dissolved in a solution of one or more miscible solvents and subsequently deposited onto the MALDI sample target. It is most widely used due to its simple and rapid processing. Typically sample volumes of matrix-analyte samples are around 1-2 μl . The droplet is then dried in air. Other variations use air flows or slightly reduced air pressure (Weinberger, 1993; Vorm, 1994) for improved homogeneity of the crystal structure. Crystal structures and size of the dried droplet can vary significantly due to preparation conditions like solvent evaporation rate, temperature, analyte concentrations and more. The analyte molecules are usually homogeneously distributed in the crystal structure. High polarity of sample solutions can lead to very inhomogeneous crystal distributions. Additionally, varying ionization states of analyte molecules or matrix-analyte interactions, as well as heterogeneous orientation of the matrix crystals or variations of crystal structures due to inhomogeneous analyte concentrations could also lead to possible 'sweet spots', i.e. certain positions of the crystallized sample droplet where best MALDI performance is achieved.

6.8 Surface Preparation

To enhance sensitivity predeposited matrix layers can be applied increasing homogeneity of crystallization. Also, mixtures of different matrices have been applied to soften the ablation process improving sensitivity for the analyte molecules. Additionally, sample plates with special designed surfaces can also influence the matrix crystallization process and improve analyte dispersion homogeneity. Hydrophobic surfaces can avoid draining of excess sample solutions and help concentrating the spotted sample (Jaskolla, 2009).

Furthermore, various other sample target plate materials and surface structures have been applied in for investigations of analyte sensitivity (Kassler, 2009; Pittenauer, 2011), as well as for offline monitoring of tribological experiments directly from tribometry sample surfaces (Gabler, 2012; Widder, 2015).

6.9 Atmospheric pressure-MALDI

Due to their soft ionization together with ESI, MALDI mass spectrometry is used as key technology in proteomics for peptides, proteins and larger biomolecules. They are used as complementary methods enabling a broad range of compounds to be analyzed. The ESI source is used to analyze liquid samples and ionization occurs under atmospheric pressure. To be coupled to mass analyzers vacuum gradient systems must be applied for ESI. Common MALDI experiments are carried out in vacuum. Its pulsed ionization mechanisms are well suited for time-of-flight mass spectrometers, which are the main analyzer technique used for MALDI.

The development of MALDI sources operating at intermediate and atmospheric pressure lead to interchangeable ion sources on the same mass spectrometer. AP-MALDI is performed outside the mass spectrometer at atmospheric pressure. The transport of ions into the mass analyzer can make use of the same pressure interface as ESI with the additional advantage of possible MS/MS fragmentation experiments.

6.9.1 Advantages

In general, the spectra of vacuum MALDI and AP-MALDI have similar features. However, AP-MALDI shows some significant advantages over the vacuum MALDI technique. First of all, AP-MALDI is a significantly softer ionization technique than traditional vacuum MALDI. This results in less fragmentation of analyte ions during the ionization pro-

cess. A possible reason could be the cooling through collisions of the ions with the background gas. Second, the AP-MALDI ion source is commonly interchangeable with an ESI ion source, which has the benefit of yielding complementary information with only considerable additional sample handling efforts (Navare, 2010).

Additionally, all sample targets and positioning devices are located outside of the vacuum chamber. This makes sample handling relatively simple in AP-MALDI and is especially convenient for high sample through-puts. One different beneficial aspect of AP-MALDI is the broad range of different matrices which are available. Since they do not have to be vacuum stable more substances are suitable for analysis in atmospheric pressure. Also liquid analytes can be investigated via AP-MALDI and pumping time for evacuation after sample and target changes can be omitted (de Hoffmann, 2007).

6.9.2 Disadvantages

The use of quadrupoles and octopoles for beam collimation into the mass spectrometer can limit the mass range. Furthermore, the transmission of the analyte ions through the capillary into the mass spectrometer significantly reduces the sensitivity of atmospheric pressure analysis, whereas ion production itself should yield similar amounts of ions as traditional vacuum MALDI systems.

7 ToF-SIMS

7.1 Introduction

Secondary ion mass spectrometry (SIMS) has been very important for high-resolution material analysis and characterization for several decades. Several key factors have made it a unique but widely available analytical technique. First, the possibility to measure all elements of the periodic system from H (atomic number 1) to U (92) along with isotopes and molecular species are very exclusive characteristics. Secondly, the SIMS measurement technique has extremely high sensitivity extending down to the ppm and ppb range. These outstanding properties paired along with very high surface resolution in the order of nm yield an exceptionally powerful method for material and surface analysis (Fearn, 2015).

One main improvement over the course of ToF-SIMS applications was the development of dual beam instruments. Here, dynamic SIMS for depth profiling of near surface and bulk regions using high ion beam currents and static SIMS used to produce complex mass spectra of surface layers were combined to merge both qualities in one instrument. For all of these reasons the SIMS-technique has been applied in a wide range of research areas and material characterization. This introduction to time-of-flight secondary ion mass spectrometry (ToF-SIMS) will be given in order to understand the main specific principles and its contribution to this work.

7.2 Principles and ion formation

7.2.1 General principle

The mass spectrometry technique of time-of-flight secondary ion mass spectrometry is used to analyze the chemical composition of samples in vacuum conditions. Secondary ions are sputtered from a target sample by the ion beam generated in the primary ion gun. For this purpose, the specimen's surface is bombarded by means of a beam of primary ions with energies between 0.1 and 20 keV. Subsequently, a large variety of sputtered particles are produced through the primary ion bombardment.

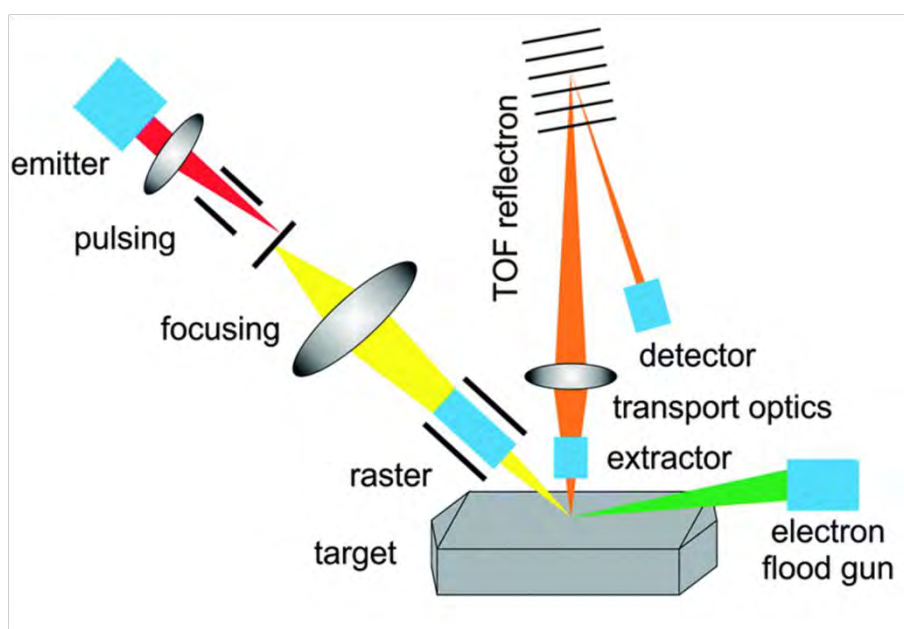


Figure 7-1: Schematic depiction of the functional principle of a ToF-SIMS instrument (Hofmann, 2014).

Electrons and photons are emitted along with respattered primary ions as well as mono-atomic and poly-atomic particles of the sample material. These secondary ions can be of positive, negative or neutral charge. The sputtered secondary ions are extracted into the flight tube via an extraction potential and electronically detected by means of a micro-channel plate. Through an inlet they are extracted into the mass spectrometer and become detected and analyzed. Depending on the system's mode of operation, various signal out-

puts can be obtained: mass spectral analysis, ion mapping, depth profiles and 3D-imaging. A schematic representation of the principal instrumental design of a ToF-SIMS instrument is given in Figure 7-1.

7.2.2 Basics of ToF-SIMS theory

In general, mass spectrometry is able to analyze ionized atomic or molecular sample analytes which are transported into the gas phase. In secondary ion mass spectrometry (SIMS), the mass-to-charge ratio (m/z) of secondary ions is measured. The secondary ions are generated by means of an ion beam bombardment of the probed target surface. Ionization, i.e. the formation of the secondary ions, occurs in the very close vicinity of the emission of the particles from the surface. The process of ionization itself is strongly influenced by surface parameters such as chemical composition or bonding conditions. The sputtering and ionization processes are complex events (Sigmund, 1969) and can in general be described by the basic SIMS-equation

$$I_s^x = I_p C_x S \gamma F \quad (\text{Eq. 7.1})$$

I_s^x = secondary ion current of species x

I_p = primary ion beam current

C_x = concentration of species x

S = sputter ion yield

γ = ionisation efficiency

F = transmission

Since the measured counts of secondary ions, I_s^x , are directly proportional to the concentration C_x of the investigated analyte species x, it is readily evident that quantification in SIMS should be a considerably simple task. However, as the chemical state of the emitting surface has a major influence on the measured signal of the secondary ions, which is also referred to as the matrix effect, quantification can be challenging for certain surface mate-

rials and conditions (Fearn, 2015). For many samples like complex biological systems or others with heterogeneous chemistry distributed over the surface this can be a handicap for valid quantification or the development of relevant analyte standards. For homogeneous matrices and surfaces, such as silicon-based samples or semiconductors in general, quantification can be readily carried out using implant standards, whereby a known amount of a certain element is implanted into the matrix material for depth profiling.

Other key parameters such as the sputter yield S and the ionization efficiency γ depend on several fundamental factors relating to the selection of ion beam parameters as well as to the properties of the target material. In general, the sputter yield S is the amount of removed target material during the course of ion bombardment. It is mainly influenced through the energy, the mass and the charge of the ion beam used. This means, ion beam bombardment by heavier ion species will lead to increased sputter yields, as the energy will be transmitted in areas closer to the target sample's top surface. The target material's elemental composition and properties significantly influence the sputter yield as well. For a given ion beam energy the resulting sputter yield can vary by a factor 3-5 (Laegreid, 1961).

For some target substrates such as covalent materials, it is important to minimize the damaged area as heavy ion bombardment will rapidly destroy the chemical structure. The damage cross section σ is defined as the mean area damaged by one single primary ion and is also related to the secondary ion intensity

$$I_m = I_{m0} e^{-\sigma I_p} \quad (\text{Eq. 7.2})$$

- I_m = recorded molecule signal
- I_{m0} = original surface density of species m
- I_p = primary ion beam current
- σ = disappearance cross-section

The damage cross section increases with the mass and energy of the primary ions, as well as the angle of incidence to the surface normal, as was shown by Galera et al. (Galera, 1991), similarly to the sputter yield S . The efficiency of the secondary ions E for the primary ion beam can therefore be described as

$$E = \frac{S}{\sigma} \quad (\text{Eq. 7.3})$$

E = secondary ion efficiency

S = Sputter yield

σ = disappearance cross-section

For increased analyte ion efficiencies E it is therefore essential to optimize the sputter yield S and reduce the damage cross section σ to minimal size. The use of cluster ions such as e.g. Au_3^+ , Bi_3^+ , Bi_2^+ or C_{60}^+ allows for a significant increase in ion yield. The change of the primary ion projectile to cluster species leads to energy distribution of the total energy of the ion beam within all atoms of the cluster upon impact. Thus, the way the cluster ion beam impacts the analyte surface leads to lower impact energies per atom and therefore less damage to the subjacent atomic structure of the sample. Hence, cluster ion beams lead to increased surface areas for surface molecules to be ejected and increased depth resolution through lower surface penetration of the cluster ion beam (Fearn, 2015).

The general tendency of a specific element or molecule to form secondary ions, either positive or negative, is dependent on the ionization energy and also the electron affinity of the measured ion species. For example, elements of the first main groups of the periodic table of the elements (alkaline metals, alkaline earth metals) have lower ionization energies (lower electron binding energies) and more readily form positive ions. Conversely, elements of the seventh main group (halogens) exhibit high electron affinities (higher electron binding energies) and more likely form negative ions.

7.3 Instrumentation

7.3.1 Ion generation

Many single processes occur during the formation of secondary ion. In a first step, the beam of primary ions is collimated and accelerated to establish the desired energy. The energy of the primary ion beam is then transferred through elastic and inelastic collisions with particles in the vicinity of the impacted surface area. As the ion beam is being rastered over the target surface the bombardment of primary ions can cause certain atoms or molecules to receive enough energy in a proper and relevant direction, as to overcome the surface binding energies. In this way these particles are sputtered away from the target surface and become the emitted secondary ions. An visualization of sputtering events is shown in Figure 7-2. A similar process of desorption ionization for ion generation is seen in other mass spectrometry techniques such as matrix-assisted laser desorption ionization (MALDI).

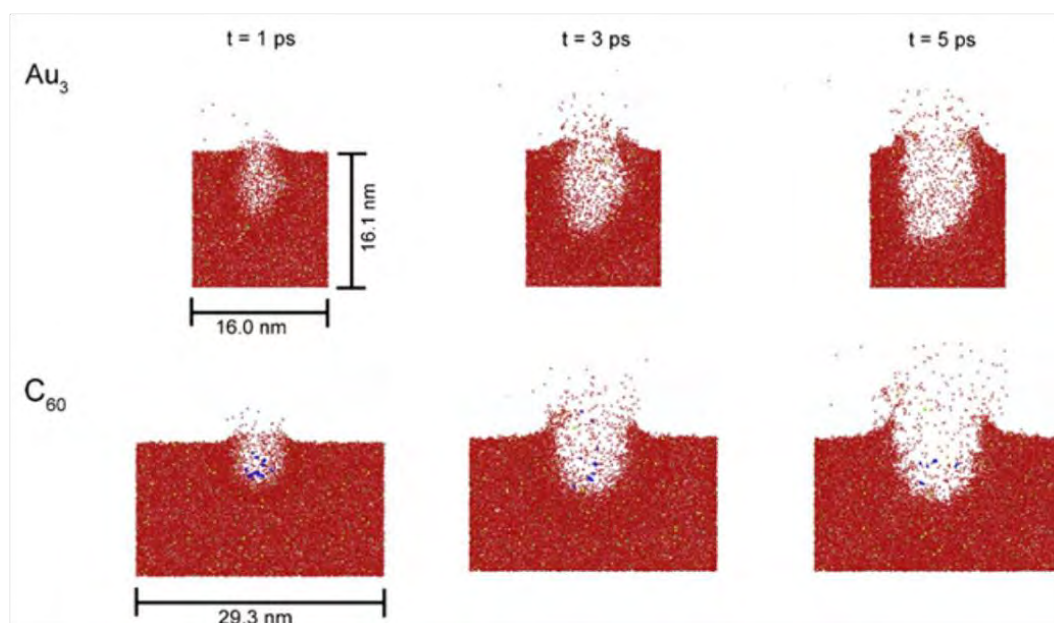


Figure 7-2: Cross-sectional view of collision events using C_{60} and Au_3 primary ions (Russo, 2006).

The approximate depth of the origin of the emitted particles can vary during SIMS-analysis due to the multiple complex collision processes occurring during sputtering but is often stated to be around 2-3 atomic layers (Winters, 1976). Thus, this method of surface examinations is often considered as being highly surface sensitive. Emitted particles can emerge of locations of up to 10 nm away from the initial impact site of the primary ion beam (Bolbach, 1992). Depending on the molecular structure and occurring species, the depth of emission for molecular particles from organic samples may also vary (Shard, 2015).

Throughout the course of all processes of generation of secondary ions the sample remains in its genuine solid state and the chemical composition and distribution of the elements is not altered. One major advantage of analyzing samples via the ToF-SIMS technique is that contrasting to other mass spectrometry methods the sample is kept in its native state and all chemical information is also preserved. Additionally, also the location of any obtained information is acquired which allows for elemental and molecular maps of the analyzed target to be established (Fearn, 2015).

For general ion generation two main models can be named: the *bond breaking model* describes increased ionization probability for positive ion generation through flooding the surface with oxygen ions, e.g. O_2^+ (Gnaser, 1999). The *electron tunneling model* predicts mainly negative secondary ion generation by decreasing the work function through inducing submonolayers of Cs into the surface layers to enable charge transfer to the sputtered atoms (Ming, 1986; Grehl, 2003).

7.3.2 Ion beam sources

In recent years substantial developments have been established in the area of ion beam sources. In general, the main primary ion beam source in a dual-beam ToF-SIMS device is a liquid metal ion gun (LMIG) to produce a focused ion beam for high lateral resolution. Previously, sources used gallium and gold ions, but recent advancements for less destructive analysis, often of soft organic or polymeric materials, focus on bismuth ion sources, since it shows improved secondary ion yields especially for the use of cluster ions (Brunelle, 2005; Straif, 2009). Cluster ion beams use charged particles comprised of multiple atoms. The LMIG technology consists of a heated field-emission tip which is coated with the metal alloy to extract a mixture of metal cluster ions. Subsequently, the ions are mass-selected and electrostatically focused to form an intense but laterally defined metal cluster ion beam.

Other cluster ions for primary ion beams include carbon fullerenes (C_{60}^+) and also Ar_n^+ gas cluster ion beams, which consist of up to around 2500 atoms. These gas-phase cluster ion sources are conventional electron impact (EI) techniques to ionize the vapor-phase clusters. After extraction and mass-filtering the ions are focused through beam-minimizing apertures and lenses to acquire a spatially well-defined cluster ion beam (Fearn, 2015).

In general, the main advantage of these cluster ion beam sources is that upon impact of the cluster ion on the sample surface the large cluster particle breaks into all consisting single atoms and the kinetic energy of the cluster particle is distributed over all atoms of the cluster. Thus, multiple separate low-energy particle impacts occur which leads to significantly reduced localized impact energies compared to high-energy single ion impacts. As a consequence, damage of the molecular surface microstructure is substantially reduced. For larger atom counts within one cluster ion a much wider crater is formed and the damage cascade and material mixing is greatly reduced in the subjacent bulk material. Also, much more particles from the top sample layers are ejected consisting of larger in-

tact fragments, compared to high-energy impacts and thus, yielding enhanced and cleaner mass spectra with less fragmentation and more intact parent molecules of the desired target material (Kayser, 2013). For larger clusters the lateral size of the impact crater increases as the depth of the damage in the bulk material decreases. In general, the focus of the ion beam from LMIG sources is much better than for large cluster ions and is consequently used in static ion mapping. Depth profiling and soft removal of material is carried out using larger cluster ions from the sputter gun.

7.4 Time-of-Flight mass analysis

To record a mass spectrum, after generation of the secondary ions and ejection from the target the surface ions are separated according to their mass-to-charge ratio (m/z). To analyze the mass of the secondary ions several different mass analyzers such as quadrupole, magnetic sector, ion trap time-of-flight (ToF) or Orbitrap are available (de Hoffmann, 2007). Most commonly the rather simple method of time-of-flight detection is used, where secondary ions are separated using the time they need to travel a certain distance within a flight tube in the mass analyzer. Within this tube no further electric or magnetic fields are used for separation of the ions. A general overview of the flight process of ions passing through the field-free drift tube is depicted in Figure 7-3.

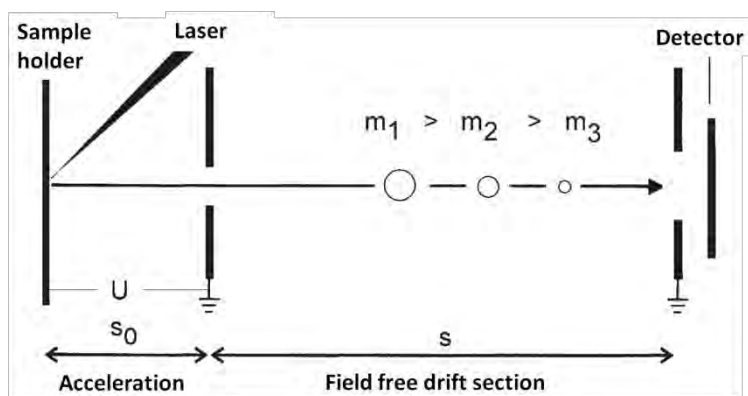


Figure 7-3: General schematic of a time-of-flight process (cf. Gross, 2012).

Each pulse of the primary ion beam rastered over the surface generates a corresponding short pulse of secondary ions migrating away from the target surface. Through the fixed potential V of an extraction plate the secondary ions are accelerated towards the time-of-flight mass analyzer device. After extraction and acceleration the secondary ions float through a field-free tube, where all ions carry the same kinetic energy $E_{kin} = mv^2/2$. Using the initial energy of the charged particle $E_{el}=qU=ezU=zV$ passing through the potential U , the mass-to-charge ratio of the ionized particles in dependence of their flight duration is obtained according to

$$\frac{m}{z} = \frac{2 \cdot V \cdot t^2}{L^2} \quad (\text{Eq. 7.4})$$

L = length of the flight tube

V = acceleration potential

t = time to pass the flight tube

where L is the length of the field-free tube, V is the fixed acceleration potential and t is the time period of the ions flying through the flight tube until impact onto the ion detector, also called time-of-flight. In this flight tube, lighter ions travel at a faster pace and need less time to cover the distance to arrive at the detector (Fearn, 2015). The time ions need to travel through the flight tube is dependent on the mass-to-charge ratio, according to equation 7.4. Each separate arrival time of particles will be transformed into the respective m/z ratio generating peaks in a mass spectrum or each single initial primary ion beam pulse. For higher ionic masses the flight times are significantly longer and ions do not collectively reach the ideal velocities within the flight tube. Thus, the mass resolution becomes lower and it is more difficult to keep good signal quality.

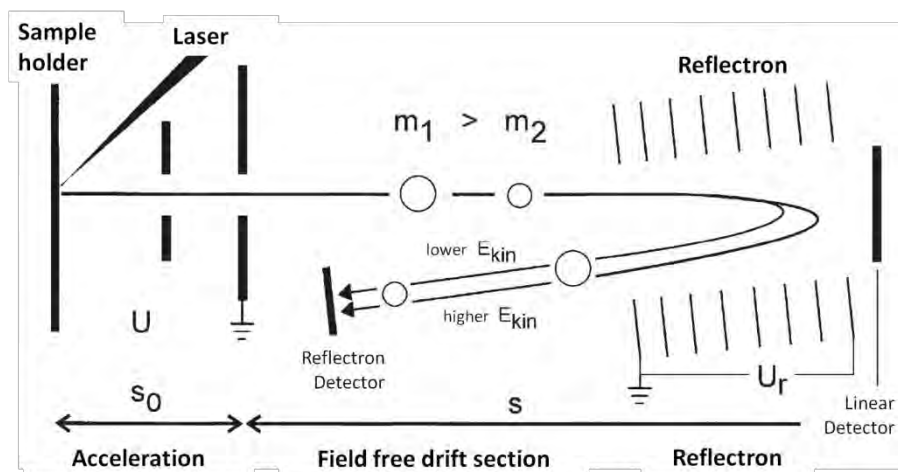


Figure 7-4: General depiction of a reflectron mass analyzer (cf. Gross, 2012).

To overcome this challenge of small differences in initial energy and angle of the ions a series of high-voltage ring electrodes are arranged at the head of the linear drift tube and acts as ion mirror, which is called the reflectron, depicted in Figure 7-4. As certain voltages are applied to the electrodes the reflectron can improve the resolution especially of higher mass ions by narrowing the extent of flight times for single m/z ratios. A decelerating voltage slows incoming ions down whereat faster ions travel further into the reflectron. Slower ions get deflected earlier. In the end, both, fast and slower moving ions of the same m/z ratio reach the detector at the same time, i.e. within an as small as possible time frame. This is narrowing the peak width of the generated mass spectra. Typical ToF-SIMS mass resolutions (M/dM) can be up to 20.000. Other major advantages are very high transmission rates, the ability of parallel ion detection of the entire mass range, as well as the unlimited mass range and the self-calibration using low mass fragments. Limits of detection are dependent on many properties of the used instrument und its key components.

7.5 Ion detection

For the detection of the secondary ions microchannel plates are used. After traveling through the drift tube of the mass analyzer the secondary ions become detected at impact

on the microchannel plate. A microchannel plate detector is a planar array of small glass channels leading from one side to the opposite. The width of the microchannels is typically about 6-10 μm in diameter. For production small hollow glass capillaries with electron emissive coating are fused and then sliced into separate plates. In microchannel plates the amplification of ion signals is achieved. A single ion will hit the wall of a channel it entered and a cascade of secondary electrons is emitted. In this way, multiple electrons are emitted from the backside of the microchannel plates. Using these plates operated in series amplification of up to 10^8 (one single ion impact event yielding an output of up to 10^8 secondary electrons) can be possible. Subsequently, outgoing electrons are being detected, usually measuring the total current using a resistive anode detector. Several unique properties are combined in microchannel plates such as e.g. high signal gain, high lateral and high temporal resolution making them useful for various applications. Depending on the type of particles the design of the microchannel plate detector can vary regarding resolution, sensitivity, signal throughput, imaging region, and others.

Additionally, a stable vacuum pressure as low as possible are essential for high surface sensitivity in ToF-SIMS. Vacuum pressure in today's ToF-SIMS analysis chambers can be as low as 10^{-10} mbar. This can be achieved through certain arrangements of various pumping techniques such as roughing pumps, turbo molecular pumps, ion pumps and sublimation gettering pumps. Low vacuum pressures are substantial to keep the probed surface free from contaminations (Fearn, 2015). Furthermore, maximization of the inelastic mean free path of the secondary ions is important to reduce energy losses of gas phase scattering effects on the way of the analyte ion into the mass analyzer.

7.6 Analysemethoden

7.6.1 Static SIMS

To obtain *high-resolution mass spectra* from target surfaces short pulses of solely primary projectile beam pulses with durations in the range of nano-seconds are used to irradiate the predefined surface region. Subsequent process sequences of static SIMS measurements include the extraction and acceleration into the time-of-flight analyzer, followed by separation according to the ions' m/z -ratio to produce a mass spectrum which is representative only for this one ion pulse's impact area. In this way, the primary ion beam is scanned over the desired area. Confined to their recording position, the sum of the different mass spectra can provide spatial distribution mapping images of specific molecule peaks.

Very short pulse durations of primary ion beams ensure high mass resolutions of up to 18.000 ($M/\Delta M$) (Iontof, 2019). Since the surface is not sputtered away and only analysis of the surface is achieved this procedure is referred to as the static SIMS method. Therefore, the ion beam dose of primary ions is rigorously controlled to minimize the interactions of the ion beam and target atoms or molecules. Thus, in static SIMS sub-monolayer removal of less than 1 % of the surface material is achieved. Low doses of primary ions and reduced interactions of ion beam and surface atoms and molecules allow static SIMS analysis to be effectively non-destructive to the surface structure and the use of further surface characterization via other techniques is possible (Fearn, 2015).

While the mass spectrum is recorded the lateral coordinates of each single position is documented. For data evaluation specific ions may be selected and correlation with their spatial distribution yield ion mappings for the predefined region of interest. Lateral resolutions of >100 nm may be achieved depending on the pulse time of the primary ion beam.

7.6.2 Dynamic SIMS

For many scientific problems it is essential to gain knowledge about how the elemental composition varies with depth. Diffusion of atoms or characterization of layer interfaces

can be such applications as well as changes of elemental composition throughout the bulk region during/after material processing measures or detection of specific bulk material features below the surface region. To measure mass spectra as a function of depth the ion sputter gun, an additional ion source, is applied. The sputter ion gun is used to ablate surface layers of material to allow analysis below the original surface level. The ion beam dose far exceeds the limit of the static SIMS analysis and removes larger quantities of sample particles. The chemical composition within the emerging sputter crater is made accessible in this way by analyzing nascent surface layers in between sputter beam pulses. This type of ToF-SIMS measurement is termed dynamic SIMS and is significantly more destructive to the sample surface and microstructure in comparison to the static SIMS method.

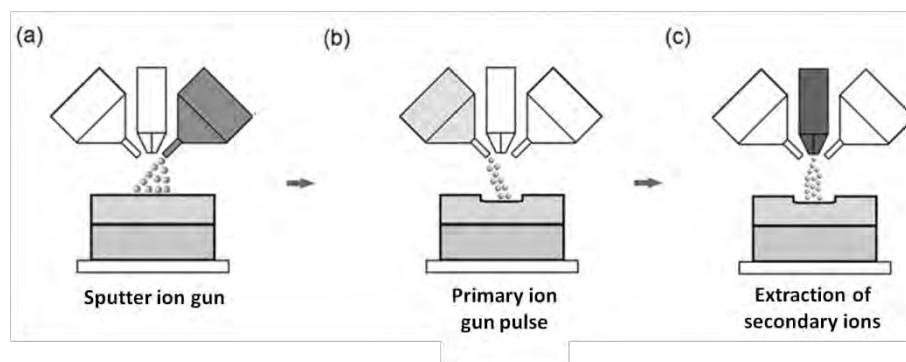


Figure 7-5: General depiction of the three main steps in dynamic SIMS depth profiling: high energy sputtering beam a); low energy analytical beam b); acceleration into the mass analyzer c) (cf. Fearn, 2015).

In a first step the sputter ion beam is scanned over the defined region of interest, which typically can be of up to $500 \mu\text{m} \times 500 \mu\text{m}$. The sputter ion beam has significantly higher ion doses compared to the analytical primary ion beam, generally in the range of tens or hundreds of nAs. For constant sputter rates the current should be kept stable and thus, material can be removed in a controlled way. High sputter rates and intense sputter ion beams large amounts of sample material can be removed but also may cause a change in the chemical composition of the sample affecting the secondary ion yields. For optimiza-

tion of the measurement accuracy and less altering of the target structure the ion beam has to be carefully controlled.

Secondly, after the sputter beam has ablated a surface layer the primary ion beam for analysis is applied to a specified area within the sputter crater. To avoid any edge effects, i.e. interference of material on the edges of the sputter crater, the analysis area is commonly chosen to be somewhat smaller than the larger sputter crater. Subsequently, secondary ions are emitted as described in previous sections and can be detected and analyzed in the ToF-SIMS instrument. Sputtering and primary analysis ion beams are again alternatingly repeated sequentially for further analysis until a specified depth is reached. For imaging, certain m/z -peaks of the mass spectra from the detected secondary ions can be selected and depth profiles of those particles can be generated and display. For compensation of the emission of charged ions and to avoid charging build ups on the target surface low energy (~ 20 eV) electron flood guns are used to neutralize the sample surface, especially for insulating samples (Fearn, 2015).

8 Electrospray Ionization

8.1 Overview

Similar to AP-MALDI, described in chapter 6.9, electrospray ionization (ESI) is an ionization source operating in atmospheric pressure. Therefore, an atmospheric pressure interface is necessary to transfer ions, generated at atmospheric pressure, into the high vacuum of the mass spectrometry system. To overcome the high differences in pressures separate intermediate pumping systems are applied and ions are transferred through lenses with small orifices (skimmer).

During the transfer of the ions into the vacuum chamber ion losses are induced. Since higher total ion yields are obtained due to the fast thermal stabilization at atmospheric pressures, these losses are usually more than compensated. One other significant advantage is the simplicity of the direct coupling of preceding separation techniques such as HPLC or others. Very beneficial is also the very easy introduction of analyte samples into the ionization chamber and subsequent transfer into the mass spectrometer, eliminating complex procedures for the sample transfer into vacuum (de Hoffmann, 2007).

ESI became popular when Fenn et al (Fenn, 1989) obtained multiply charged ions of protein samples in 1989. First, ESI was mainly used for protein samples and biopolymers but was extended also the analysis of small molecules as well. This method showed high sensitivities and easy handling of the ESI source and coupling to HPLC equipment was a simple task in lab application.

8.2 Electrospray ionization process

Ionization in ESI is achieved through application of a strong electric field of approximately 10^6 V/m to a capillary tube. Inside the tube is a liquid containing the analyte molecules moving with relative low velocities of around 1-10 $\mu\text{l}/\text{min}$. The potential difference of around 3 to 6 kV is applied onto the capillary and a counter electrode in a distance of up to 20 mm (de Hoffmann, 2007).

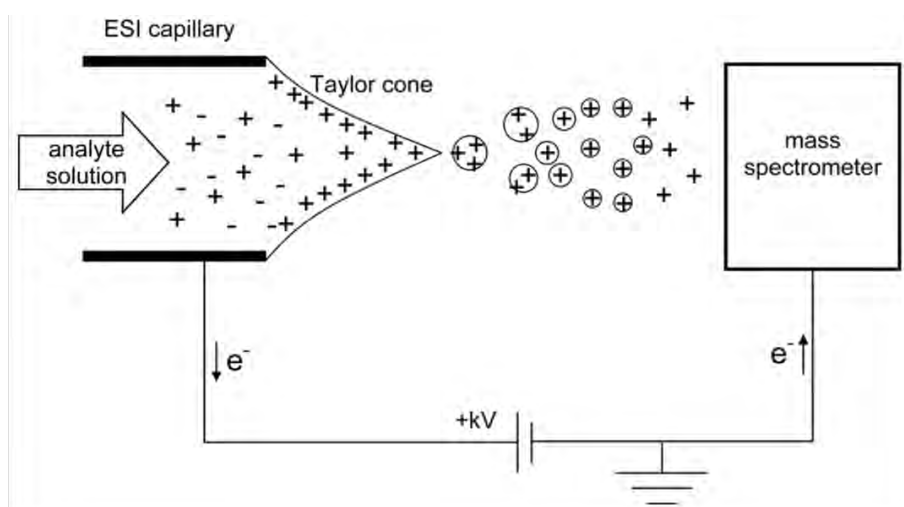


Figure 8-1: Schematic depiction of electrospray ionization process (positive ion mode) (Konermann, 2012).

The ionization process starts with the electrospray dispersion of the analyte containing fluid. During the application of the potential difference the fluid in the spray tube is formed into an elliptic shape (see Figure 8-1). Two separate forces are at an equilibrium in this state (Wilm, 2011):

- 1) The surface tension is applying a force onto the liquid surface to prevent dissolution and hold the fluid together.
- 2) The electrostatic force of the Coulomb attraction applies a force onto the liquid towards the direction of the counter electrode.

At the limit of a certain onset voltage, the elliptical shape of the surface will instantly flip to show a pointed cone. A fine spray is then emitted from the tip of this cone. After Sir Geoffrey Taylor, who investigated this behavior, it is called the Taylor-cone. He showed, that equilibrium between forces of surface tension and electrostatic attraction for a cone of a fluid is reached for a semi-vertical opening angle of 49.3° (Taylor, 1964). When a critical threshold voltage is exceeded, the Taylor-cone becomes instable and inverts to emit a jet of liquid droplets (also called Coulomb fission (Gomez, 1994; Gu, 2007)). In this way the electrospray process is initiated, where analyte ions in the fluid can be transferred to the gas phase and into the mass spectrometer device. Usually, the applied voltage is slightly above the threshold voltage to achieve stable jet conditions. The newly formed droplets at the apex of the sharp cone tip are charged close to the Rayleigh-limit, the maximum number of charges allowed in one drop depending on size and surface tension (Smith, 2002). After the droplets are generated, the containing solvent begins to evaporate as neutral particles. Hence, the resulting surface charge density increases. When again the Rayleigh-limit is reached for the secondary droplet a novel Taylor-cone is formed and newly generated smaller droplets are ejected which are highly charged. In this way, a large amount of finely dispersed small droplets is achieved until the smallest droplets only contain single analyte molecules (Wilm, 2011). These ions are then detected via the mass spectrometer.

In general, the spray is slightly focused off-axis to the inlet of the analyzer because the smallest droplets are found in the outer sphere of the entire spray plume due to electrostatic repulsion of the droplets. Therefore, the highest ion intensities are achieved for probing this region of droplet samples. So, the spray plume generated via a Taylor-cone consists of finely dispersed liquid droplets without preceding evaporation of significant amounts of solvent molecules (Wilm, 2011).

In general, two main models are proposed for explanation of the exact ionization mechanisms (de la Mora, 2000; Rohner, 2004; Cole, 2011; Wang, 2011; Wilm, 2011). An general depiction is given in Figure 8-2. One is called the *ion evaporation model* (IEM), where ions located at the surface of the generated droplets would overcome inner attraction forces and will be emitted from the surface into the gas-phase. The second one is called the *charge residue model* (CRM), wherein after consecutive solvent evaporation and Coulomb fission of smaller and smaller droplets through Taylor-cone generation in the electrospray the analyte molecules obtain the charges of the dissipated droplets and form gas-phase ions.

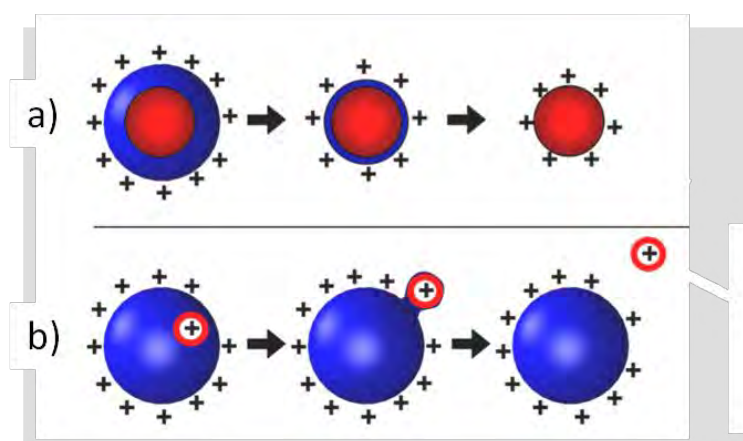


Figure 8-2: Ionization mechanisms in ESI: charge residue model (CRM) a); ion evaporation model (IEM) b) (cf. Konermann, 2012).

8.2.1 The ion evaporation model

Originally, this theory of the ion generation process was proposed by Iribarne and Thomson around 1976 (Iribarne, 1976). When the solvent evaporates after the ejection process the droplets start to shrink. After reaching a certain size, the field strength of their surface and the Coulomb repulsion become large enough to overcome the attraction forces of the droplet. The energy needed to increase the droplet's surface for the ion to be expelled is surpassed and therefore, it becomes possible for solvated ions to directly be emitted into the gas-phase from the surface of the droplets before complete solvent evaporation.

8.2.2 The charged residue model

The model was described by Dole in 1968 (Dole, 1968). It describes the shrinking process of the highly charged droplets via solvent evaporation. Eventually, an increased field strength on the surface leads to formation of an additional Taylor-cone wherefrom other even smaller charged droplets are expelled. After several repetition steps of droplet formation small droplets which in average contain only single analyte ions. After solvent evaporation and declustering the molecular ion is released. Thus, the analyte molecule stays inside of the droplet until the entire amount solvent molecules is evaporated. The charges remain within the small droplets and lead to formation of the gas-phase analyte ions.

9 Bibliography

- (Adamson, 1967) Adamson, A. W., & Gast, A. P. (1967). *Physical chemistry of surfaces*. John Wiley & Sons.
- (Allara, 1985) Allara, D. L., & Nuzzo, R. G. (1985). Spontaneously organized molecular assemblies. 2. Quantitative infrared spectroscopic determination of equilibrium structures of solution-adsorbed n-alkanoic acids on an oxidized aluminum surface. *Langmuir*, *1*(1), 52-66.
- (Allen, 1969) Allen, C. M., & Drauglis, E. (1969). Boundary layer lubrication: monolayer or multilayer. *Wear*, *14*(5), 363-384.
- (Archard, 1953) Archard, J.F. (1953), Contact and rubbing of flat surfaces, *J. Appl. Phys.*, *24*, 981-988.
- (Archard, 1980) Archard, J. F. (1980). Wear theory and mechanisms. In Peterson, M. B. & Winer, W. O. (Eds) *Wear control handbook*. American Society of Mechanical Engineers.
- (Axén, 2000) Axén, N., Hogmark, S., & Jacobson, S. (2000). Friction and Wear Measurement Techniques. In Bhushan, B. (Ed.) *Modern tribology handbook* (pp. 493). CRC press.
- (Bailey, 1955) Bailey, A. I., & Courtney-Pratt, J. S. (1955). The area of real contact and the shear strength of monomolecular layers of a boundary lubricant. *Proc. R. Soc. Lond. A*, *227*(1171), 500-515.
- (Barnes, 2001) Barnes, A. M., Bartle, K. D., & Thibon, V. R. (2001). A review of zinc dialkyldithiophosphates (ZDDPS): characterisation and role in the lubricating oil. *Tribology International*, *34*(6), 389-395.
- (Beare, 1935) Beare, W. G., & Bowden, F. P. (1935). Physical properties of surfaces I-Kinetic friction. *Philosophical Transactions of the Royal Society of London. Series A, Mathematical and Physical Sciences*, *234*(741), 329-354.
- (Bell, 1990) Bell, J., Coy, R., & Spikes, H. (1990). Cryogenic studies of zinc dialkyl dithiophosphate anti-wear films. In *Proceedings of the Japan International Tribology Conference* (pp. 505-10).
- (Bhansali, 1980) Bhansali, K.J. (1980), Wear coefficients of hard-surfacing materials, in *Wear Control Handbook*, Peterson, M.B. and Winer, W.O. (Eds.), ASME, 373-383.
- (Bolbach, 1992) Bolbach, G., Viari, A., Galera, R., Brunot, A., & Blais, J. C. (1992). Organic film thickness effect in secondary ion mass spectrometry and plasma desorption mass spectrometry. *International journal of mass spectrometry and ion processes*, *112*(1), 93-100.
- (Bowden, 1940) Bowden, F. P., & Leben, L. (1940). The friction of lubricated metals. *Phil. Trans. R. Soc. Lond. A*, *239*(799), 1-27.

- (Bowden, 1959) Bowden, F. P., & Tabor, D. (1959). *Reibung und Schmierung fester Körper*. Springer-Verlag.
- (Boyd, 1945) Boyd, J. (1945). The friction properties of various lubricants at high pressures. *Trans. ASME*, 67, 51-59.
- (Braun, 2007) Braun, J. (2007). Additives. In Mang, T., Dresel, W. (Eds) *Lubricants and lubrication* (pp. 88). John Wiley & Sons.
- (Brunelle, 2005) Brunelle, A., Touboul, D., & Laprèvote, O. (2005). Biological tissue imaging with time-of-flight secondary ion mass spectrometry and cluster ion sources. *Journal of Mass Spectrometry*, 40(8), 985-999.
- (Burwell, 1957) Burwell J T. Survey of possible wear mechanisms. *Wear*: 119–141 (1957)
- (Busch, 2007) Busch, C. (2007). Solid Lubrication. In Mang, T., Dresel, W. (Eds) *Lubricants and lubrication* (pp. 694). John Wiley & Sons.
- (Campbell, 1939) Campbell, W. E. (1939). Variables Influencing the Coefficient of Static Friction Between Clean and Lubricated Metals. *Trans. ASME*, 61, 633.
- (Campen, 2015) Campen, S., Green, J.H., Lamb, G.D., Spikes, H.A. (2015.) In situ study of model organic friction modifiers using liquid cell AFM: self-assembly of octadecylamine. *Tribol. Lett.* 58, 1–15.
- (Çavdar, 1991) Çavdar, B., & Ludema, K. C. (1991). Dynamics of dual film formation in boundary lubrication of steels part III. Real time monitoring with ellipsometry. *Wear*, 148(2), 347-361.
- (Clark, 1935) Clark, G. L., Lincoln, B. H., & Sterrett, R. R. (1935). Fundamental physical and chemical forces in lubrication. In *Proc. API* (Vol. 16, pp. 68-80).
- (Cole, 2011) Cole, R. B. (Ed.). (2011). *Electrospray and MALDI mass spectrometry: fundamentals, instrumentation, practicalities, and biological applications*. John Wiley & Sons.
- (Czichos, 2010) Czichos, H., Habig, K. H. (2010). Tribologische Systeme. In *Tribologie-Handbuch: Tribometrie, Tribomaterialien, Tribotechnik*. Springer-Verlag.
- (Czichos, 2014) Czichos, H. (2014). Tribosystems. In Mang T. (Ed.) *Encyclopedia of Lubricants and Lubrication* (pp. 2178). Springer Berlin Heidelberg.
- (Daniel, 1951) Daniel, S. G. (1951). The adsorption on metal surfaces of long chain polar compounds from hydrocarbon solutions. *Transactions of the Faraday Society*, 47, 1345-1359.
- (Davey, 1950) Davey, W. (1950). Boundary Lubrication of Steel. Blends of Acids, Esters and Soaps in Mineral Oils. *Industrial & Engineering Chemistry*, 42(9), 1837-1841.
- (de Barros, 2003) de Barros, M. I., Bouchet, J., Raoult, I., Le Mogne, T., Martin, J. M., Kasrai, M., & Yamada, Y. (2003). Friction reduction by metal sulfides in boundary lubrication studied by XPS and XANES analyses. *Wear*, 254(9), 863-870.
- (de Barros-Bouchet, 2005) de Barros-Bouchet, M. I., Martin, J. M., Le-Mogne, T., & Vacher, B. (2005). Boundary lubrication mechanisms of carbon coatings by MoDTC and

- ZDDP additives. *Tribology International*, 38(3), 257-264.
- (de Gee, 1982) de Gee, A. W. J. (1982). „Adhäsionsverhalten von Werkstoffen und Maßnahmen zur Verhinderung des „Fressens“ von Bewegungselementen. *Reibung und Verschleiß von Werkstoffen, Bauteilen und Konstruktionen*“, Grafenau, Expert Verlag, 75.
- (de Hoffmann, 2007) de Hoffmann, E. , & Stroobant, V. (2007). Mass spectrometry: principles and applications. John Wiley & Sons.
- (de la Mora, 2000) de la Mora, J. F., Van Berkel, G. J., Enke, C. G., Cole, R. B., Martinez-Sanchez, M., & Fenn, J. B. (2000). Electrochemical processes in electrospray ionization mass spectrometry. *Journal of Mass Spectrometry*, 35(8), 939-952.
- (DIN 51834-1, 2010) DIN 51834-1. (2010). Testing of lubricants - Tribological test in the transitory oscillation apparatus - Part 1: General working principles
- (Dokos, 1946) Dokos, S. J. (1946). Sliding friction under extreme pressure-I. *Trans. ASME*, 68, A148-A156.
- (Dole, 1968) Dole, M., Mack, L. L., Hines, R. L., Mobley, R. C., Ferguson, L. D., & Alice, M. B. (1968). Molecular beams of macroions. *The Journal of Chemical Physics*, 49(5), 2240-2249.
- (Douglas, 2005) Douglas, D. J., Frank, A. J., & Mao, D. (2005). Linear ion traps in mass spectrometry. *Mass spectrometry reviews*, 24(1), 1-29.
- (Dowson, 1979) Dowson, D. (1979). *History of tribology*. Addison-Wesley Longman Limited.
- (Drauglis, 1970) Drauglis, E., Allen, C. M., Jones Jr, W. H., Hartman, N. F., & Genco, J. M. (1970). *Thin Film Rheology of Boundary Lubricating Surface Films. Part I*. BATTELLE MEMORIAL INST COLUMBUS OHIO COLUMBUS LABS.
- (Dreisewerd, 2003) Dreisewerd, K. (2003). The desorption process in MALDI. *Chemical reviews*, 103(2), 395-426.
- (Dresel, 2007-a) Dresel, W. (2007). Synthetic Base Oils. In Mang, T., Dresel, W. (Eds) *Lubricants and lubrication* (pp. 64). John Wiley & Sons.
- (Dresel, 2007-b) Dresel, W. (2007). Lubricating Greases. In Mang, T., Dresel, W. (Eds) *Lubricants and lubrication* (pp. 648). John Wiley & Sons.
- (Durst, 2008) Durst, O. (2008). *Korrosions- und Verschleißigenschaften neuartiger kohlenstoffhaltiger PVD-Schichten* (Doctoral dissertation, Technische Universität Darmstadt).
- (Evans, 2005) Evans, R. D., More, K. L., Darragh, C. V., & Nixon, H. P. (2005). Transmission electron microscopy of boundary-lubricated bearing surfaces. Part II: Mineral oil lubricant with sulfur-and phosphorus-containing gear oil additives. *Tribology Transactions*, 48(3), 299-307.
- (Fearn, 2015) Fearn, S. (2015). *An Introduction to time-of-flight secondary ion mass spectrometry (ToF-SIMS) and its application to materials science*. Morgan & Claypool Publishers.

- (Fein, 1965) Fein, R. S., & Kreuz, K. L. (1965). Chemistry of boundary lubrication of steel by hydrocarbons. *ASLE TRANSACTIONS*, 8(1), 29-38.
- (Fenn, 1989) Fenn, J. B., Mann, M., Meng, C. K., Wong, S. F., & Whitehouse, C. M. (1989). Electrospray ionization for mass spectrometry of large biomolecules. *Science*, 246(4926), 64-71.
- (Ferrante, 1977) Ferrante, J. (1977). Exoelectron emission from a clean, annealed magnesium single crystal during oxygen adsorption. *ASLE TRANSACTIONS*, 20(4), 328-332.
- (Fink, 1932) Fink, M., & Hofmann, U. (1932). Zur Theorie der Reiboxydation. *Archiv für das Eisenhüttenwesen*, 6 (4), 161-164
- (Fox, 2004) Fox, N. J., Tyrer, B., & Stachowiak, G. W. (2004). Boundary lubrication performance of free fatty acids in sunflower oil. *Tribology letters*, 16(4), 275-281.
- (Franek, 1996) Franek, F., & Pauschitz, A. (1996). *Tribologie – Konstruktive Richtlinien zur Reibungs-, Verschleiß- und Schmierungstechnik*. (Vol. 277). Schriftenreihe des Wirtschaftsförderungsinstitutes.
- (Fujita, 2004) Fujita, H., & Spikes, H. A. (2004). The formation of zinc dithiophosphate antiwear films. *Proceedings of the Institution of Mechanical Engineers, Part J: Journal of Engineering Tribology*, 218(4), 265-278.
- (Furey, 1959) Furey, M. J. (1959). Film formation by an antiwear additive in an automotive engine. *ASLE Transactions*, 2(1), 91-100.
- (Gabler, 2012) Gabler, C., Pittenauer, E., Dörr, N., & Allmaier, G. (2012). Imaging of a tribolayer formed from ionic liquids by laser desorption/ionization-reflectron time-of-flight mass spectrometry. *Analytical chemistry*, 84(24), 10708-10714.
- (Gabler, 2012) Gabler, C., Pittenauer, E., Dörr, N., & Allmaier, G. (2012). Imaging of a tribolayer formed from ionic liquids by laser desorption/ionization-reflectron time-of-flight mass spectrometry. *Analytical chemistry*, 84(24), 10708-10714.
- (Gabler, 2014) Gabler, C., Dörr, N., & Allmaier, G. (2014). Influence of cationic moieties on the tribolayer constitution shown for bis (trifluoromethylsulfonyl) imide based ionic liquids studied by X-ray photoelectron spectroscopy. *Tribology International*, 80, 90-97.
- (Gabler, 2014) Gabler, C. (2014). *Tribochemical and chemical reactions of potential ionic liquid lubricants in contact with metal surfaces* (Doctoral dissertation, Technische Universität Wien).
- (Gaines, 1960) Gaines Jr, G. L. (1960). Some observations on monolayers of carbon-14 labeled stearic acid. *Journal of Colloid Science*, 15(4), 321-339.
- (Galera, 1991) Galera, R., Blais, J. C., & Bolbach, G. (1991). Molecular sputtering and damage induced by kiloelectron ions in organic monolayer—metal systems. *International Journal of Mass Spectrometry and Ion Processes*, 107(3), 531-543.

- (Gane, 1973) Gane, N., & Skinner, J. (1973). The generation of dislocations in metals under a sliding contact and the dissipation of frictional energy. *Wear*, 25(3), 381-384.
- (Georges, 1994) Georges, J. M., Tonck, A., & Mazuyer, D. (1994). Interfacial friction of wetted monolayers. *Wear*, 175(1-2), 59-62.
- (Gnaser, 1999) Gnaser, H. (1999). *Low-energy ion irradiation of solid surfaces*. Springer.
- (Gomez, 1994) Gomez, A., & Tang, K. (1994). Charge and fission of droplets in electrostatic sprays. *Physics of Fluids*, 6(1), 404-414.
- (Grehl, 2003) Grehl, T. (2003). *Improvements in TOF-SIMS Instrumentation for Analytical Application and Fundamental Research* (Doctoral dissertation, Westfälische Wilhelms-Universität Münster).
- (Gross, 2012) Gross, J. H. (2012). *Massenspektrometrie: Ein Lehrbuch*. Springer-Verlag.
- (Grossiord, 1998) Grossiord, C., Martin, J. M., Le Mogne, T., & Palermo, T. (1998). In situ MoS₂ formation and selective transfer from MoDPT films. *Surface and coatings Technology*, 108, 352-359.
- (Groszek, 1970) Groszek, A. J. (1970). Heats of preferential adsorption of boundary additives at iron oxide/liquid hydrocarbon interfaces. *ASLE TRANSACTIONS*, 13(4), 278-287.
- (Gu, 2007) Gu, W., Heil, P. E., Choi, H., & Kim, K. (2007). Comprehensive model for fine Coulomb fission of liquid droplets charged to Rayleigh limit. *Applied physics letters*, 91(6), 064104.
- (Hardy, 1922) Hardy, W. B., & Doubleday, I. (1922). Boundary lubrication.—The paraffin series. *Proc. R. Soc. Lond. A*, 100(707), 550-574.
- (Hardy, 1925) Hardy, W., & Bircumshaw, I. (1925). Bakerian Lecture. Boundary Lubrication. Plane Surfaces and the Limitations of Amontons' Law. *Proceedings of the Royal Society of London. Series A, Containing Papers of a Mathematical and Physical Character*, 108(745), 1-27.
- (Hardy, 1931) Hardy, W. B. (1931). Problems of the boundary state. *Philosophical Transactions of the Royal Society of London. Series A, Containing Papers of a Mathematical or Physical Character*, 230(681-693), 1-37.
- (Harper, 1967) Harper, W. R. (1967). *Contact and frictional electrification*. Clarendon press.
- (Haydon, 1963) Haydon, D. A. (1963). Boundary potentials and adsorption at the oil-metal interface. *Kolloid-Zeitschrift und Zeitschrift für Polymere*, 188(2), 141-147.
- (Heinicke, 1984) Heinicke, G. (1984). *Tribochemistry*. Akademie-Verlag.
- (Heinke, 1975) Heinke, G. (1975). Verschleiß - eine Systemeigenschaft Auswirkungen auf die Verschleißprüfung. *Materialwissenschaft und Werkstofftechnik*, 6(5), 164-169.
- (Hermance, 1958) Hermance, H. W., & Egan, T. F. (1958). Organic deposits on precious metal contacts. *Bell System Technical Journal*, 37(3), 739-776.

- (Hillenkamp, 1990) Hillenkamp, F., Karas, M., Ingendoh, A., & Stahl, B. (1990). Matrix assisted UV-laser desorption/ionization: A new approach to mass spectrometry of large biomolecules. *Biological Mass Spectrometry, Burlingame et al.,(eds.), Elsevier Science Pub., Amsterdam*, 49-60.
- (Hillenkamp, 2013) Hillenkamp, F., Jaskolla, T. W., & Karas, M. (2013). The MALDI process and method. *MALDI MS: A Practical Guide to Instrumentation, Methods, and Applications*. Wiley Blackwell.
- (Hirayama, 2012) Hirayama, T., Torii, T., Konishi, Y., Maeda, M., Matsuoka, T., Inoue, K., Hino, M., Yamazaki, D., & Takeda, M. (2012). Thickness and density of adsorbed additive layer on metal surface in lubricant by neutron reflectometry. *Tribology International*, 54, 100-105.
- (Hofmann, 2014) Hofmann, J. P., Rohnke, M., & Weckhuysen, B. M. (2014). Recent advances in secondary ion mass spectrometry of solid acid catalysts: large zeolite crystals under bombardment. *Physical Chemistry Chemical Physics*, 16(12), 5465-5474.
- (Hokkirigawa, 1997) Hokkirigawa, K. (1997), Wear maps of ceramics, Bulletin of the Ceramic Society of Japan, 1, 19-24.
- (Holm, 1967) Holm, R. (1967). *Electric contacts: theory and application*. Springer.
- (Holmberg, 2012) Holmberg, K., Andersson, P., & Erdemir, A. (2012). Global energy consumption due to friction in passenger cars. *Tribology International*, 47, 221-234.
- (Holmberg, 2014) Holmberg, K., Andersson, P., Nylund, N. O., Mäkelä, K., & Erdemir, A. (2014). Global energy consumption due to friction in trucks and buses. *Tribology International*, 78, 94-114.
- (Holmberg, 2015) Holmberg, K., & Erdemir, A. (2015). Global impact of friction on energy consumption, economy and environment. *FME Trans*, 43(3), 181-5.
- (Holmberg, 2017-a) Holmberg, K., Kivikytö-Reponen, P., Härkisaari, P., Valtonen, K., & Erdemir, A. (2017). Global energy consumption due to friction and wear in the mining industry. *Tribology International*, 115, 116-139.
- (Holmberg, 2017-b) Holmberg, K., & Erdemir, A. (2017). Influence of tribology on global energy consumption, costs and emissions. *Friction*, 5(3), 263-284.
- (Hsu, 2005) Hsu, S. M., & Gates, R. S. (2005). Boundary lubricating films: formation and lubrication mechanism. *Tribology International*, 38(3), 305-312.
- (Hu, 2005) Hu, Q., Noll, R. J., Li, H., Makarov, A., Hardman, M., & Graham Cooks, R. (2005). The Orbitrap: a new mass spectrometer. *Journal of mass spectrometry*, 40(4), 430-443.
- (Hwang, 2016) Hwang, Y. L., Horng, J. H., Kao, W. H., Sawae, Y., & Bartz, W. J. (2016). Special Issue on “Advances in Engineering Tribology Technology”. *Advances in Mechanical Engineering*, 8(1).
- (Iontof, 2019) Iontof.com. (2019). TOF-SIMS (Time of flight secondary ion mass spectrometry) technique for surface analysis. [online] Available at: <https://www.iontof.com/tof-sims-secondary-ion-mass-spectrometry.html>

- [Accessed 17 Feb. 2019].
- (Iribarne, 1976) Iribarne, J. V., & Thomson, B. A. (1976). On the evaporation of small ions from charged droplets. *The Journal of Chemical Physics*, 64(6), 2287-2294.
- (Israelachvili, 1981) Israelachvili, J. N., Fisher, L. R., Horn, R. G., & Christenson, H. K. (1981). Measurement of Adhesion and Short-Range Forces between Molecularly Smooth Surfaces in Undersaturated Vapours and in Organic Liquids. In *Tribology Series* (Vol. 7, pp. 55-69). Elsevier.
- (Jaskolla, 2009) Jaskolla, T. W., Karas, M., Roth, U., Steinert, K., Menzel, C., & Reihls, K. (2009). Comparison between vacuum sublimed matrices and conventional dried droplet preparation in MALDI-TOF mass spectrometry. *Journal of the American Society for Mass Spectrometry*, 20(6), 1104-1114.
- (John, 1998) John, P. W. (1998). *Statistical design and analysis of experiments* (Vol. 22). Siam.
- (Johnston, 1991) Johnston, G. J., Wayte, R., & Spikes, H. A. (1991). The measurement and study of very thin lubricant films in concentrated contacts. *Tribology Transactions*, 34(2), 187-194.
- (Joly-Pottuz, 2005) Joly-Pottuz, L., Dassenoy, F., Belin, M., Vacher, B., Martin, J. M., & Fleischer, N. (2005). Ultralow-friction and wear properties of IF-WS 2 under boundary lubrication. *Tribology letters*, 18(4), 477-485.
- (Jost, 1966) Jost, H. P. (1966). *Lubrication: Tribology; Education and Research; Report on the Present Position and Industry's Needs (submitted to the Department of Education and Science by the Lubrication Engineering and Research Working Group)*. HM Stationery Office.
- (Kapsa, 1982) Kapsa, P., & Martin, J. M. (1982). Boundary lubricant films: a review. *TRIBOLOGY international*, 15(1), 37-42.
- (Karas, 1985) Karas, M., Bachmann, D., & Hillenkamp, F. (1985). Influence of the wavelength in high-irradiance ultraviolet laser desorption mass spectrometry of organic molecules. *Analytical chemistry*, 57(14), 2935-2939.
- (Karas, 1987) Karas, M., Bachmann, D., Bahr, U., & Hillenkamp, F. (1987). Matrix-assisted ultraviolet laser desorption of non-volatile compounds. *International journal of mass spectrometry and ion processes*, 78, 53-68.
- (Karas, 1988) Karas, M., & Hillenkamp, F. (1988). Laser desorption ionization of proteins with molecular masses exceeding 10,000 daltons. *Analytical chemistry*, 60(20), 2299-2301.
- (Kassler, 2009) Kassler, A., Pittenauer, E., Doerr, N., & Allmaier, G. (2009). Electrospray ionization and atmospheric pressure matrix-assisted laser desorption/ionization mass spectrometry of antioxidants applied in lubricants. *Rapid Communications in Mass Spectrometry: An International Journal Devoted to the Rapid Dissemination of Up-to-the-Minute Research in Mass Spectrometry*, 23(24), 3917-3927.
- (Kato, 2000) Kato, K., & Adachi, K. (2000). Wear Mechanisms. In Bhushan, B. (Ed.) *Modern tribology handbook* (pp. 273). CRC press.

- (Kayser, 2013) Kayser, S., Rading, D., Moellers, R., Kollmer, F., & Niehuis, E. (2013). Surface spectrometry using large argon clusters. *Surface and Interface Analysis*, 45(1), 131-133.
- (Kenbeck, 2009) Kenbeck, D., & Bunemann, T.F. (2009). Organic Friction Modifiers. In Rudnick (Ed) *Lubricant Additives* (pp. 195). CRC Press.
- (Konermann, 2012) Konermann, L., Ahadi, E., Rodriguez, A. D., & Vahidi, S. (2012). Unraveling the mechanism of electrospray ionization. *Analytical Chemistry* 85 (1), 2-9.
- (Kornfeld, 1976) Kornfeld, M. I. (1976). Frictional electrification. *Journal of Physics D: Applied Physics*, 9(8), 1183.
- (Koshima, 2010) Koshima, H., Kamano, H., Hisaeda, Y., Liu, H., & Ye, S. (2010). Analyses of the adsorption structures of friction modifiers by means of quantitative structure-property relationship method and sum frequency generation spectroscopy. *Tribology Online*, 5(3), 165-172.
- (Kubo, 2006) Kubo, T., Fujiwara, S., Nanao, H., Minami, I., & Mori, S. (2006). TOF-SIMS analysis of boundary films derived from calcium sulfonates. *Tribology Letters*, 23(2), 171-176.
- (Kubo, 2008) Kubo, T., Fujiwara, S., Nanao, H., Minami, I., & Mori, S. (2008). Boundary film formation from overbased calcium sulfonate additives during running-in process of steel-DLC contact. *Wear*, 265(3-4), 461-467.
- (Laegreid, 1961) Laegreid, N., & Wehner, G. K. (1961). Sputtering yields of metals for Ar⁺ and Ne⁺ ions with energies from 50 to 600 eV. *Journal of Applied Physics*, 32(3), 365-369.
- (Landman, 1990) Landman, U., Luedtke, W. D., Burnham, N. A., & Colton, R. J. (1990). Atomistic mechanisms and dynamics of adhesion, nanoindentation, and fracture. *Science*, 248(4954), 454-461.
- (Li, 2009) Li, L. (2009). *MALDI mass spectrometry for synthetic polymer analysis* (Vol. 175). John Wiley & Sons.
- (Liang, 2003) Liang, H., Totten, G. E., & Webster G. M. (2003). Lubrication and Tribology Fundamentals. In Totten G. E. (Ed) *Fuels and Lubricants Handbook: Technology, Properties, Performance, and Testing*. American Society for Testing & Materials.
- (Lim, 1987) Lim, S. C., & Ashby, M. F. (1987). Overview no. 55 wear-mechanism maps. *Acta metallurgica*, 35(1), 1-24.
- (Ludema, 2010) Ludema, K.C. (2010). Friction. In Booser E.R. (Ed) *CRC Handbook of Lubrication, Theory and Practice of Tribology, Volume II Theory and Design*. (pp. 31/44). CRC Press.
- (Lüdermann, 2002) Lüdermann, H. C., Redmond, R. W., & Hillenkamp, F. (2002). Singlet-singlet annihilation in ultraviolet matrix-assisted laser desorption/ionization studied by fluorescence spectroscopy. *Rapid communications in mass spectrometry*, 16(13), 1287-1294.

- (Lundgren, 2006) Lundgren, S. M., Persson, K., Kronberg, B., & Claesson, P. M. (2006). Adsorption of fatty acids from alkane solution studied with quartz crystal microbalance. *Tribology Letters*, 22(1), 15-20.
- (Makarov, 1999) Makarov, A. A. (1999). Mass spectrometer. *U.S. Patent No. 5,886,346*. Washington, DC: U.S. Patent and Trademark Office.
- (Makarov, 2000) Makarov, A. (2000). Electrostatic axially harmonic orbital trapping: a high-performance technique of mass analysis. *Analytical chemistry*, 72(6), 1156-1162.
- (Mamyrin, 1973) Mamyrin, B. A., Karataev, V. I., Shmikk, D. V., & Zagulin, V. A. (1973). The mass-reflectron, a new nonmagnetic time-of-flight mass spectrometer with high resolution. *Zh. Eksp. Teor. Fiz*, 64, 82-89.
- (Mamyrin, 2001) Mamyrin, B. A. (2001). Time-of-flight mass spectrometry (concepts, achievements, and prospects). *International Journal of Mass Spectrometry*, 206(3), 251-266.
- (Mang, 2007-a) Mang, T. (2007). Lubricants in the Tribological System. In Mang, T., Dresel, W. (Eds) *Lubricants and lubrication* (pp. 7). John Wiley & Sons.
- (Mang, 2007-b) Mang, T., Lingg, G. (2007). Base Oils. In Mang, T., Dresel, W. (Eds) *Lubricants and lubrication* (pp. 34). John Wiley & Sons.
- (Mang, 2014) Mang, T. (2014). *Encyclopedia of Lubricants and Lubrication*. Springer Berlin Heidelberg.
- (Martin, 2000) Martin, J. M., Grossiord, C., Le Mogne, T., & Igarashi, J. (2000). Transfer films and friction under boundary lubrication. *Wear*, 245(1-2), 107-115.
- (Marshak, 2011) Marshak, S. (2011). *Earth: Portrait of a Planet*. WW Norton & Company.
- (Martin, 2005) Martin, J. M., & Minfray, C. (2005). Antiwear chemistry in presence of ZDDP. In *World Tribology Congress III* (pp. 599-600). American Society of Mechanical Engineers.
- (Marucci, 2002) Marrucci, L., Paparo, D., Cerrone, G., Solimeno, S., Russo, R., Lenza, T. L., & Siano, P. (2002). Optical analysis of surfaces by second-harmonic generation: Possible applications to tribology. *Tribotest*, 8(4), 329-337.
- (Minfray, 2004) Minfray, C., Martin, J. M., De Barros, M. I., Le Mogne, T., Kersting, R., & Hagenhoff, B. (2004). Chemistry of ZDDP tribofilm by ToF-SIMS. *Tribology Letters*, 17(3), 351-357.
- (Ming, 1986) Ming, L. Y., & Lang, N. D. (1986). Mechanisms of atomic ion emission during sputtering. *Nuclear Instruments and Methods in Physics Research Section B: Beam Interactions with Materials and Atoms*, 14(4-6), 403-413.
- (Morina, 2006) Morina, A., Neville, A., Priest, M., & Green, J. H. (2006). ZDDP and MoDTC interactions and their effect on tribological performance - tribofilm characteristics and its evolution. *Tribology Letters*, 24(3), 243-256.
- (Morina, 2007-a) Morina, A., & Neville, A. (2007). Tribofilms: aspects of formation, stability and removal. *Journal of Physics D: Applied Physics*, 40(18), 5476.

- (Morina, 2007-b) Morina, A., & Neville, A. (2007). Understanding the composition and low friction tribofilm formation/removal in boundary lubrication. *Tribology International*, 40(10-12), 1696-1704.
- (MS-Museum, 2019) MS-Museum. (2019). *Mass Spectrometry*. [online] Retrieved from <http://www.ms-museum.org/mass-spectrometry>. [Accessed 10 Apr. 2019].
- (Mücke, 1980) Mücke, W. (1980). Zur Anwendung der statistischen Versuchsplanung in der Tribotechnik. *Schmierungstechnik-11-n*, 5, 140.
- (Nakayama, 2006) Nakayama, K., & Martin, J. M. (2006). Tribochemical reactions at and in the vicinity of a sliding contact. *Wear*, 261(3-4), 235-240.
- (Navare, 2010) Navare, A. T. (2010). *Development of high-sensitivity atmospheric pressure (ap) matrix-assisted laser desorption/ionization (maldi) and open air ionization techniques for the analysis of biomolecules by mass spectrometry* (Doctoral dissertation, Georgia Institute of Technology).
- (Nicholas, 1959) Nicholas, J. F. (1959). The dissipation of energy during plastic deformation. *Acta metallurgica*, 7(8), 544-548.
- (Nicholls, 2005) Nicholls, M. A., Do, T., Norton, P. R., Kasrai, M., & Bancroft, G. M. (2005). Review of the lubrication of metallic surfaces by zinc dialkyl-dithiophosphates. *Tribology international*, 38(1), 15-39.
- (Paul, 1953) Paul, W., & Steinwedel, H. (1953). Ein neues Massenspektrometer ohne Magnetfeld. *Zeitschrift für Naturforschung A*, 8(7), 448-450.
- (Paul, 1960) Paul, W., & Steinwedel, H. (1960). *U.S. Patent No. 2,939,952*. Washington, DC: U.S. Patent and Trademark Office.
- (Percipio, 2018) Enterprise.percipio-big-data.com. (2019). *Percipio*. [online] Available at: <https://enterprise.percipio-big-data.com> [Accessed 17th April 2018].
- (Pittenauer, 2011) Pittenauer, E., Kassler, A., Haubner, R., & Allmaier, G. (2011). Different target surfaces for the analysis of peptides, peptide mixtures and peptide mass fingerprints by AP-MALDI ion trap-mass spectrometry. *Journal of proteomics*, 74(7), 975-981.
- (Premierbiosoft, 2019) Premierbiosoft.com. (2019). *Mass Spectrometry: Introduction, Principle of Mass Spectrometry, Components of Mass Spectrometer, Applications*. [online] Available at: http://www.premierbiosoft.com/tech_notes/mass-spectrometry.html [Accessed 19 Feb. 2019].
- (Proteomics, 2019) Creative Proteomics. (2019). *MALDI-TOF Mass Spectrometry*. [online] Creative Proteomics. Available at: <https://www.creative-proteomics.com/technology/maldi-tof-mass-spectrometry.htm> [Accessed 3 Mar. 2019].
- (Rabinowicz, 1980) Rabinowicz, E. (1980), Wear coefficients — metals, Wear Control Handbook, Peterson, M.B. and Winer, W.O. (Eds.), ASME, 475.
- (Ratoi, 2000) Ratoi, M. V. C. H. A., Anghel, V., Bovington, C., & Spikes, H. A. (2000). Mechanisms of oiliness additives. *Tribology International*, 33(3-4), 241-247.
- (Repka, 2017) Repka, M., Dörr, N., Brenner, J., Gabler, C., McAleese, C., Ishigo, O., &

- Koshima, M. (2017). Lubricant-surface interactions of polymer-coated engine journal bearings. *Tribology International*, 109, 519-528.
- (Rigo, 2014) Rigo, J., & Feinle, P. (2014). SRV Tribometer. In Mang, T. (Ed.) Encyclopedia of lubricants and lubrication. 1949-1956. Springer Berlin Heidelberg.
- (Rohner, 2004) Rohner, T. C., Lion, N., & Girault, H. H. (2004). Electrochemical and theoretical aspects of electrospray ionisation. *Physical chemistry chemical physics*, 6(12), 3056-3068.
- (Roll, 1934) Roll, F., & Pulewka, W. (1934). Beitrag zur Entstehung der Reiboxydation. *Zeitschrift für anorganische und allgemeine Chemie*, 221(2), 177-181.
- (Russel, 1965) Russell, J. A., Campbell, W. E., Burton, R. A., & Ku, P. M. (1965). Boundary lubrication behavior of organic films at low temperatures. *ASLE TRANSACTIONS*, 8(1), 48-58.
- (Russo, 2006) Russo Jr, M. F., Wojciechowski, I. A., & Garrison, B. J. (2006). Sputtering of amorphous ice induced by C60 and Au3 clusters. *Applied Surface Science*, 252(19), 6423-6425.
- (Sakurai, 1962) Sakurai, T., Ikeda, S., & Okabe, H. (1962). The Mechanism of Reaction of Sulfur Compounds with Steel Surface During Boundary Lubrication, Using S35 as a Tracer. *ASLE TRANSACTIONS*, 5(1), 67-74.
- (Schlag, 2012) Schlag, E. W. (Ed.). (2012). *Time-of-flight mass spectrometry and its applications*. Newnes.
- (Setz, 2005) Setz, P. D., & Knochenmuss, R. (2005). Exciton mobility and trapping in a MALDI matrix. *The Journal of Physical Chemistry A*, 109(18), 4030-4037.
- (Shard, 2015) Shard, A. G., Spencer, S. J., Smith, S. A., Havelund, R., & Gilmore, I. S. (2015). The matrix effect in organic secondary ion mass spectrometry. *International Journal of Mass Spectrometry*, 377, 599-609.
- (Sharma, 2015) Sharma, V., Gabler, C., Doerr, N., & Aswath, P. B. (2015). Mechanism of tribofilm formation with P and S containing ionic liquids. *Tribology International*, 92, 353-364.
- (Sheasby, 1991) Sheasby, J. S., Caughlin, T. A., & Habeeb, J. J. (1991). Observation of the antiwear activity of zinc dialkyldithiophosphate additives. *Wear*, 150(1-2), 247-257.
- (Sigmund, 1969) Sigmund, P. (1969). Theory of sputtering. I. Sputtering yield of amorphous and polycrystalline targets. *Physical review*, 184(2), 383.
- (Smith, 1989) Smith, D. P. E., Hörber, H., Gerber, C., & Binnig, G. (1989). Smectic liquid crystal monolayers on graphite observed by scanning tunneling microscopy. *Science*, 245(4913), 43-45.
- (Smith, 2002) Smith, J. N., Flagan, R. C., & Beauchamp, J. L. (2002). Droplet evaporation and discharge dynamics in electrospray ionization. *The Journal of Physical Chemistry A*, 106(42), 9957-9967.
- (Snow, 2014) Snow, J. T. (2014). *The environmental, elemental and proteomic plasticity of Trichodesmium in the (sub) tropical atlantic* (Doctoral dissertation, Uni-

- versity of Southampton).
- (Sommer, 2010) Sommer, K., Heinz, R., & Schöfer, J. (2010). *Verschleiß metallischer Werkstoffe*. Wiesbaden: Vieweg+ Teubner, 90(4).
- (Spikes, 1993) Spikes, H. A. (1993). Boundary lubrication and boundary films. In *Tribology Series* (Vol. 25, pp. 331-346). Elsevier.
- (Spikes, 2004) Spikes, H. (2004). The history and mechanisms of ZDDP. *Tribology Letters*, 17(3), 469-489.
- (Spikes, 2015) Spikes, H. (2015). Friction modifier additives. *Tribology Letters*, 60(1), 5.
- (Stanton, 1923) Stanton, T. E. (1923). *Friction*. Longmans, Green and Company.
- (Stephens, 1946) Stephens, W. E. (1946). A Pulsed Mass Spectrometer with Time Dispersion. *Phys. Rev.*, 69, 691.
- (Stipanovic, 2003) Stipanovic, A. J. (2003). Hydrocarbon Base Oil Chemistry. In Totten G. E. (Ed) *Fuels and Lubricants Handbook: Technology, Properties, Performance, and Testing*. American Society for Testing & Materials.
- (Straif, 2009) Straif, C. J., & Hutter, H. (2009). Investigation of polymer thin films by use of Bi-cluster-ion-supported time of flight secondary ion mass spectrometry. *Analytical and bioanalytical chemistry*, 393(8), 1889-1898.
- (Stratmann, 2017) Stratmann, A., Jacobs, G., Hsu, C. J., Gachot, C., & Burghardt, G. (2017). Antiwear tribofilm growth in rolling bearings under boundary lubrication conditions. *Tribology International*, 113, 43-49.
- (Stribeck, 1902) Stribeck, R. (1902). Die wesentlichen Eigenschaften der Gleit- und Rollenlager. *Z. des Verein. Deut. Ing.*, 46, 1341-1348.
- (Stump, 2002) Stump, M. J., Fleming, R. C., Gong, W. H., Jaber, A. J., Jones, J. J., Surber, C. W., & Wilkins, C. L. (2002). Matrix-assisted laser desorption mass spectrometry. *Applied Spectroscopy Reviews*, 37(3), 275-303.
- (Tanaka, 1988) Tanaka, K., Waki, H., Ido, Y., Akita, S., Yoshida, Y., Yoshida, T., & Matsuo, T. (1988). Protein and polymer analyses up to m/z 100 000 by laser ionization time-of-flight mass spectrometry. *Rapid communications in mass spectrometry*, 2(8), 151-153.
- (Taylor, 1964) Taylor, G. I. (1964). Disintegration of water drops in an electric field. *Proceedings of the Royal Society of London. Series A. Mathematical and Physical Sciences*, 280(1382), 383-397.
- (Tolstoi, 1967) Tolstoi, D. M. (1967). Significance of the normal degree of freedom and natural normal vibrations in contact friction. *Wear*, 10(3), 199-213.
- (Topolovec-Miklozic, 2008) Topolovec-Miklozic, K., Lockwood, F., & Spikes, H. (2008). Behaviour of boundary lubricating additives on DLC coatings. *Wear*, 265(11-12), 1893-1901.
- (Trillat, 1931) Trillat, J. J. (1937). The adsorption of oils in relation to lubrication. *I. Mech. E. Proceedings of the General Discussion on Lubrication and Lubricants*, 2, 55-59.

- (Uetz, 1979) Uetz, H., Sommer, K., & Khosrawi, M. A. (1979). Übertragbarkeit von Versuchs- und Prüfergebnissen bei abrasiver Verschleissbeanspruchung auf Bauteile. *VDI-Berichte*, 354, 107-124.
- (Varenberg, 2013) Varenberg, M. (2013). "Towards a unified classification of wear". *Friction*. 1 (4): 333–340.
- (Varlof, 1999) Varlof, K., Martin, J. M., Vacher, B., & Inoue, K. (1999). Tribochemical interactions between micellar calcium borate and ZDDP: evidence for borophosphate tribofilm by EELS. In *Tribology Series* (Vol. 36, pp. 433-438). Elsevier.
- (Vorm, 1994) Vorm, O., Roepstorff, P., & Mann, M. (1994). Improved resolution and very high sensitivity in MALDI TOF of matrix surfaces made by fast evaporation. *Analytical Chemistry*, 66(19), 3281-3287.
- (Walton, 1977) Walton, A. J. (1977). Triboluminescence. *Advances in Physics*, 26(6), 887-948.
- (Wang, 2011) Wang, R. (2011). *On the mechanism of electrospray ionization and electrospray-based ambient ionization methods* (Doctoral dissertation, ETH Zurich).
- (Weinberger, 1993) Weinberger, S.R., Boernsen, K.O., Finchy, J.W., Robertson, V., and Musselman, B.D. (1993) Proceedings, 41st Annual ASMS Conference on Mass Spectrometry and Allied Topics; San Francisco, CA, May 31–June 5, 1993, pp. 775a–775b.
- (Widder, 2015) Widder, L., Ristic, A., Brenner, F., Brenner, J., & Hutter, H. (2015). Modified-Atmospheric Pressure-Matrix Assisted Laser Desorption/Ionization Identification of Friction Modifier Additives Oleamide and Ethoxylated Tallow Amines on Varied Metal Target Materials and Tribologically Stressed Steel Surfaces. *Analytical chemistry*, 87(22), 11375-11382.
- (Wiley, 1955) Wiley, W. C., & McLaren, I. H. (1955). Time-of-flight mass spectrometer with improved resolution. *Review of scientific instruments*, 26(12), 1150-1157.
- (Wilm, 2011) Wilm, M. (2011). Principles of electrospray ionization. *Molecular & cellular proteomics*, 10(7), M111-009407.
- (Winters, 1976) Winters, H. F., & Coburn, J. W. (1976). Influence of the altered layer on depth profiling measurements. *Applied Physics Letters*, 28(4), 176-179.
- (Wortmann, 1976) Wortmann, J., & Feller, H.G. (1976.) Exo-Elektronenemission nach tribo-mechanischer Oberflächenbeanspruchung. *Z. Metallkunde* 67, 688.
- (Yamaguchi, 1998) Yamaguchi, E. S., Ryason, P. R., Yeh, S. W., & Hansen, T. P. (1998). Boundary film formation by ZnDTPs and detergents using ECR. *Tribology transactions*, 41(2), 262-272.
- (Yin, 1997) Yin, Z., Kasrai, M., Fuller, M., Bancroft, G. M., Fyfe, K., & Tan, K. H. (1997). Application of soft X-ray absorption spectroscopy in chemical characterization of antiwear films generated by ZDDP Part I: the effects of physical parameters. *Wear*, 202(2), 172-191.

- (Yu, 2007) Yu, L. G., Yamaguchi, E. S., Kasrai, M., & Bancroft, G. M. (2007). The chemical characterization of tribofilms using XANES—Interaction of nanosize calcium-containing detergents with zinc dialkyldithiophosphate. *Canadian Journal of Chemistry*, *85*(10), 675-684.
- (Zhang, 2015) Zhang, J., & Meng, Y. (2015). Boundary lubrication by adsorption film. *Friction*, *3*(2), 115-147.
- (Zhang, 2016) Zhang, J., & Spikes, H. (2016). On the mechanism of ZDDP antiwear film formation. *Tribology Letters*, *63*(2), 24.
- (Zink, 1978) Zink, J. I. (1978). Triboluminescence. *Accounts of Chemical Research*, *11*(8), 289-295.
- (Zum Gahr, 1987) Zum Gahr K.-H.: Microstructure and wear of materials, Elsevier, Amsterdam, 1987, 560 pp.

10 Aim of thesis

The field of tribology has attracted increasing attention in recent surface science. Friction, wear and lubrication between objects in contact are essential in numerous fields of science and industrial applications. Boundary tribofilms have been subject of research since the early days of lubrication science. They consist of chemical reaction products of lubricant components used within the tribo-contact and can have major influence on the entire behavior of tribological systems. Driven by the need for improved energy efficiency interest in surface interactions and the understanding of interaction mechanisms has risen substantially during the last decades.

Much of the information gained over the past century has been gathered in investigations of specific problems. For great and deep understanding of the mechanisms in surface interactions and influences on tribology, a broad insight in surface chemistry, materials science and the contact mechanical aspects is needed. To add a contribution to this understanding and support strategies for system optimization, in this work a new method for the characterization and identification of lubrication additives and chemical reaction products in boundary tribofilms was applied. In this respect, the main focus of the thesis was to develop a method to apply the known instrumentation of atmospheric pressure matrix assisted laser desorption/ionization (AP-MALDI) onto tribologically stressed surfaces for identification of model additives used in the applied lubricants.

To lay groundwork for the development of such a method, the planned objective was to determine and characterize existing boundary tribofilms on heavily stressed surfaces of a field sample lubricated with various types of additives (*Publication A*). Herein, a basic investigation of a used and deteriorated tribologically stressed sample at end-of-lifetime was accomplished, which can be seen as state of the art approach for analysis of worn surfaces. A limiting aspect of applied surface analytical methods is the lack of data about structural information or molecular weight of chemical components featured on the ex-

aminated surface. However, this information can be detrimental for elucidation of lubricant additive behavior on the surface and its contribution to friction and wear. Since AP-MALDI brings the potential to provide missing structural information, the aim was to develop a method which allows for original tribologically stressed surfaces to be analyzed by this soft ionization technique without the necessity of transferring samples into vacuum conditions. Therefore, a feasibility study was to be conducted with two model organic friction modifier additives (*Publication B*). The possibility was shown to successfully identify both additives through the AP-MALDI method directly from base oil blends without further application of any separation techniques. As a next step, detailed structural characterization of tribological contact areas and present boundary tribofilms of used additives was to be performed (*Publication C*). Therefore, new target sample holders were designed and constructed for investigations of various sample configurations (disc and cylinder). In a first step, various sample materials of different chemical composition, as well as varying surface roughness were tested for sensitivity and additive ion intensities in AP-MALDI. Furthermore, the stressed surfaces from tribological experiments were supposed to be analyzed. With the help of high resolution Orbitrap mass analysis definite identification of used additive molecules within additive tribofilms was aimed for. For verification of AP-MALDI results, as well as to complement findings with further elucidation of tribolayers and degradation fragments from applied friction modifier additives ESI and ToF-SIMS measurements were applied.

As an approach to the scientific results presented, the applied analytical methods were described. Prior, a basic introduction focused on lubricant additivation and the assessment of tribological interactions forming boundary tribofilms was given, including a brief overview on general tribological aspects and phenomena.

11 Scientific work published

11.1 Publication A

Triboanalysis of hypoid gear components in drive trains

Triboanalysis of hypoid gear components in drive trains

von L. Widder, A. Grafl, A. Lebel, C. Tomastik, J. Brenner^{*)}

Eingereicht: 29. 11. 2010

Nach Begutachtung angenommen: 15. 1. 2011

Kurzfassung

Getriebesysteme werden im tribologischen Kontakt sehr hoch belastet und daher sind für einen langlebigen und wartungsfreien Betrieb ein verfeinertes Oberflächendesign und verbesserte Materialeigenschaften unentbehrlich. Um dies zu erreichen müssen die Mechanismen für Oberflächenschädigungen, Schmierstoffalterung, erhöhte Reibung und morphologische Veränderung wohl verstanden sein. Für diesen Artikel wurde ein Hypoidgetriebe nach einem Langzeit-Testversuch mit hoher Belastung detailliert untersucht um kritische Veränderungen der Getriebekomponenten zu evaluieren. Die gefundenen Ergebnisse sind die Grundlage, um Einflüsse, die auf den Tribo-Prozess zurückzuführen sind, aufzuklären und um Strategien zur Systemoptimierung zu untermauern.

Schlüsselwörter: Hypoidgetriebe, Tribologie, Oberflächenanalyse, Verschleiß, Triboschicht, Querschleiff

Keywords: Hypoid gear, Tribology, surface analysis, wear, tribo-layer, cross-section

1 Introduction

Tribosystems undergo changes over time mainly due to lubricant ageing and surface alteration. Amongst other things this is expressed in changes of viscosity and formation of wear debris, resulting in component topography and morphology changes. Projected goal of recent investigations was to determine and characterize surfaces and tribo-layers on tribologically stressed surfaces of a hypoid gearbox system in the state after a severe long-term test run. The knowledge gain about tribo-processes and the presence and composition of tribo-layers can support the search for concepts to improve friction behavior and material performance subsequently. Therefo-

re, the combination of methods for the characterization of surface and tribo-layers of a hypoid gear is evaluated.

2 Experimental Details

For this research a standard steel hypoid gear after a severe long-term test was investigated. Single teeth were separated by Wire Electrical Discharge Machining (WEDM). The lubricant used in these investigations was based on ester/polyalphaolefine blends and main additives are sulfur carriers and phosphonates/phosphates. Oil characterization was done for both, the fresh lubricant before and the used oil after the test run. Each gear sample was rinsed extensively using petroleum ether before measurements. For the characterization of the system Optical Microscopy, Confocal White Light Microscopy, SEM/EDS analysis (Scanning Electron Microscopy / Energy Dispersive X-ray Spectroscopy), XPS (X-ray Photoelectron Spectroscopy), Nanoindentation, ToF-SIMS (Time of Flight-Secondary Ion Mass Spectrometry) and Computational Simulations were used. An overview of investigation methods applied herein is given in **Table 1**. Detailed information about wear measurement with Confocal White Light Microscopy is published in [1]. [2] gives an overview which kind of information is gained with different characterization methods.

3 Results

3.1 Tooth flanks

Oil characterization shows the decrease of kinematic viscosity at 40 °C from 63.2 mm²/s (fresh oil) to 55.2 mm²/s (used oil). Investigations of elemental composition of the used oil reveals major wear elements such as iron and manganese. Traces of aluminum, copper and chromium are also found.

Abstract

In tribological contact gear systems are heavily loaded and therefore improved surface design and material properties are essential for long life and maintenance-free operation. Thus, mechanisms leading to surface deterioration, lubricant ageing, enhanced friction and morphological changes need to be well understood. In this work a hypoid gear system is analyzed in detail to evaluate critical changes of gear system components after a severe long term test run. Results are the basis to elucidate possible effects due to the tribo-process and to support strategies for system optimization.

For a first overview of the condition of the gear system standard optical microscopy was used. With this method special characteristics and macro-features of the worn surface were determined. Optical microscopy of the surface of the hypoid gear tooth flanks shows three different types of surface structure with differing visual properties.

First, pinion tooth flanks exhibit unstressed surface area at the concave pinion drag heel side. Herein, no contact of opposing pinion/gear teeth had occurred and the original surface structure of the production process can be seen. Thus, no alteration and surface modification on the basis of steel/steel tribo-contact has happened.

Clearly different appearance is exhibited on tribologically stressed areas where steel/steel contact has occurred. Due to surface modification and change in topography, these contact areas appear much darker in optical microscopy. Original grinding grooves of the

^{*)} Dipl.-Ing. Lukas Widder

AC²T research GmbH, Austrian Center of Competence for Tribology, 2700 Wiener Neustadt, Österreich

Vienna University of Technology, Institute of Chemical Technologies und Analytics, 1060 Wien, Österreich

Dipl.-Ing. Alexander Grafl

Dipl.-Ing. (FH) Astrid Lebel, MSc

Dipl.-Ing. Christian Tomastik

Josef Brenner

AC²T research GmbH, Austrian Center of Competence for Tribology, 2700 Wiener Neustadt, Österreich

Method	Information	Depth of Penetration
Oil analysis (e.g. Viscometry, Inductively Coupled Plasma Optical Emission Spectrometry (ICP-OES))	Viscosity, elemental composition, density, water content, total acid, base numbers	
Optical Microscopy	Topography	Surface
Confocal White Light Microscopy	Topography	Surface
SEM / EDS (Scanning Electron Microscope / Energy-dispersive X-ray Spectroscopy)	Elemental composition and surface structure	< 1 µm
XPS (X-ray Photoelectron Spectroscopy)	Elemental composition, chemical bonding energies, depth profiles	< 10 nm
Nanoindentation	Hardness, Young's Modulus	50 nm - 5 µm
ToF-SIMS (Time of Flight-Secondary Ion Mass Spectrometry)	Elemental composition, depth profiles	Submonolayers
Computational Simulation	Line of contact	

Table 1: Overview of methods used for the investigation of gear components

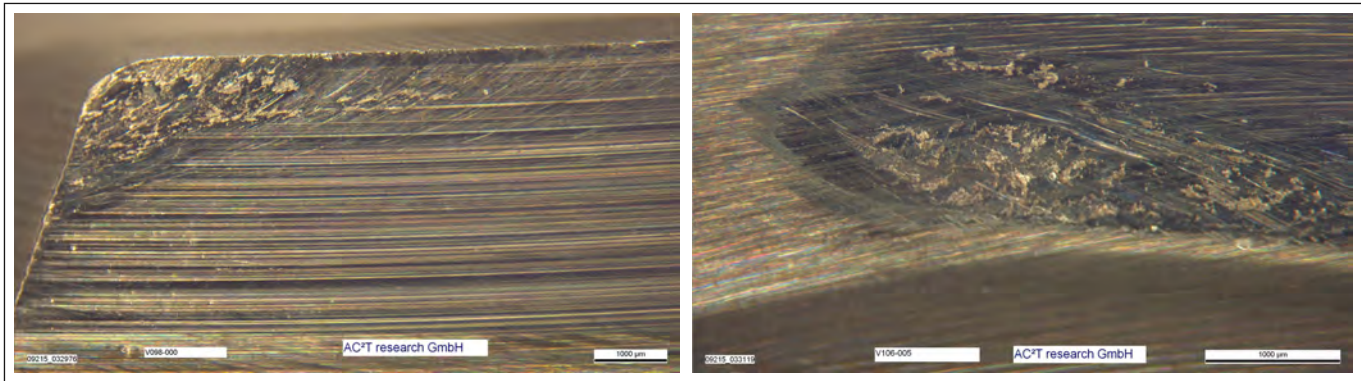


Figure 1: Optical microscopy of severe wear areas of gear (left), pinion (right)

production process are still visible herein but evidently the steel surface has undergone radical alteration as a result of heavy load contact.

Additionally, two specific regions reveal extraordinary surface deformation. Both, on the concave pinion drag heel side tooth flank bottom and the convex gear drag heel side tooth flank top severe wear zones are visible on the surface (Figure 1). Therein, original processing grooves are worn off and new types of wear tracks appear. As small bright spots are obvious, in various places surface material is removed and pits and cavities occur.

Measurements with confocal white light microscopy reveal much more details of the worn surface. The comparison of scans of un-stressed and stressed surface shows the smoothing of the heavier loaded surface. The applied load and test duration has abraded existing surface asperities and altered the original surface structure of the contact areas. Additionally, the drag and coast side of the gear teeth have differing load stress during operation and therefore smoothing of the surface is unequally pronounced. Detailed images of the severe wear zone reveal major differences in height and confirm removal of surface material and the existence of several pits and cavities in the heavily stressed areas (Figure 2).

SEM analysis of the tooth flank bottom reveals major accumulation of wear debris and contamination particles on the surface. Particles of various shapes and structures are gathered at the bottom. The major part was of round shape and of sizes from $\sim 0.5 \mu\text{m}$ to $\sim 5 \mu\text{m}$. EDS analysis of these particles detected only iron and oxygen. Other particles had more cubic and crystal-like structure and EDS revealed a fairly high amount of calcium. Particles of more bulky and shapeless structure consisted mainly of iron and oxygen, but also copper was detected. When BSE (back scattered electron) mode was used, elemental contrast of the surface of the tooth flank is visible in readily distinguishable bright and dark areas. Whereas in bright areas mainly iron from steel substrate could be detected, dark areas seem to be covered by various residues and showed clearly different

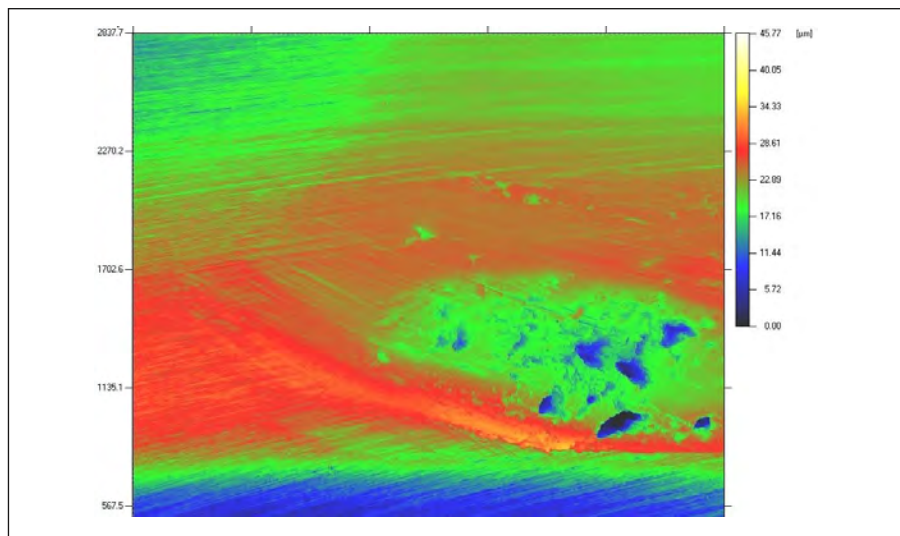


Figure 2: Confocal white light microscopy picture of pinion wear area

composition. In these regions SEM analyses showed existence of sulfur, phosphorus, silicon and also traces of copper were found.

Carbon was also detected in small amounts but this generally derives from atmospheric surface contaminations.

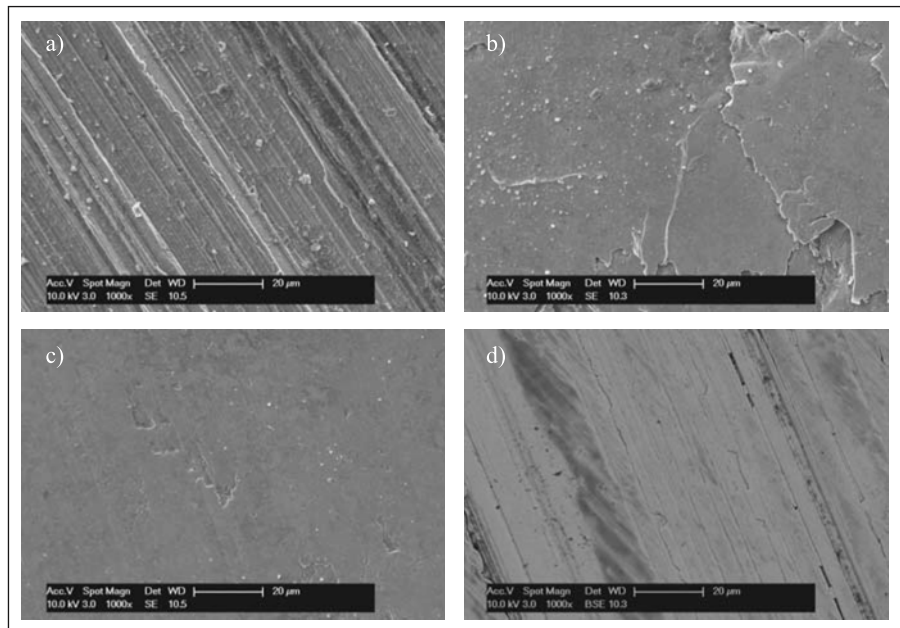


Figure 3: SEM pictures of original grooves at tooth bottom including particles (a); severe wear area with strong plastic deformation (b); flattened surface of heavy load area (c); less loaded area at tooth top including oil residues (dark) (d)

For further investigations of the tooth flanks quasi-line scans of the surface were made. From the tooth bottom to its top SEM images were taken every 250 μm with a picture width of 125 μm . These picture series gives a great overview of the surface's condition in each segment (**Figure 3**). At the tooth flank bottom, as mentioned above, an accumulation of particles and contaminations is visible. Moreover, the original surface finish of the production process is unaltered in this region.

Towards the middle of the tooth flank, which is exposed to higher loads, plastic deformation becomes apparent. In this region of low load also previous mentioned dark areas of oil residues containing sulfur, silicon and phosphorus appeared. As load increases towards the line of contact, these dark areas become less and plastic deformation reaches its maximum. Within this area original processing grooves have almost completely vanished due to severe plastic deformation. Furthermore, oil residue tribolayers for the most part disappear in this region. Proceeding further towards the top of the tooth flank, again reduced surface alteration occurs as the surface stress level decreases and more and more original grinding grooves appear. In addition, increasing oil residues become visible again as the tooth flank top is exposed to less load.

In the course of these line scans, also previously mentioned severe wear zone of the pinion tooth flank was imaged by SEM. Heavy plastic deformation and the removal of material is evident as the steel substrate is absolutely evened out and pits and cavities are clearly visible in this area. Top surface layers seem smeared out and appear to be pushed on top of each other under a very high local load and pressure.

For one pinion tooth flank three different quasi-line scans were made on each, the drag and the coast side. It is apparent that the region of extreme load level varies in distance to the tooth top when going from heel to toe side. At the pinion drag heel side the distance is approximately 2.75-5.5 mm from the top. In the middle of the pinion tooth the distance is around 1.75-4.0 mm whereas at the toe side offset of the most plastically deformed region to the tooth top further decreased to 0.75-2.5 mm. For pinion coast heel, middle and toe side the varying distances of the most stressed surfaces from the top of the tooth were around 2.0-4.5 mm, 1.75-4.75 mm and 0.5-2.5 mm, respectively. Furthermore, the coast side of the teeth generally shows less tribological stress. On this side less plastic deformation and also less oil residues could be detected.

XPS analysis of the pinion tooth flank did not reveal any major differences between the heavily stressed and less loaded areas. Typical profiles show a thin oxide layer and traces of phosphorus and sulfur. In the stressed surface areas around 10 at% (atomic percent) phosphorus and roughly 2 at% sulfur were

present. Reference measurements in the unstressed region also show concentrations of phosphorus and sulfur. Phosphorus intensities decreased to around 6 at% which was about half the value of the stressed area and sulfur intensities are even slightly increased to approximately 3 at% in the less loaded surface region.

3.2 Cross Sections

For further investigations cross sections of the severe wear zones of both, the gear and the pinion teeth were made. Optical microscopy of polished cross sections do not reveal any micro-structure of the steel bulk material. However, in the wear zone pits from broken out material and small fissures in the uppermost tooth flank surface layers could be seen. When etched with a solution of hydrochloric and picric acid in methanol, micro-structure of the base material becomes visible.

In the severe wear zone there are three regions visible with entirely different appearance (**Figure 4**).

- The outermost layer, where the surface is most stressed and deteriorated, appears white and no clear micro-structure can be seen. In the cross section this white etching layer has a maximum thickness of around 20 μm .
- A slightly broader layer between the bulk material and the white etching layer is apparent. This layer has much darker appearance than both, the bulk material and the brighter outer layer and seems to have very coarse grain structure.

- The structure of the bulk material seems more or less homogeneous.

Interestingly enough, another feature that could be seen under the microscope was, that in contrast to the etched bulk structure different behaviour was observed at the top land edge of the gear tooth cross section. Here, to a depth of around 50 μm the grain boundaries were emphasized along the entire top land edge after etching.

Another characteristic which can be seen by optical microscopy in cross-sections of the tooth flanks is that the bright and dark etching layers in the severe wear zones and on the tooth flank's surface seem to occur at slightly protruding convexities for both, the gear and the pinion. Furthermore, cavities and cracks on the tooth flank surface visible by optical microscopy seem to only occur in the white etching layer and do not reach further into the bulk material.

SEM images after etching procedure clearly show three different regions of varying surface conditions. This correlates with results of surface characterization gained by optical microscopy. The outermost layer shows very fine micro-structure and seems to be less affected by the etching solution. In addition, surface cavities and thin fissures, are captured in very close detail (**Figure 4**). This kind of surface deterioration of the severe wear zone only occurs in this fine structured layer and does not advance into the second layer. The intermediate layer between the white etching layer and bulk material reveals very coarse structure and seems to be much more affected by etching. EDS investigations of the steel material in these areas do not show any variation

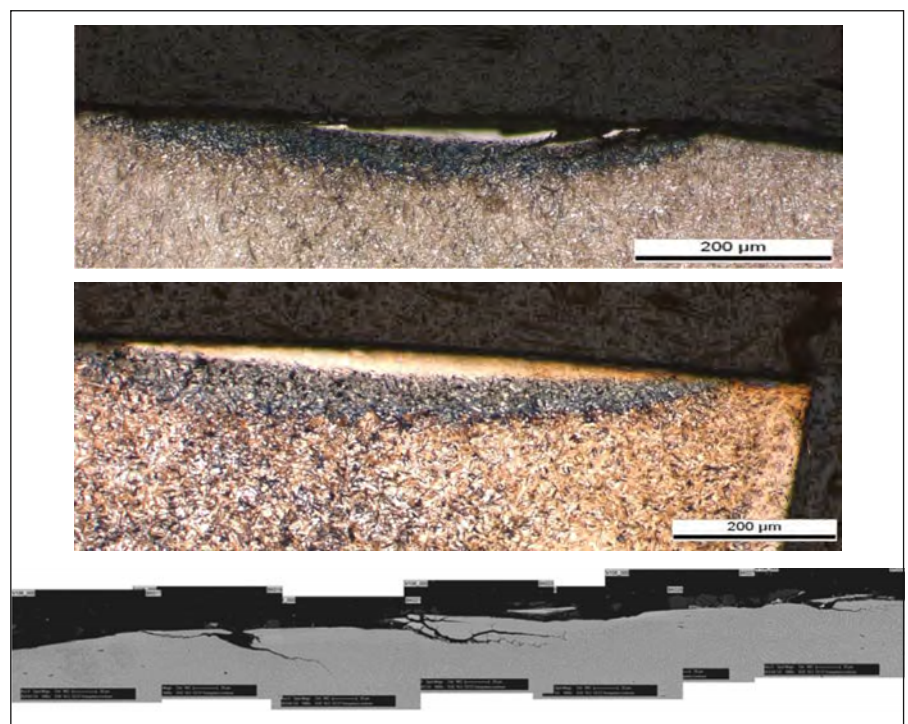


Figure 4: Optical microscopy of cross sections of severe wear areas of pinion (top) and gear (middle); SEM picture series of pinion wear area (bottom)

in elemental composition. However, complementary to optical microscopy, also SEM analysis of the gear tooth showed coarse embrittlement at grain boundaries at the top land edge of the cross section.

For further characterization of properties of these altered surface layers nanoindentation was used. Therefore, a line of nano indents was made across the bright and dark etching layer well into the bulk material while hardness (H) and reduced Young's Modulus (E_R) were measured (Table 2). For reference values another line scan from the tooth flank surface into the bulk was made in 1.5 mm distance.

Embedded cross sections of both, pinion and gear tooth were also analyzed by ToF-SIMS. From investigations using high current bunched mode it is evident, that at the surface of the tooth flanks in the region of severe wear a major amount of oxygen is present. For this oxygen aggregation primarily iron oxide is accounted for but also minor amounts of manganese and chromium oxides are present. Mainly, these increased oxide ion intensities are found at sites of fine cracks and burst off material (Figure 5). This is confirmed by burst alignment mode with high lateral resolution, where high oxide ion intensities of iron, manganese and chromium are detected

	E_R (GPa)	H (GPa)
Reference area	210	9,5
White etching zone	200 - 230	10 - 21
Dark etching zone	170	4,3

Table 2: Reduced Young's Modulus (E_R) and Hardness (H) of severe wear area

in particular inside pits and along the very thin fissures in the outermost brittle white etching layer.

Additionally, at the unstressed top land of the gear tooth heavy oxidation at the grain boundaries was detected. However, no iron oxide is present in this region and oxides consist mainly of manganese and chromium oxides (Figure 6). In the bulk material manganese as a steel additive is binding undesirable sulfur as manganese sulfide. It is clearly visible that the increased amount of manganese at the top land area is only correlated to the accumulation of its oxide as no sulfur and manganese sulfide is detected in this region.

Furthermore, one other obvious aspect visible in ToF-SIMS measurements is the decrease of iron, manganese and chromium ion intensities towards the sample edge of the cross section at the severe wear zone for both, the pinion and the gear tooth. However, the decre-

ase of yield of ions definitely already starts further inwards the bulk region than could be estimated by the dark etching area visible in optical microscopy images.

4 Discussion

Images of optical microscopy show areas of severe wear on both, the pinion drag side and the gear drag side. These wear zones appear on corresponding sites at the gear drag heel side top and the pinion drag heel side bottom of the teeth. Similar behavior is seen throughout the gear and pinion on every tooth at the same position. An unstressed region, visible at the pinion tooth flank, is as processed and no contact to the opposite tooth occurs. Apparently, the gear and pinion do not engage in a smooth sliding motion but instead a rather intense collision of the gear top and the pinion bottom seems to take place, at least temporarily in the test run. As these regions experience extreme tribological stress levels, this leads to severe wear and surface deterioration.

Particles which can be seen on the tooth bottom are wiped from the tooth flank by the curved sliding motion of the engaged pinion and gear teeth and gather at the non-contact zone at the bottom. These particles mainly consist of globular wear debris of the steel surface but also other contaminations are present. Additionally, oil and additive residues are smeared down from the tooth surface and gathered at the bottom. Carbon present at the surface usually derives from atmospheric contaminations.

As the different gear teeth have been separated by WEDM, zinc and copper residues most probably derive from this cutting process. The influence of this cutting process and cleaning procedures on the residues, especially sulfur, is evident. Oil analysis showed much more sulfur than phosphorus contained in the oil but EDS and XPS measurements of oil residues on the surface only reveals traces of sulfur much below the amount of phosphorus. Furthermore, surface sulfur and phosphorus is detected also on the unstressed surface which points out the strong bonding of additives onto the surface.

The SEM image series give a detailed picture of the variation of the plastic deformation across the tooth flank. The distance of the heavy load region to the tooth top varies from heel to toe side as the line of contact from pinion and gear in hypoid gears describes an s-like curve across the tooth flank. This correlates with results of computational simulations of the kinematics which were performed in tandem with the experimental and analytical investigations but are not described in this paper. In the region of highest load the original processing grooves of the tooth surface are completely evened out. In addition, in this area no additive tribolayers are visible due to the shear stress of the tooth surfaces. In less tribologically stressed areas lubricant additives are not instantly removed and residues

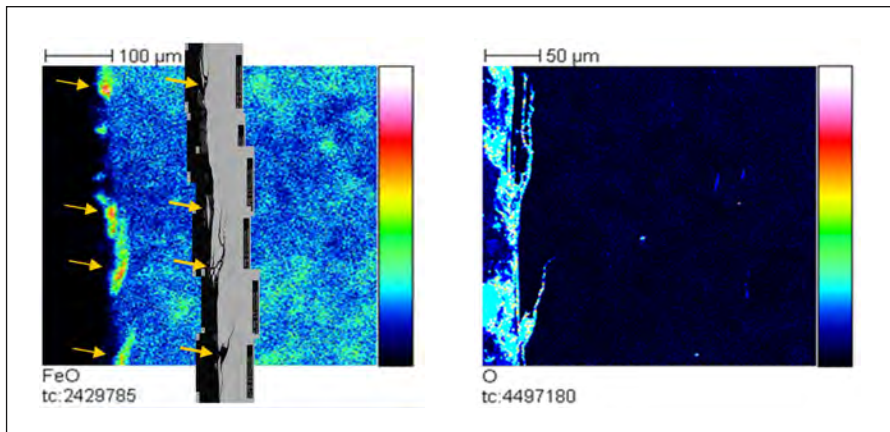


Figure 5: ToF-SIMS images of embedded cross sections of pinion's severe wear area: iron oxide overview (left); detailed view of oxygen in small fissures (right)

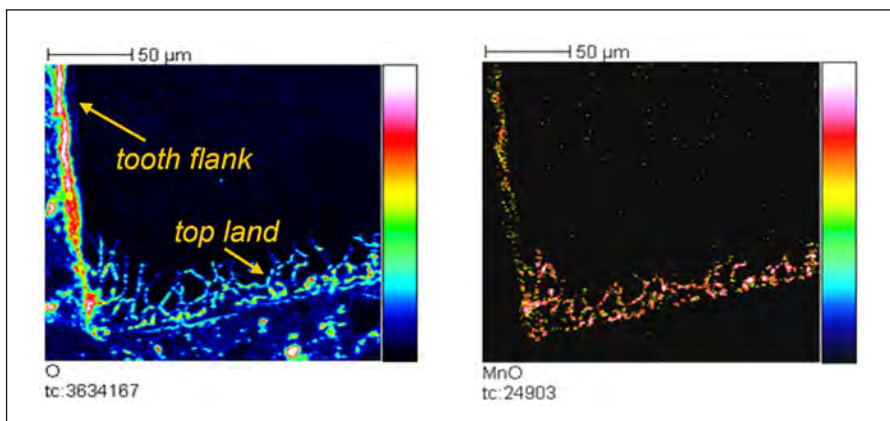


Figure 6: ToF-SIMS images of the embedded gear tooth cross section: oxides at tooth flank and top land (left); major manganese oxides at unstressed top land (right)

can still be detected. Furthermore, as load decreases from the line of contact to the top and bottom of the tooth flank, the original grinding grooves of the production process become more pronounced and less plastic deformation is visible.

The region of severe wear at the pinion drag side shows extreme surface alteration, removal of material and surface layers seem to be smeared over each other. Repeated impingement at the same location on the tooth flanks and resulting high pressure and temperature led to a change in microstructure of the steel. Analysis of etched cross sections reveals different layers at this severe wear zone. The modification and microstructure of the two resulting surface layers is deviant to the structure of the bulk material. Thus, the mechanical properties change and lead to different surface reactions when repeated impact at the same position of the tooth flank occurs.

Nanoindentation reveals the very different properties of these two layers and the main body of the gear teeth. While the outermost white etching layer exhibits increased values for hardness, it is also much more brittle than subjacent material as pits and cracks only occur in this surface layer. The underlying surface modification with a coarsely appearing structure after etching leads to softening of the subjacent material layer which may be due to local extreme thermal conditions generated by friction. Influence of the etching process on the mechanical values evaluated by nanoindentation is unknown. However, the differentiation of the varying regions on unetched polished samples was not clearly visible by nanoindenter analysis.

ToF-SIMS measurements of the cross sections reveal major oxygen intensities at the surface of the heavily worn area. Evidently, oxides appear at the very surface of this severe wear zone. Oxides of iron and to a lesser extent of manganese and chromium are found at the surface of the white etching layer as well as inside pits and cracks (**Figure 5**). Also inside the very small fissures, where new surface is generated and provided for oxidation ToF-SIMS investigations detected high oxide ion intensities.

Furthermore, a general decrease of ion intensity yield can be noticed towards the sample edge of the cross section, which is attributed to the change in structure of the material and consequently a change of the sputter coefficient of both, the white and dark etching layers. In addition, heavy manganese and chromium oxidation at the grain boundaries is found throughout the gear tooth top land whereas no iron oxide ions were detected in this region. However, the origin thereof is unknown as no unstressed reference sample was available for being inspected.

5 Conclusion

Results of these investigations show that the combination of several analytical methods yields a significant overview on the condition of a given tribosystem. A vast spectrum of information is gained and leads to profound insight of tribological processes on the surface while the system is in motion and heavy load is applied.

The details of analytical investigation reveal relevant procedures during the friction pro-

cess especially tribomechanical and tribochemical alterations of the mating surfaces. Understanding of the reasons of energy loss and wear on the surface is the key for system optimization. On the basis of these results essential knowledge is achieved for the improvement of future gear systems.

6 Acknowledgements

This work was supported by the COMET K2-program and carried out in the project „XTribology“ by AC²T research GmbH – Austrian Competence Center for Tribology.

Thankfully acknowledged is the support and fruitful cooperation contributed to this work by Mr. Dipl.-Ing. Schöfmann (MAGNA Powertrain AG & Co KG) and by Mr. Prof. Hutter, providing the possibility of ToF-SIMS measurements (Vienna University of Technology, Institute of Chemical Technologies and Analytics).

7 Literature

- [1] Wopelka Th., Jech M., Böhm J., Franek F.: Comparison of different wear measurement methods for a piston ring – cylinder liner system on a model tribometer, Technische Akademie Esslingen (TAE), International Colloquium on Tribology Lubricants, 2008
- [2] Stadler A., Brenner J., Pauschitz A., Wendrinsky J., Schindel A., Nauer G.: Surface analytics of different boundary layers on steel discs formed in a lubricated tribocontact during laboratory tests as compared to field application, Analytical and Bioanalytical Chemistry, Vol 390, No 6, 01.03.2008, pp 1527-1535, 2008

Hier sollte auch IHRE Firmen-Information zu finden sein!

Wenn auch Sie die Leser von T + S über Ihre aktuellen Broschüren und Kataloge informieren möchten, empfehlen wir Ihnen, diese neue Werbemöglichkeit zu nutzen.

Für weitere Informationen – wie Gestaltung, Platzierung, Kosten – wenden Sie sich bitte gleich an Nicole Stickel, die Ihnen jederzeit gerne mit Rat und Tat zur Verfügung steht.

Telefon (0 71 59) 92 65-13
 Telefax (0 71 59) 92 65-20
 E-Mail: stickel@expertverlag.de
 Internet: www.expertverlag.de

expert  **verlag**®
 Erlesene Weiterbildung®

11.2 Publication B

Atmospheric pressure matrix-assisted laser desorption/ionization mass spectrometry of friction modifier additives analyzed directly from base oil solutions



Atmospheric pressure matrix-assisted laser desorption/ionization mass spectrometry of friction modifier additives analyzed directly from base oil solutions

Lukas Widder,^{a,b} Josef Brenner^b and Herbert Hutter^a

^aVienna University of Technology, Institute of Chemical Technologies and Analytics, 1040 Vienna, Austria. E-mail: Widder@ac2t.at

^bAC2T Research GmbH, Austrian Center of Competence for Tribology, 2700 Wiener Neustadt, Austria

To develop new products and to apply measures of quality control quick and simple accessibility of additive composition in automotive lubrication is important. The aim of this study was to investigate the possibility of analyzing organic friction modifier additives by means of atmospheric pressure matrix-assisted laser desorption/ionization mass spectrometry (AP-MALDI-MS) from lubricant solutions without the use of additional separation techniques. Analyses of selected friction modifier ethoxylated tallow amines and oleic acid amide were compared using two ionization methods, positive-ion electrospray ionization (ESI) and AP-MALDI, using a LTQ Orbitrap mass spectrometer. Pure additives were characterized from solvent solutions, as well as from synthetic and mineral base oil mixtures. Detected ions of pure additive samples consisted mainly of $[M + H]^+$, but also alkali metal adducts $[M + Na]^+$ and $[M + K]^+$ could be seen. Characterizations of blends of both friction modifiers from the base oil mixtures were carried out as well and showed significant intensities for several additive peaks. Thus, this work shows a method to directly analyze friction modifier additives used in the automotive industry from an oil blend via the use of AP-MALDI without any further separation steps. The method presented will further simplify the acquisition of data on lubricant composition and additives. Furthermore, it allows the perspective of analyzing additive reaction products directly from formulated oil blends.

Keywords: AP-MALDI, mass spectrometry, lubrication, additives, friction modifier

Introduction

Atmospheric pressure matrix-assisted laser desorption/ionization mass spectrometry (AP-MALDI-MS)^{1–3} has evolved as an important method for the analysis of small molecules in recent years.^{4,5} This technique allows the investigation of surface-bound molecules of thin films and adsorbed layers. Surface analysis using AP-MALDI is mainly used in the field of proteomics and for investigations of biomolecules^{6–10} due to its relatively soft ionization process.^{1,11} AP-MALDI has not yet been widely applied to additive chemistry but research has been undertaken on ethoxylated surfactants and anti-

oxidants.^{4,5} In an atmospheric environment generally lower ion intensities are achieved, whereas in AP-MALDI experiments more volatile molecule species are also accessible, which would be lost in vacuum-MALDI systems. For this work the sensitive technique of AP-MALDI was expanded for the investigation of surface-active friction-modifier additives in automotive lubrication.

Lubrication of gear and transmission systems is commonly required in the automotive industry. Modern quality standards on lubrication cannot be satisfied without high-performance

additives since natural base oils and additives do not meet these requirements.¹²⁻¹⁴ Therefore, synthetic lubricants and a large amount of additive types have been developed over the past decades. Lubrication additives are intended to serve in various roles, such as antioxidants, dispersants, viscosity index improvers, friction modifiers, corrosion inhibitors, as well as many others, and are widely used in commercial lubricants to optimize system performance.¹⁵⁻¹⁷ In this work the focus was on the additive group of friction modifiers.

Organic friction modifiers are one widely used group of lubricant additives. Their properties improve fuel efficiency due to reduced wear and friction and enhanced friction stability.¹⁷ Organic friction modifiers take effect in the boundary lubrication regime. The structure of friction modifiers usually includes a polar head group and an alkyl chain. These molecules provide a cushioning effect in minor surface contacts due to a physisorption process of the polar groups.¹⁸⁻²⁰ Through adhesive hydrogen bonding of the polar head groups, organic friction modifiers are adsorbed onto the metal surface and Van der Waals forces between the long alkyl chains lead to a stabilized alignment of adjacent molecules.²¹ In this way adsorbed layers are formed on the metal surfaces.

It was shown in previous studies that friction modifiers can form thick layers in tribologically stressed surface contacts.^{22,23} These tribolayers are generally formed by additive molecules as well as reaction products of both the additives and the base lubricant.²⁴ As tribolayers alter the contact surface they are the main influence on changes in friction behavior of a tribological system. Knowledge about what chemical composition of surface layers is to be expected from certain lubricants is essential for improvement of the design of both contact surfaces and the lubricant formulation.

Conventional organic friction modifiers include alkoxyated tallow amines and oleamide,²⁵⁻²⁷ which have been in use for several years in the formulation of automotive lubricants. Both friction modifiers are used for their ability to improve friction behavior as well as for their properties as corrosion inhibitors.¹⁷ Tallow amines are nitrogen derivatives mainly from natural sources, such as beef tallow, and derived fatty acids. For use as friction modifier these fatty amines are ethoxylated with ethylene oxide.²⁷ Ethoxylated tallow amines, therefore, are a mixture of molecules with a distribution of different carbon-chain lengths²⁷ and polyoxyethylene chains. Their molecular weight distribution can readily be observed by mass spectrometry.

Work for this research was carried out on a linear ion trap tandem mass spectrometer (LIT-MS) with an Orbitrap mass analyzer for high resolution and mass accuracy.^{2,28,29} Additionally, to confirm the AP-MALDI ionization behavior of both organic friction modifiers, electrospray ionization (ESI) was applied as well. Mass analysis using the same detection system should yield similar results as was shown in recent investigations.^{5,11} LIT-collision induced dissociation (CID) MS was applied for fragmentation experiments in ESI to confirm the chemical structures of the investigated analytes.

In a first step, pure friction-modifier additives were measured individually from solutions of suitable solvents as stated in the Methods using positive-ion ESI and AP-MALDI. Whereas surface-bound molecules are not readily accessible in direct infusion electrospray ionization mass spectrometry, an advantage of AP-MALDI is the possibility to ionize selectively the polar molecules of adsorbed additive layers on metal surfaces derived from liquid lubricant films. Friction-modifier additives were investigated via AP-MALDI in base oils individually and, eventually, blends of both friction modifiers with base oils were analyzed directly from the target surface without the use of any further separation techniques. These results promise improved access to lubricant composition.

Methods

Chemicals and reagents

Ethoxylated tallow amines were purchased from Chem Service Inc. (West Chester, PA, USA) and oleic acid amide (98%) was purchased from Sigma-Aldrich (Vienna, Austria). Acetonitrile (LC-MS Chromasolv[®] grade), methanol (LC-MS Chromasolv[®] grade), 2-propanol (LC-MS Chromasolv[®] grade), water (LC-MS Chromasolv[®] grade), and acetic acid (99.9%, analytical grade, p.a.) were obtained from Sigma-Aldrich (Vienna, Austria). Stocks of synthetic base oil consisting of polyalphaolefines (PAO, 6 cSt; base oil group IV) and hydrocracked mineral base oil of Nexbase 3043 (base oil group III) were generously provided by LUKOIL Lubricants Austria GmbH (Vienna, Austria). For use in the AP-MALDI experiments the matrix α -cyano-4-hydroxycinnamic acid (CHCA) was purchased from Sigma-Aldrich (St. Louis, MO, USA).

Mass spectrometry

Electrospray ionization linear ion trap Orbitrap mass spectrometry

Mass spectrometric measurements were undertaken on an LTQ Orbitrap XL[™] hybrid tandem mass spectrometer (Thermo Fisher, Bremen, Germany). The IonMax[™] atmospheric pressure ionization source was equipped with an ESI probe for direct-infusion experiments. Orbitrap mass analyses for high resolution and mass accuracy were performed in positive-ion ESI. Applied experimental conditions for the ESI ion source were: transfer capillary temperature 275°C, spray voltage 4 kV, capillary voltage 11 V, nitrogen sheath gas 10 arbitrary units. Helium was used as the collision gas for low-energy collision-induced dissociation (LE-CID) experiments with normalized collision energy of 30%. The obtained resolution for mass and CID spectra was given as full width at half maximum (FWHM) of 30,000. Mass accuracy was calibrated externally and all measurements were performed with mass accuracy better than 5 ppm.

Pure samples of ethoxylated tallow amine and oleamide were dissolved in isopropanol/water (4:1, v/v) and isopropanol/water (7:3, v/v), respectively. Samples were applied to the MS-system via direct infusion with a flow rate of 5 $\mu\text{l min}^{-1}$. The

acquisition time for ESI-MS experiments was set to 0.5 min to obtain a sufficient signal-to-noise ratio.

AP-MALDI-MS

AP-MALDI experiments were conducted using an AP-MALDI PDF+ ion source obtained from MassTech (Columbia, MD, USA). All measurements using the AP-MALDI PDF+ ion source were carried out in the positive-ion mode. The wavelength of the all-solid-state triple-frequency Nd:YAG laser source was 355 nm operated at a repetition rate of 10 Hz. The laser pulse width was at 3–5 ns (FWHM) with a pulse energy of 200 μ J, which could be attenuated from 100% to 0%. The pulse delay for pulsed dynamic focusing (PDF) was set to 25 μ s to optimize ion signals.³⁰ The temperature of the transfer capillary was set to 275 °C and the automatic gain control was turned off to secure an equal acquisition time for each single-scan event.^{2,31} Overall acquisition time for all the AP-MALDI experiments was set to 0.5 min. Matrix solutions of CHCA were prepared at concentrations of 10 mg ml⁻¹ in acetonitrile/water (1:1, v/v).

Pure additive samples of ethoxylated tallow amines were dissolved in mixtures of acetonitrile/water (1:1, v/v), whereas samples of pure oleic acid amide were dissolved in methanol/water (2:1, v/v). Concentrations of both additives in the solutions spotted on the target plate were 5 μ l ml⁻¹ and 2 μ l ml⁻¹, respectively. For the investigations of additives in base oil solutions the friction modifiers were dissolved in synthetic and mineral oils at a concentration of 20 μ l ml⁻¹ and diluted in acetonitrile/water (1:1, v/v) to a concentration of 0.1 μ l ml⁻¹ in the spotted droplet. Blends of both pure additives in one solution were dissolved in a solvent mixture of methanol/acetonitrile/water (5:3:3, v/v/v) or in base oil at a concentration of 0.1 μ l ml⁻¹ and 10 μ l ml⁻¹ for ethoxylated tallow amines and oleic acid amides, respectively. All solutions were thoroughly mixed with the matrix solution and a small amount of acetic acid (<1%, v/v) was added to enhance protonation and increase the signal-to-noise ratio. All the given additive concentration values represent the spotted droplet including matrix solutions. The gold-coated stainless-steel target was cleaned carefully with methanol before each AP-MALDI experiment. An amount of 1 μ l was spotted onto the AP-MALDI gold-coated target. Several 1 μ l spots were set side by side, although each spot was only used once for an AP-MALDI measurement.

Results

ESI-MS

Mass spectra of the chosen friction modifier additives were measured using positive-ion ESI to confirm the peak identification of the AP-MALDI experiments. Owing to the poor deprotonation abilities of the aminic and amidic head groups of the additives used, experiments in negative-ion mode were not performed in this study.^{5,32}

Ethoxylated tallow amines exhibited a homologous series of peaks with a different hydrocarbon chain length and varying

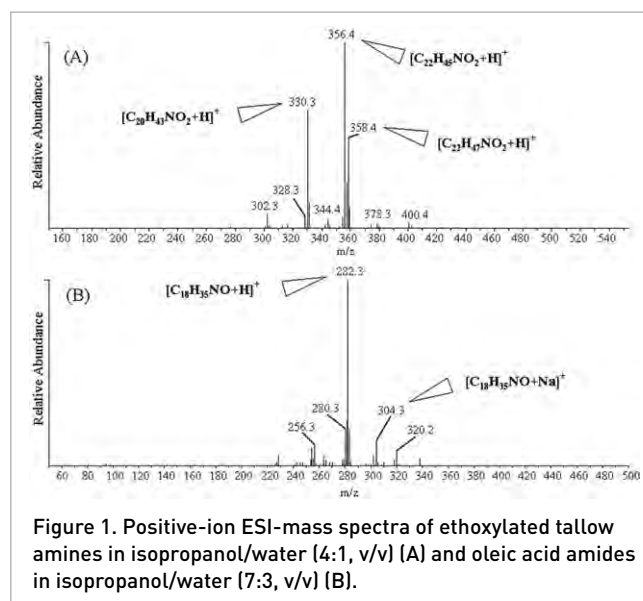


Figure 1. Positive-ion ESI-mass spectra of ethoxylated tallow amines in isopropanol/water [4:1, v/v] (A) and oleic acid amides in isopropanol/water [7:3, v/v] (B).

number of adhering ethoxy groups, as seen in Figure 1. The observed chain lengths range from 14 carbon atoms to 18 carbon atoms. Although most hydrocarbon moieties were saturated, unsaturated hydrocarbon chains with one or two double bonds were detected also. The m/z values of the measured peaks correspond to a number of adhering ethoxy groups, from one to three. Different types of ion species could be observed and identified. Peaks with the highest intensities were found at m/z values of 330.3, 356.4, and 358.4. These m/z values correspond to chain lengths of 16 and 18 carbon atoms including one double bond for m/z 356.4 and saturated carbon chains for m/z 330.3 and m/z 358.4. Additional to these protonated molecule species $[M + H]^+$, sodium adducts $[M + Na]^+$ were observed. A list of measured m/z values of major peaks for ethoxylated tallow amines is given in Table 1.

Cationized molecule species of oleamide samples included $[M + H]^+$ at an m/z value of 282.3, as well as alkali metal adducts $[M + Na]^+$ and $[M + K]^+$ at m/z values of 304.3 and 320.2, respectively. A list of measured m/z values of major peaks for oleic acid amide is given in Table 2.

Additionally, CID fragmentation experiments of high-intensity peaks were conducted to confirm the structural appearance of used additive substances. Spectra of fragmented additive peaks are shown in Figure 2. Fragmentation of the high-intensity peak at m/z 356.4 of ethoxylated tallow amines shows a prominent peak at m/z 338.3, which has a mass difference of 18.0 Da and represents the loss of a terminal oxygen as H_2O . The product ion at m/z 312.3 was formed by a mass loss of 44.0 Da and corresponds to one ethoxy side chain (C_2H_5O). A mass loss of 250.3 Da correlates to a dispatched carbon chain ($C_{18}H_{34}$), which leads to a secondary amine with two ethoxy groups at m/z 106.1. The fragment corresponding to the carbon chain itself could not be detected at m/z 250.3 due to the low ionizability of hydrocarbons in ESI-MS.

Fragmentation of the oleic acid amide peak at m/z 282.3 led to two main product ions with high-intensity peaks at

Table 1. Peak identification of ethoxylated tallow amines as seen in positive-ion ESI and AP-MALDI experiments.

<i>m/z</i>	Number of carbon atoms in chain	Number of double bonds	Number of ethoxy groups	Adduct ion	Ion composition
296.294	17	2	1	H ⁺	[C ₁₉ H ₃₇ NO + H] ⁺
298.310	17	1	1	H ⁺	[C ₁₉ H ₃₉ NO + H] ⁺
300.289	14	1	2	H ⁺	[C ₁₈ H ₃₇ NO ₂ + H] ⁺
302.304	14	0	2	H ⁺	[C ₁₈ H ₃₉ NO ₂ + H] ⁺
312.325	18	1	1	H ⁺	[C ₂₀ H ₄₁ NO + H] ⁺
316.320	15	0	2	H ⁺	[C ₁₉ H ₄₁ NO ₂ + H] ⁺
328.320	16	1	2	H ⁺	[C ₂₀ H ₄₁ NO ₂ + H] ⁺
330.336	16	0	2	H ⁺	[C ₂₀ H ₄₃ NO ₂ + H] ⁺
342.336	17	1	2	H ⁺	[C ₂₁ H ₄₃ NO ₂ + H] ⁺
344.351	17	0	2	H ⁺	[C ₂₁ H ₄₅ NO ₂ + H] ⁺
352.320	16	0	2	Na ⁺	[C ₂₀ H ₄₃ NO ₂ +Na] ⁺
354.336	18	2	2	H ⁺	[C ₂₂ H ₄₃ NO ₂ + H] ⁺
356.351	18	1	2	H ⁺	[C ₂₂ H ₄₅ NO ₂ + H] ⁺
358.367	18	0	2	H ⁺	[C ₂₂ H ₄₇ NO ₂ + H] ⁺
372.346	16	1	3	H ⁺	[C ₂₂ H ₄₅ NO ₃ + H] ⁺
374.361	16	0	3	H ⁺	[C ₂₂ H ₄₇ NO ₃ + H] ⁺
378.333	18	1	2	Na ⁺	[C ₂₂ H ₄₅ NO ₂ +Na] ⁺
380.350	18	0	2	Na ⁺	[C ₂₂ H ₄₇ NO ₂ +Na] ⁺
398.361	18	2	3	H ⁺	[C ₂₄ H ₄₇ NO ₃ + H] ⁺
400.377	18	1	3	H ⁺	[C ₂₄ H ₄₉ NO ₃ + H] ⁺

m/z 265.3 and *m/z* 247.2. These mass differences of 17.1 Da and 35.1 Da, respectively, correspond to losses of (NH₃) and (NH₃ + H₂O). A low-intensity peak at *m/z* 264.3 represents the loss of a water molecule with mass loss 18.0 Da (H₂O). Peaks of the homologous series between *m/z* 240 and *m/z* 80 correspond to differing hydrocarbon chain lengths separated by the mass of single CH₂ groups, where varying components of the amide head group are attached.

Table 2. Peak identification of oleic acid amides as seen in positive-ion ESI and AP-MALDI experiments.

<i>m/z</i>	Number of carbon atoms	Number of double bonds	Adduct ion	Ion composition
226.215	14	1	H ⁺	[C ₁₄ H ₂₇ NO + H] ⁺
228.230	14	0	H ⁺	[C ₁₄ H ₂₉ NO + H] ⁺
254.246	16	1	H ⁺	[C ₁₆ H ₃₁ NO + H] ⁺
256.261	16	0	H ⁺	[C ₁₆ H ₃₃ NO + H] ⁺
280.262	18	2	H ⁺	[C ₁₈ H ₃₃ NO + H] ⁺
282.277	18	1	H ⁺	[C ₁₈ H ₃₅ NO + H] ⁺
302.243	18	2	Na ⁺	[C ₁₈ H ₃₃ NO+Na] ⁺
304.259	18	1	Na ⁺	[C ₁₈ H ₃₅ NO+Na] ⁺
318.217	18	2	K ⁺	[C ₁₈ H ₃₃ NO+K] ⁺
320.232	18	1	K ⁺	[C ₁₈ H ₃₅ NO+K] ⁺

AP-MALDI-MS

Pure ethoxylated tallow amine samples dissolved in acetonitrile/water (1:1, v/v) and pure oleic acid amide samples dissolved in methanol/water (2:1, v/v) were measured to compare *m/z* values of additive peaks of ESI-MS and examine the accessibility of additive samples via the AP-MALDI method.

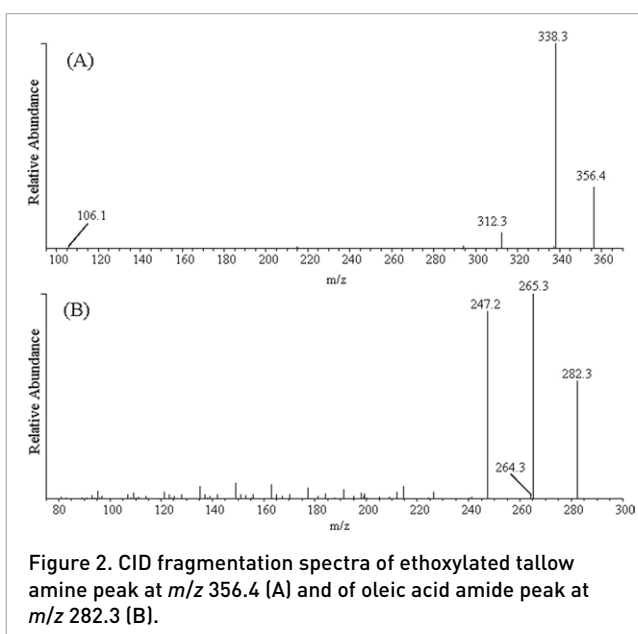
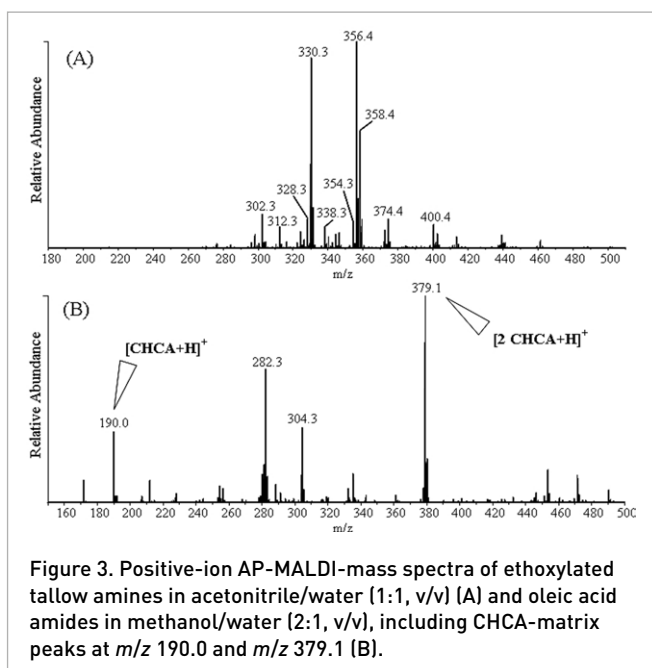


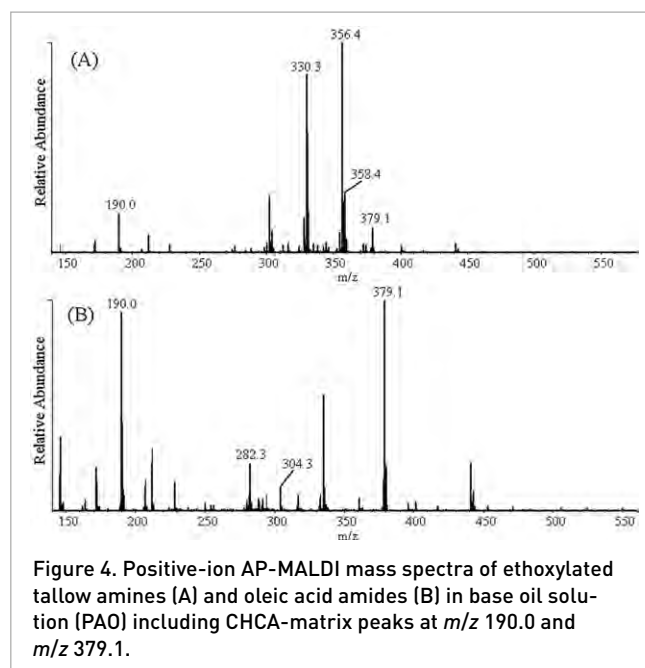
Figure 2. CID fragmentation spectra of ethoxylated tallow amine peak at *m/z* 356.4 (A) and of oleic acid amide peak at *m/z* 282.3 (B).



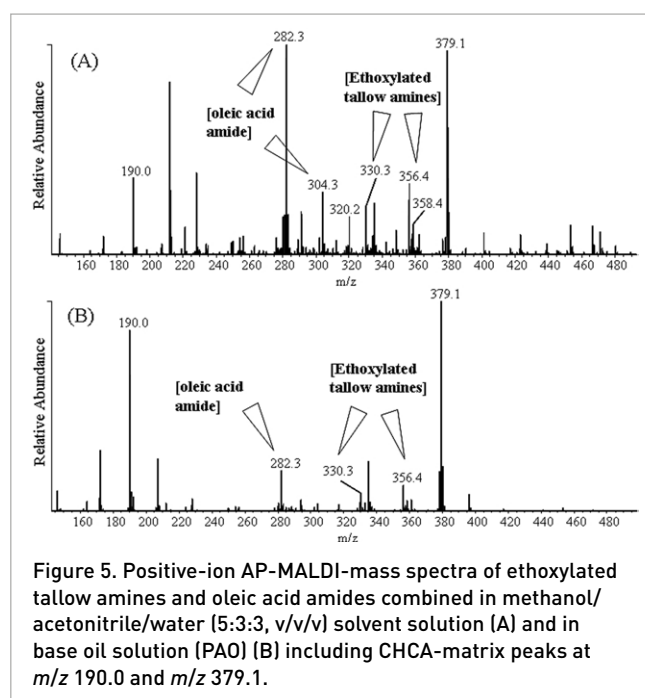
AP-MALDI measurements of both friction modifier additives in solvent solutions are shown in Figure 3. Peaks of the homologous series with different chain lengths and a varying number of ethoxy groups were observed, similar to ESI-MS measurements for ethoxylated tallow amines. The CHCA matrix was not visible due to suppression effects of the ethoxylated tallow amines, which show a higher ionization efficiency. High-intensity peaks of $[M + H]^+$ ions were observed at m/z values of 330.3, 356.4, and 358.4, as seen before in ESI-MS experiments [Figure 3(A)].

AP-MALDI measurements of pure oleic acid amide samples exhibited two major peaks of ion species $[M + H]^+$ and $[M + Na]^+$ at m/z 282.3 and m/z 304.3, respectively [Figure 3(B)]. Additional to the ESI measurements, various peaks of the CHCA-matrix single molecules were detected where $[M + H]^+$ had the highest intensity at m/z 190.0. Matrix adduct ions were also clearly visible, as well as a high-intensity matrix cluster ion consisting of two matrix molecules at m/z 379.1 for $[2M + H]^+$. AP-MALDI CID fragmentation experiments of high intensity peaks at m/z 356.4 and m/z 282.3 for ethoxylated tallow amines and oleic acid amines, respectively, exhibited similar spectra as fragmentation experiments using the ESI method.

Subsequently, pure additives were dissolved in synthetic oil PAO and mineral oil Nexbase 3043 (not shown), which were used as base oils. Measurements utilizing the AP-MALDI method can be seen in Figure 4(A). Peaks of the significant homologous series are clearly visible and also minor matrix peaks were detected when measuring ethoxylated tallow amines in both base oils. Observed ionic species for the tallow amines were only $[M + H]^+$ with no other adduct ions visible. Compared to measurements of sample additives in solvents, similar or even slightly higher peak intensities could be reached.



Additionally, the oleic acid amide was dissolved in PAO and Nexbase 3043 (not shown). Major peaks at the same m/z values appeared as when measured by ESI-MS in pure solvents [Figure 4(B)]. Ion species $[M + H]^+$ and sodium adducts $[M + Na]^+$ with a mass difference of +22 u were of significant intensity. Peak intensity of matrix $[M + H]^+$ and matrix cluster ions $[2M + H]^+$ at m/z 190.0 and m/z 379.1, respectively, exceeded the intensities of additive peaks. Overall peak intensity of the oleamide additive in base oil was around one-sixth of the intensities of the major peaks for ethoxylated tallow amines in PAO.



For further experiments, both additives were dissolved in the same solvent mixture of methanol/acetonitrile/water (5:3:3, v/v/v) and combined with the matrix solution. When measured by AP-MALDI, peaks of significant intensity of ion species $[M + H]^+$ of both additives could be detected. The spectra included high-intensity peaks at m/z 330.3, 356.4, and 358.4 of ethoxylated tallow amines [Figure 5(A)], as well as the peak at m/z 282.3 of oleic acid amide [Figure 5(B)]. For oleic acid, amide alkali metal adduct ions of $[M + Na]^+$ and $[M + K]^+$ were detected at m/z 304.3 and m/z 320.2, respectively. Additional to the additive peaks, minor matrix peaks were observed.

Subsequently, both additives combined were dissolved in PAO. The base oil mixture was added to the matrix solution and measured via AP-MALDI. Again, distinct peaks of both additives had significant intensities and were clearly visible. Additive peaks at m/z values of 282.3 and 356.4 obviously correspond to ethoxylated tallow amines and oleic acid amide, respectively. Generally, most matrix fragment and cluster peaks were of lower intensity than exhibited when measuring both additives together in the solvent mixture.

Conclusion

Both friction modifier additives analyzed could be successfully identified via the AP-MALDI method. Measurements were undertaken directly from the base oil mixture without the use of any separation techniques. Thus, we believe this is the first attempt to analyze friction-modifier additives directly from a formulated base oil mixture using AP-MALDI.

However, intensities of all the major peaks for both additives in the formulated base oils were slightly lower in comparison to analyzing each additive individually, either in solvents or in base oil. Since no difference could be detected between analysis in the synthetic and mineral base oil, results are shown only for additives in synthetic oil PAO. Matrix peaks could be observed more clearly when both additives were analyzed in one sample on account of lower suppression effects due to the lower concentration of ethoxylated tallow amines. Nonetheless, peak intensities for both, ethoxylated tallow amines and oleic acid amide, still had a significant signal-to-noise ratio sufficient for an effective identification. Comparison to ESI-MS and CID experiments confirmed the m/z values of friction modifier additives obtained in AP-MALDI.

The results presented herein provide a valuable gain in knowledge for the analysis of selected additives directly from the base oil mixtures without prior separation steps. In future experiments use of the AP-MALDI method has to be stretched to a wider range of additive molecules in the field of tribometry.

Acknowledgments

The work presented was funded by the "Austrian COMET Programme" (Project XTribology, no. 824187), the European Regional Development Fund (ERDF) and the country of Lower

Austria within the project "OnLab" and carried out at the "Excellence Centre of Tribology" (AC2T research GmbH).

References

1. V.V. Laiko, M.A. Baldwin and A.L. Burlingame, "Atmospheric pressure matrix-assisted laser desorption/ionization mass spectrometry", *Anal. Chem.* **72**(4), 652 (2000). doi: <http://dx.doi.org/10.1021/ac990998k>
2. V.V. Laiko, S.C. Moyer and R.J. Cotter, "Atmospheric pressure MALDI/ion trap mass spectrometry", *Anal. Chem.* **72**(21), 5239 (2000). doi: <http://dx.doi.org/10.1021/ac000530d>
3. S.C. Moyer, L.A. Marzilli, A.S. Woods, V.V. Laiko, V.M. Doroshenko and R.J. Cotter, "Atmospheric pressure matrix-assisted laser desorption/ionization mass spectrometry", in *Proceedings of the 47th ASMS Conference on Mass Spectrometry and Allied Topics*, Dallas (1999).
4. S.D. Hanton, D.M. Parees and J. Zweigenbaum, "The fragmentation of ethoxylated surfactants by AP-MALDI-QIT", *J. Am. Soc. Mass Spectrom.* **17**(3), 453 (2006). doi: <http://dx.doi.org/10.1016/j.jasms.2005.11.013>
5. A. Kassler, E. Pittenauer, N. Doerr and G. Allmaier, "Electrospray ionization and atmospheric pressure matrix-assisted laser desorption/ionization mass spectrometry of antioxidants applied in lubricants", *Rapid Commun. Mass Spectrom.* **23**(24), 3917 (2009). doi: <http://dx.doi.org/10.1002/rcm.4326>
6. V.V. Laiko, N.I. Taranenko, V.D. Berkout, M.A. Yakshin, C.R. Prasad, H.S. Lee and V.M. Doroshenko, "Desorption/ionization of biomolecules from aqueous solutions at atmospheric pressure using an infrared laser at $3\mu\text{m}$ ", *J. Am. Soc. Mass Spectrom.* **13**(4), 354 (2002). doi: [http://dx.doi.org/10.1016/S1044-0305\(02\)00341-0](http://dx.doi.org/10.1016/S1044-0305(02)00341-0)
7. A.J. Madonna, K.J. Voorhees, N.I. Taranenko, V.V. Laiko and V.M. Doroshenko, "Detection of cyclic lipopeptide biomarkers from *Bacillus* species using atmospheric pressure matrix-assisted laser desorption/ionization mass spectrometry", *Anal. Chem.* **75**(7), 1628 (2003). doi: <http://dx.doi.org/10.1021/ac020506v>
8. S.C. Moyer, C.E. Von Seggern and R.J. Cotter, "Fragmentation of cationized phosphotyrosine containing peptides by atmospheric pressure MALDI/ion trap mass spectrometry", *J. Am. Soc. Mass Spectrom.* **14**(6), 581 (2003). doi: [http://dx.doi.org/10.1016/S1044-0305\(03\)00142-9](http://dx.doi.org/10.1016/S1044-0305(03)00142-9)
9. N.I. Taranenko, V.M. Doroshenko, A.K. Shukla and M.M. Shukla, "Applications of AP-MALDI ion trap mass spectrometry for the analysis of phosphopeptides", *Am. Lab.* **36**(10), 34 (2004).
10. E. Pittenauer, M. Zehl, O. Belgacem, E. Raptakis, R. Mistrik and G. Allmaier, "Comparison of CID spectra of singly charged polypeptide antibiotic precursor ions

- obtained by positive-ion vacuum MALDI IT/RTOF and TOF/RTOF, AP-MALDI-IT and ESI-IT mass spectrometry”, *J. Mass Spectrom.* **41**(4), 421 (2006). doi: <http://dx.doi.org/10.1002/jms.1032>
11. B.B. Schneider, C. Lock and T.R. Covey, “AP and vacuum MALDI on a QqLIT instrument”, *J. Am. Soc. Mass Spectrom.* **16**(2), 176 (2005). doi: <http://dx.doi.org/10.1016/j.jasms.2004.10.004>
 12. D.C. Kramer, B.K. Lok and R.R. Krug; “The evolution of base oil technology”, *Am. Soc. Test. Mater. ASTM Special Technical Publication* **1407**, 25 (2001).
 13. W.J. Heilman, I.-C. Chiu, W. Song and J.C.W. Chien, “New synthetic hydrocarbon base oils”, *National Petrochemical and Refiners Association Annual Meeting Papers* **126**, (2001).
 14. D.C. Kramer, J.N. Ziemer, M.T. Cheng, C.E. Fry, R.N. Reynolds, B.K. Lok, M.L. Sztenderowicz and R.R. Krug, “Influence of group II & III base oil composition on VI and oxidation stability”, *NLGI Spokesman* **63**, 20 (2000).
 15. J. Braun, “Additives”, in *Lubricants and Lubrication*, Ed by T. Mang and W. Dresel. Wiley-VCH, Weinham, p. 43 (2003).
 16. F. Rounds, “Changes in friction and wear performance caused by interactions among lubricant additives”, *Lubr. Sci.* **1**(4), 333 (1989). doi: <http://dx.doi.org/10.1002/ls.3010010404>
 17. D. Kenbeck and T. Bunemann, “Organic friction modifiers”, in *Lubricant Additives: Chemistry and Applications*, Second Edition, Ed by L.R. Rudnick. CRC Press, Boca Raton, p. 195 (2009).
 18. J.-H. Choo, A.K. Forrest and H.A. Spikes, “Influence of organic friction modifier on liquid slip: a new mechanism of organic friction modifier action”, *Tribol. Lett.* **27**(2), 239 (2007). doi: <http://dx.doi.org/10.1007/s11249-007-9231-z>
 19. H.A. Spikes, “Boundary lubrication and boundary films”, *Tribol. Ser.* **25**, 331 (1993). doi: [http://dx.doi.org/10.1016/S0167-8922\(08\)70389-4](http://dx.doi.org/10.1016/S0167-8922(08)70389-4)
 20. M. Ratoi, V. Anghel, C. Bovington and H.A. Spikes, “Mechanisms of oiliness additives”, *Tribol. Int.* **33**(3-4), 241 (2000). doi: [http://dx.doi.org/10.1016/S0301-679X\(00\)00037-2](http://dx.doi.org/10.1016/S0301-679X(00)00037-2)
 21. R.P. Glovnea, A.V. Olver and H.A. Spikes, “Effectiveness of boundary lubricant additives on some coated surfaces”, *Tribol. Interface Eng. Ser.* **48**, 135 (2005). doi: [http://dx.doi.org/10.1016/S0167-8922\(05\)80016-1](http://dx.doi.org/10.1016/S0167-8922(05)80016-1)
 22. M. Ratoi, C. Bovington, H.A. Spikes, “In situ study of metal oleate friction modifier additives”, *Tribol. Lett.* **14**(1), 33 (2003). doi: <http://dx.doi.org/10.1023/A:1021714231949>
 23. V. Anghel, C. Bovington and H.A. Spikes, “Thick-boundary-film formation by friction modifier additives”, *Lubr. Sci.* **11**(4), 313 (1999). doi: <http://dx.doi.org/10.1002/ls.3010110402>
 24. A. Stadler, J. Brenner, A. Pauschitz, J. Wendrinsky, A. Schindel and G.E. Nauer, “Surface analysis of different boundary layers on steel discs formed in a lubricated tribocontact during laboratory test compared with field application”, *Anal. Bioanal. Chem.* **390**(6), 1527 (2008). doi: <http://dx.doi.org/10.1007/s00216-007-1730-0>
 25. M. Ingram, J. Noles, R. Watts, S. Harris and H.A. Spikes, “Frictional properties of automatic transmission fluids: Part I—Measurement of friction—sliding speed behavior”, *Tribol. Trans.* **54**(1), 145 (2011). doi: <http://dx.doi.org/10.1080/10402004.2010.531888>
 26. H. Zhao, A. Neville, A. Morina, R. Vickerman and J. Durham, “Improved anti-shudder performance of ATF—influence of a new friction modifier and surface chemistry”, *Tribol. Int.* **46**, 62 (2012). doi: <http://dx.doi.org/10.1016/j.triboint.2011.06.012>
 27. R. Franklin, “Nitrogen derivatives of natural fats and oils”, in *Surfactants from Renewable Resources*, Ed by M. Kjellin and I. Johansson. John Wiley & Sons, Chichester, p. 21 (2010). doi: <http://dx.doi.org/10.1002/9780470686607.ch2>
 28. S.C. Moyer, L.A. Marzilli, A.S. Woods, V.V. Laiko, V.M. Doroshenko and R.J. Cotter, “Atmospheric pressure matrix-assisted laser desorption/ionization (AP MALDI) on a quadrupole ion trap mass spectrometer”, *Int. J. Mass Spectrom.* **226**(1), 133 (2003). doi: [http://dx.doi.org/10.1016/S1387-3806\(02\)00972-7](http://dx.doi.org/10.1016/S1387-3806(02)00972-7)
 29. K.A. Kellersberger, P.V. Tan, V.V. Laiko, V.M. Doroshenko and D. Fabris, “Atmospheric pressure MALDI-Fourier transform mass spectrometry”, *Anal. Chem.* **76**(14), 3930 (2004). doi: <http://dx.doi.org/10.1021/ac0498415>
 30. P.V. Tan, V.V. Laiko and V.M. Doroshenko, “Atmospheric pressure MALDI with pulsed dynamic focusing for high-efficiency transmission of ions into a mass spectrometer”, *Anal. Chem.* **76**(9), 2462 (2004). doi: <http://dx.doi.org/10.1021/ac0353177>
 31. T.J. Garrett, M.C. Prieto-Conaway, V. Kovtoun, H. Bui, N. Izgarian, G. Stafford and R.A. Yost, “Imaging of small molecules in tissue sections with a new intermediate-pressure MALDI linear ion trap mass spectrometer”, *Int. J. Mass Spectrom.* **260**(2-3), 166 (2007). doi: <http://dx.doi.org/10.1016/j.ijms.2006.09.019>
 32. T. Henriksen, R.K. Juhler, B. Svensmark, and N.B. Cech, “The relative influences of acidity and polarity on responsiveness of small organic molecules to analysis with negative ion electrospray ionization mass spectrometry (ESI-MS)”, *J. Am. Soc. Mass Spectrom.* **16**(4), 446 (2005). doi: <http://dx.doi.org/10.1016/j.jasms.2004.11.021>

11.3 Publication C

Modified-Atmospheric Pressure-Matrix Assisted Laser Desorption/Ionization Identification of Friction Modifier Additives Oleamide and Ethoxylated Tallow Amines on Varied Metal Target Materials and Tribologically Stressed Steel Surfaces

Modified-Atmospheric Pressure-Matrix Assisted Laser Desorption/Ionization Identification of Friction Modifier Additives Oleamide and Ethoxylated Tallow Amines on Varied Metal Target Materials and Tribologically Stressed Steel Surfaces

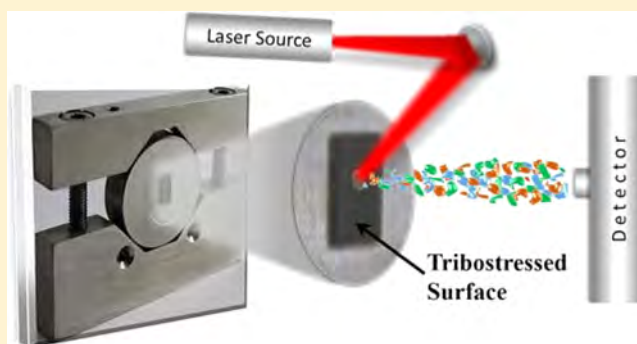
Lukas Widder,^{*,†,‡} Andjelka Ristic,[‡] Florian Brenner,[†] Josef Brenner,[‡] and Herbert Hutter[†]

[†]Institute of Chemical Technologies and Analytics, Vienna University of Technology, Getreidemarkt 9/164, 1060 Vienna, Austria

[‡]AC2T research GmbH, Austrian Center of Competence for Tribology, Viktor-Kaplan-Straße 2C, 2700 Wiener Neustadt, Austria

Supporting Information

ABSTRACT: For many tasks in failure and damage analysis of surfaces deteriorated in heavy tribological contact, the detailed characterization of used lubricants and their additives is essential. The objective of the presented work is to establish accessibility of tribostressed surfaces for direct characterization via modified atmospheric pressure-matrix assisted laser desorption/ionization-mass spectrometry (m-AP-MALDI-MS). Special target holders were constructed to allow target samples of differing shape and form to fit into the desorption/ionization chamber. The best results of desorption and ionization on different target materials and varying roughnesses were achieved on smooth surfaces with low matrix/substrate interaction. M-AP-MALDI characterization of tribologically stressed steel surfaces after pin-on-disc sliding wear tests (SRV-tribotests) yielded positive identification of used friction modifier additives. Further structure elucidation by electrospray ionization mass spectrometry (ESI-MS) and measurements of worn surfaces by time-of-flight-secondary ion mass spectrometry (TOF-SIMS) accompanied findings about additive behavior and deterioration during tribological contact. Using m-AP-MALDI for direct offline examinations of worn surfaces may set up a quick method for determination of additives used for lubrication and general characterization of a tribological system.



Atmospheric pressure-matrix assisted laser desorption/ionization-mass spectrometry (AP-MALDI-MS) was developed around the turn of the century^{1–3} and has been strongly improved over the years by using various types of mass spectrometers^{2,4–7} and different types of lasers.^{8–10} In recent years, AP-MALDI has been widely used for analytical purposes in proteomics and the emerging field of lipidomics.^{4–6,8,11–16} Only a little research has been carried out on additives such as cationic surfactants from wastewater,^{17,18} as well as ethoxylated surfactants¹⁹ and antioxidants²⁰ from lubricants, but no comprehensive study on organic friction modifiers (FM) utilizing AP-MALDI is known. Only recently, the general possibility to analyze friction modifier additives directly from base oil solutions via AP-MALDI-MS has been introduced.²¹ Furthermore, several materials have been used as AP-MALDI targets in previous studies, whereas the gold-covered metal target showed superior desorption/ionization yield.^{15,20}

Lubrication additives are important to improve friction properties of tribologically stressed surfaces.^{22–26} In this work, focus was placed on the additive group of friction modifiers as the reduction of the coefficient of friction is essential to increase energy efficiency in tribological systems.^{27–29} FM-additives are

widely used to enhance efficiency in boundary lubricant applications. In general, they appear in the form of long hydrocarbon chains with polar head groups. Typically, the polar head groups of FMs consist of amines and amides, as well as carboxylic acids and respective derivatives, i.e., detergent-like compounds.^{30–32} The additives used for the present investigations consisted of ethoxylated tallow amines (ETA) as well as oleamide (OA).

For the recent examinations, AP-MALDI was used to analyze a combination of the two FM-additives directly from the base oil solution on surfaces of various types of materials. The ionization intensity of the FM-additives on the original gold covered AP-MALDI target was compared to sample targets made of steel, aluminum, and three different copper alloys. All of these materials are widely applied throughout various tribological systems. The roughness of the alternative metal surfaces was varied, and the influence on the crystal formation, which influences the ionization efficiency, was evaluated.

Received: July 24, 2015

Accepted: October 22, 2015

Published: October 22, 2015

The objective of the herein presented work was to examine the general possibility to use the AP-MALDI method to identify oil components used as lubrication additive in a tribolayer of a tribologically stressed surface, similar to recent developments in offline monitoring of tribometrical experiments directly from disc specimens via vacuum-LDI-MS.³³ For this purpose, pin-on-disc sliding wear tests (SRV-tribotests) were conducted and the sample surface of the wear tracks was analyzed. Through modification of the AP-MALDI ionization chamber and application of especially manufactured sample holders, the use of SRV-discs and -cylinders as m-AP-MALDI sample targets became accessible. Furthermore, electrospray ionization mass spectrometry (ESI-MS) and time-of-flight-secondary ion mass spectrometry (TOF-SIMS) were used as supporting methods to identify additional fragments of single additive molecules and chemical reaction products of additive components within oil residues and tribolayers, respectively.

EXPERIMENTAL SECTION

Materials. Oleic acid amide (98.5%) was purchased from Sigma-Aldrich (Vienna, Austria), and the second friction modifier consisting of polyethoxylated tallow amines was purchased from Chem Service Inc. (West Chester, PA, USA). Additional chemicals such as acetonitrile, methanol, ethanol, water (all in LC-MS grade), and acetic acid (99.9%, analytical grade, p.a.) were purchased from Sigma-Aldrich (Vienna, Austria). Lukoil Lubricants Austria GmbH (Vienna, Austria) contributed the supply of the polyalphaolefine base oil (PAO, 6 cSt). AP-MALDI experiments were performed using α -cyano-4-hydroxycinnamic acid (CHCA) as matrix component, which was obtained from Sigma-Aldrich (Vienna, Austria).

Sample materials for experiments on varying surfaces were standard materials commonly used in industry applications. The standard AP-MALDI gold target used as reference material. Other materials include steel, aluminum, brass, bronze, and a nickel silicon bronze. All alternative target materials are listed in Table 1. For comparison of additive ionization intensities on

Table 1. Sample Description

sample	composition	description
gold	Au-covered steel	Reference AP-MALDI target
steel	100Cr6	1.3505, AISI 52100
Al	Al	aluminum
CuZn	CuZn25Al5Mn4Fe3	brass
CuSn	CuSn8P	bronze
CuNi	CuNi2Si	nickel silicon bronze

different target materials, samples were polished and additional surface grinding was used to vary the surface roughness. Sample roughness was measured via a Mahr MarSurf PS1 Perthometer, and 3D-microscopy was performed on an Alicona InfiniteFocusL applying the focus-variation method. Applied target specimens are given in Figure 1.

AP-MALDI. All m-AP-MALDI experiments were conducted using the AP-MALDI PDF+ ion source, which was obtained from MassTech (Columbia, MD, USA) on a LTQ Orbitrap XL hybrid tandem mass spectrometer (ThermoFisher Scientific, Bremen, Germany). Obtained results reached mass resolution of 60.000 (fwhm), and mass accuracy was better than 3 ppm. A frequency-tripled Nd:YAG laser with a wavelength of 355 nm was used as energy source. The pulse width of the laser was at 3–5 ns (fwhm), and it was operated at a repetition rate of 10 Hz

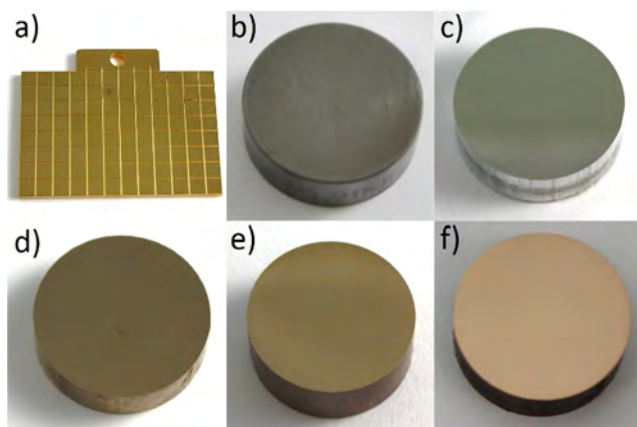


Figure 1. Variation of target materials used for analysis with new target holder: (a) Standard AP-MALDI target used as reference; (b) 100Cr6 SRV-disc used as steel sample; (c) aluminum target; (d) brass target; (e) bronze target; (f) nickel silicon bronze target.

with spiral motion. A pulse energy of 8 μ J was used while pulsed dynamic focusing (PDF)³⁴ was set to 25 μ s for signal optimization. To secure equal acquisition periods for all single scan events, automatic gain control (AGC) was turned off^{2,35} and acquisition time for one AP-MALDI experiment was set to 0.5 min. Measurements on varying surfaces were carried out on at least six different spots on one disc for each type of material. Results were used for calculation of average and maximum ion intensities. The CHCA matrix was mixed in solutions of acetonitrile/water 1:1 (v/v) in concentrations of 10 mg/mL. On unstressed surfaces, the dried droplet method was used, whereas in wear tracks the matrix was applied onto the analyte layer for modified AP-MALDI (m-AP-MALDI). The FM additive concentrations used were 2% and 0.025% in PAO for oleamide and polyethoxylated tallow amines, respectively. The base oil was warmed slightly in a water bath to enhance dissolving of the additives. To still allow homogeneous crystallization of the matrix, 40 μ L of the additive mixture was added to 1 mL of matrix solution. Droplets of 1.5 μ L were spotted onto the surface of the target samples and dried at 60 °C.

Sample Holders. For measurements on alternative target samples, special target holders for discs and cylinders of pin-on-disc tribotests were constructed out of stainless steel (Figure 2).

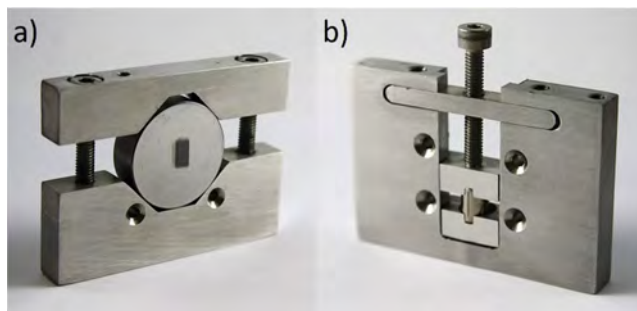


Figure 2. Novel in-house built conductive target holders made of stainless steel for m-AP-MALDI-MS: target holder for SRV-discs holding a used disc with visible wear track (a); target holder for SRV-cylinders holding a used cylinder (b). Both holders can be adapted for the use of targets of various size and shape through adjustable screws. Drilled holes on top of the target holders allow connection to the high voltage cable of the AP-MALDI system.

The in-house built target holders were fit into the ionization chamber of the AP-MALDI system. To install the new target holders, the high-voltage cable was disengaged and the original holder for the standard target was removed. Both sample holders, for cylinders and discs, respectively, are adaptable to the size and shape of the target material through adjustment screws. They are easily mounted into the AP-MALDI chamber and connected to the high-voltage cable.

Tribotests. SRV-tribotests were carried out on a reciprocating pin-on-disc tribometer (3rd generation SRV). Test parameters of 1.6 kN and a sliding speed of 1 m/s were applied for 1 h. The FM additive concentrations used for tribotesting were 2.5% and 0.05% in PAO for oleamide and polyethoxylated tallow amines, respectively. After SRV-tribotests, the samples were cleaned with ethanol. For m-AP-MALDI analysis, 1.5 μL droplets of CHCA-matrix were applied on the wear track. Oil residues collected in the cleaning process of the targets were analyzed through ESI-MS. For further elucidation of existing tribolayers after friction testing, TOF-SIMS measurements of wear tracks were conducted.

ESI-MS. Measurements using ESI-MS were performed in positive ion mode on the LTQ Orbitrap XL mass spectrometer by direct infusion (flow rate: 5 $\mu\text{L}/\text{min}$). The ESI interface was used to ionize and form the protonated molecular ions. The technique of ESI-MS is well-known to provide information on molecular mass and structure.³⁶ Orbitrap as a high resolution (>100 000) and high accuracy detector (better than 1 ppm) in combination with linear ion trap as external mass analyzer enables multiple levels of fragmentation. The following ESI ion source conditions were applied: spray capillary temperature, 275 $^{\circ}\text{C}$; spray voltage, 4.0 kV; capillary voltage, 27 V. Nitrogen (2 arbitrary units) was used as sheath gas and helium as collision gas in the linear ion trap section. LE-CID (low-energy collision-induced dissociation), like MS2 and MS3, was performed with an optimized normalized collision energy ranging from 25% to 40%. CID-generated fragment ions were detected by the high resolution Orbitrap-section of the instrument at a resolution of 60.000 (fwhm). All accurate mass measurements were acquired with a mass accuracy of 3 ppm or better. The original lubricant mixture before tribotesting was dissolved in methanol (dilution factor of 1000) and used as a reference sample. After the SRV-test, the residual lubricant was rinsed with ethanol from the disc's surface and diluted in methanol (dilution factor of 10).

TOF-SIMS. TOF-SIMS measurements were used as a complementary analytical technique to examine FM content of tribolayers after pin-on-disc tests. The device used was a TOF-SIMS 5 of Iontof GmbH (Münster, Germany). High current bunched mode was applied on the wear tracks with a pulse width of 16 ns for analysis of a $500 \times 500 \mu\text{m}^2$ region utilizing primary Bi_3^+ ion clusters of the liquid metal ion gun (LMIG) with a target current of 0.87 pA and a beam width of 2 μm .

RESULTS AND DISCUSSION

AP-MALDI. AP-MALDI measurements of a combination of lubrication additives out of a base oil solution on the gold-covered steel target were already described elsewhere in great detail.²¹ For this work, target materials have been varied to examine differences in ionization intensities and direct measurements of tribologically stressed surfaces have been undertaken. In addition to the gold-covered standard, model experiments were conducted on a 100Cr6 steel target and an aluminum target as well as three different copper alloys. Surface roughness R_a of the alternative targets was varied by polishing and two different

Table 2. Roughness R_a of Used AP-MALDI Targets

sample	polished [μm]	grinding step 1 [μm]	grinding step 2 [μm]
gold	0.021		
steel	0.007	0.019	0.035
Al	0.035	0.115	0.244
CuZn	0.016	0.023	0.039
CuSn	0.016	0.041	0.070
CuNi	0.014	0.020	0.081

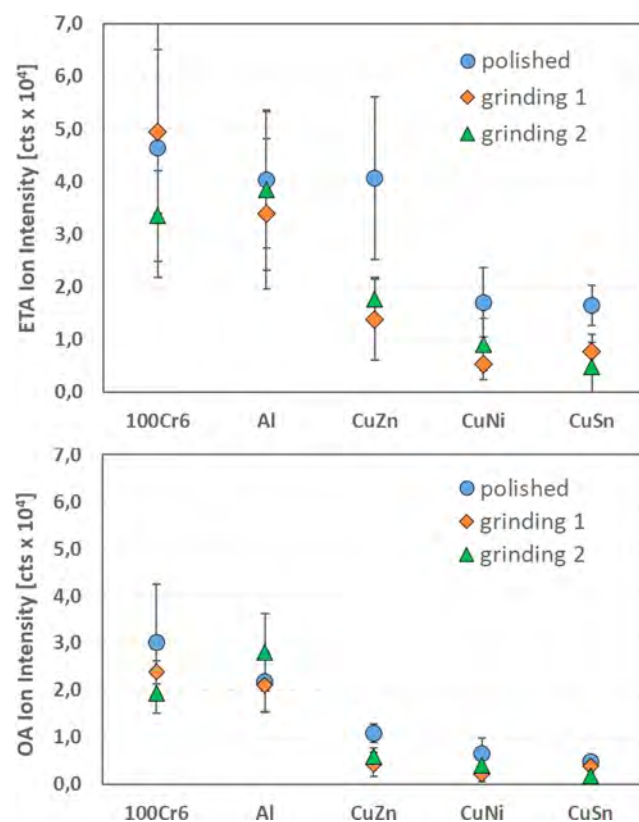


Figure 3. Average AP-MALDI ion intensities for ETA (top) and OA (bottom) on alternative target materials.

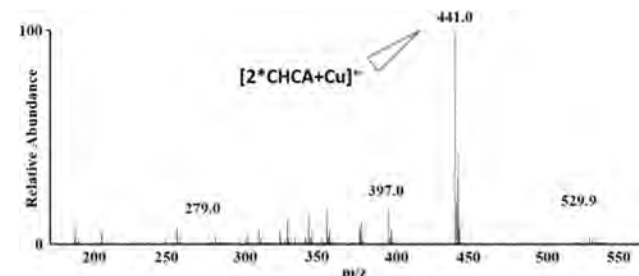


Figure 4. AP-MALDI-MS spectrum achieved on bronze target showing cluster ions of CHCA-matrix and copper.

surface grinding steps (grinding 1: lower roughness; grinding 2: higher roughness) and is given in Table 2.

Using the plain steel target, the highest ion intensities of all alternative target materials were accomplished, although values were still significantly lower than ion intensity of FM additives measured on the gold-covered target. Average ion intensity yields of ETA and OA on alternative target materials are given in Figure 3. The aluminum target showed excellent ionization properties as well and yielded only slightly lower intensities compared to the

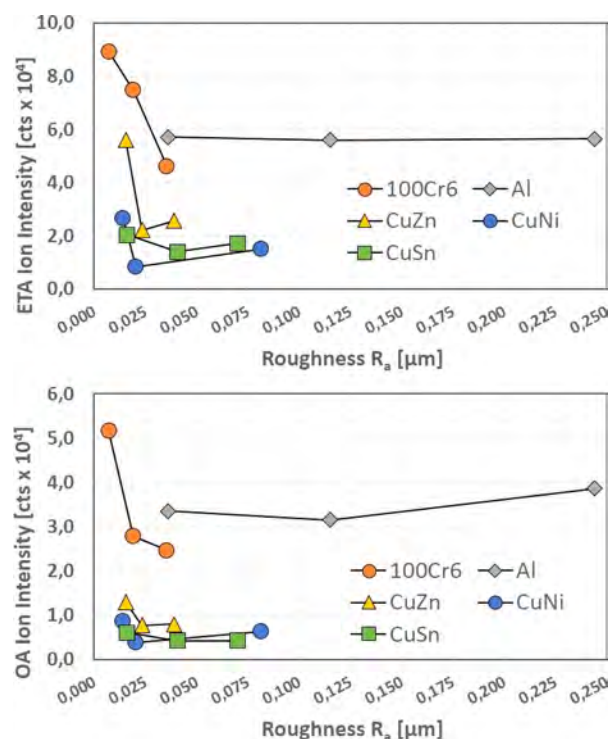


Figure 5. Maximum AP-MALDI ion intensities for ETA (top) and OA (bottom) on alternative target materials compared to surface roughness R_a .

Table 3. Decline of AP-MALDI Ion Signal Intensity When Surface Roughness Is Increased from R_a of 0.015–0.020 μm to R_a of 0.035–0.040 μm

sample target	ETA signal decline [%]	OA signal decline [%]
steel	38	11
CuZn	54	38
CuSn	31	30
CuNi	63	49

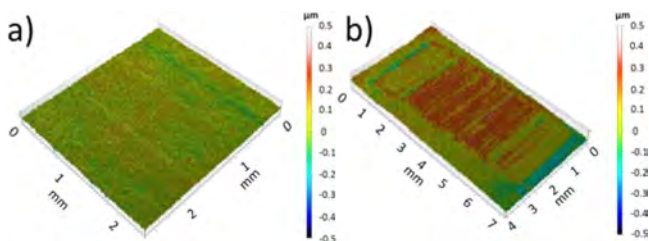


Figure 6. Focus variation of (a) the 3D-image of the original steel surface and (b) the steel surface after SRV-tribotesting.

steel target. Average ionization intensities of analytes on the gold-covered target are significantly higher than for the other materials and reach 12.5 and 9.7×10^4 cts, for ETA and OA, respectively. In general, ETA showed better ionization properties on all surfaces compared to OA. Using copper alloys, AP-MALDI experiments on polished target samples lead to significantly higher ion intensities for ETA friction modifier compared to ground surfaces, whereas for OA ionization intensities were close to the detection limit for all roughness levels. However, polished brass samples even yielded similar results as aluminum or steel targets for ETA, when in fact ion intensities significantly dropped when the target was ground to higher roughnesses.

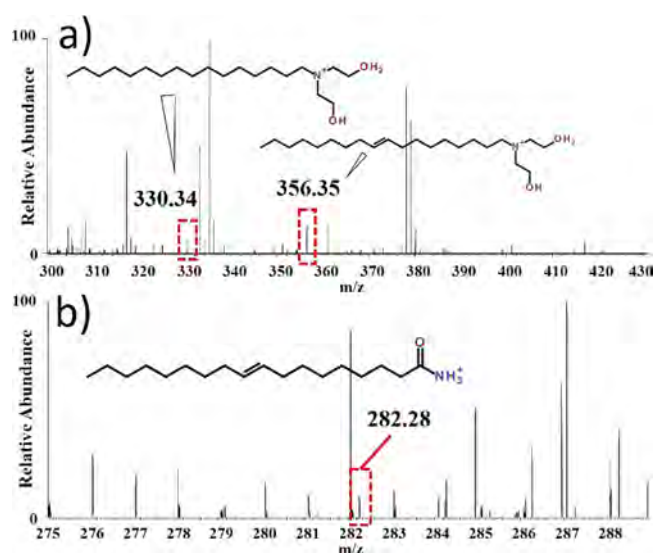


Figure 7. M-AP-MALDI mass spectra of wear track after SRV-tribotest: (a) peaks of FM additive ETA at m/z 356.35 (C18) and m/z 330.34 (C16); (b) OA additive identified at m/z 282.28.

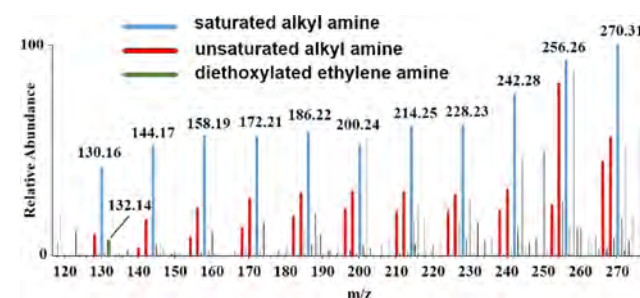


Figure 8. ETA degradation products of lubricant residues after tribotest measured via ESI-MS. Saturated alkyl amines (blue) with chain lengths of C8 (m/z 130.16) to C18 (m/z 270.31) and unsaturated alkyl amines (red) measured at 2 and 4 mass units lower. Diethoxylated ethylene amine was detected at m/z 132.14 (green).

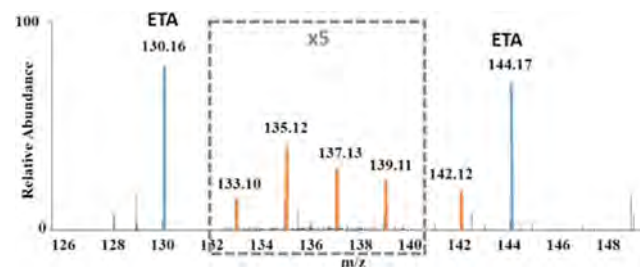


Figure 9. OA degradation products of lubricant residues after the SRV-tribotest measured via ESI-MS (orange). Ion intensity in the area within the dashed lines is multiplied 5 times.

Interestingly, along with generally low analyte ion intensities, copper alloys as target materials yielded intense peaks of cluster ions composed of matrix and copper $[2^*CHCA + Cu]^+$. These radical cation peaks appeared at m/z 441.0 ($C_{20}H_{14}O_6N_2Cu^+$) (Figure 4). Additional pronounced peaks of cluster ions of matrix fragments and copper included radical cation molecular ions m/z 279.0 ($C_{11}H_8O_3N_2Cu^+$) and m/z 397.0 ($C_{19}H_{14}O_4N_2Cu^+$), as well as the molecular cation m/z 529.9 ($C_{21}H_{14}O_6N_3Cu_2^+$).

The phenomenon of matrix and copper cluster ion formation when copper targets were used for MALDI-TOF experiments

Table 4. Overview on FM Additives and Main Degradation Products Detected via m-AP-MALDI, ESI-MS, and TOF-SIMS within Wear Tracks after SRV-Tribotesting on a Steel Surface

Name	Structure	Elemental composition	Calculated monoisotopic m/z value	Measured m/z values		
				AP-MALDI	ESI	ToF-SIMS
protonated polyethoxylated tallow amines		$C_{20}H_{44}NO_2^+$	330.3367	330.3381	330.3363	330.3275
		$C_{22}H_{46}NO_2^+$	356.3523	356.3538	356.3520	
Degradation product ions	saturated alkyl amines		$C_8H_{20}N^+$	130.1590		130.1588
			$C_9H_{22}N^+$	144.1747		144.1744
			$C_{10}H_{24}N^+$	158.1903		158.1901
			$C_{11}H_{26}N^+$	172.2060		172.2058
			$C_{12}H_{28}N^+$	186.2216		186.2214
Degradation product ions	diethoxylated ethylene amine		$C_6H_{14}NO_2^+$	132.1019		132.1017
oleic acid amide		$C_{18}H_{35}NO^+$	281.2719			281.3004
(protonated)		$C_{18}H_{36}NO^+$	282.2791	282.2802	282.2788	282.2993
Degradation product ions	unsaturated alkyl chains		$C_{10}H_{13}^+$	133.1012		133.1008
			$C_{10}H_{15}^+$	135.1168		135.1165
			$C_{10}H_{17}^+$	137.1325		137.1322
	nonenal		$C_9H_{15}O^+$	139.1117		139.1115
octyl acid amide		$C_8H_{16}NO^+$	142.1226		142.1225	

was previously reported by Esser et al.³⁷ Thus, the substrate for analyte crystals plays an important role for the achievable ion intensities. Strong surface interactions and bonding between the target material and sample/matrix crystals can have detrimental effects to the overall sensitivity. Inert materials, such as the gold-covered steel reference target, are favorable for higher sensitivity.

Comparing ion intensity maxima with surface roughness for most alternative target material polished samples yielded significantly higher intensities than ground sample surfaces. In Figure 5, an overview of the resulting ion intensities compared to surface roughness is given. Noticeably, the steel sample yielded a much steeper decline of ion intensities with increasing surface roughness than the other target materials. An interesting finding

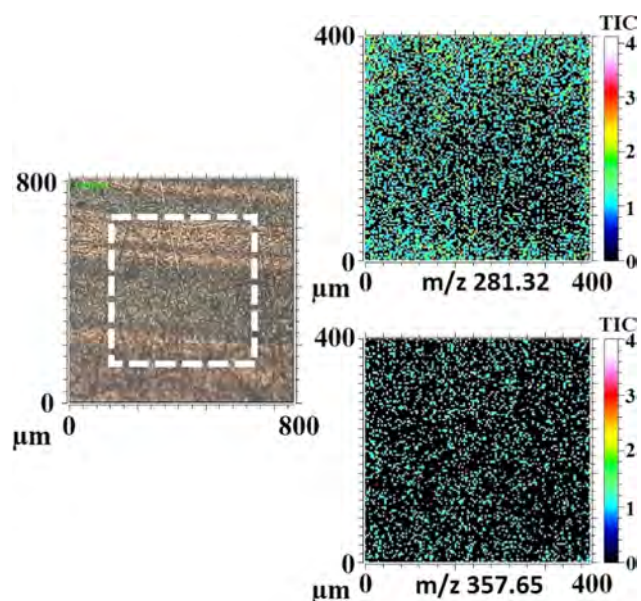


Figure 10. Region of interest for TOF-SIMS measurements (dashed line) within the wear track after SRV-tribotest and ion distribution of detected additive ions at m/z 281.32 (OA) and m/z 357.65 (ETA).

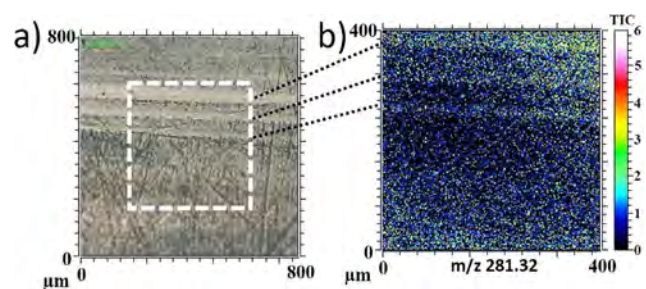


Figure 11. Area of TOF-SIMS measurements (dashed line) including tracks of more intense surface deterioration (a). Distribution of OA additive at m/z 281.32 showing significantly increased ion intensity corresponding to highly stressed areas (b).

was that aluminum targets did not show significant deviation of ion intensities with increasing surface roughness at all for both additives. However, due to the very low hardness values of the aluminum target compared to the other sample materials with an equal preparation method, only relatively high rough values were accomplished for aluminum surfaces. For the resulting roughness regime, no significant change in achievable ion sensitivity occurred for the aluminum target.

The polished brass sample led to similar values as those for steel and aluminum for ETA friction modifier additive, but surface grinding significantly decreased the resulting ion intensities. Both additional copper alloys, bronze and nickel silicon bronze, yielded a similar picture, whereas even the polished samples led to rather low ion intensities of ETA. Oleamide friction modifier in general yielded low intensity peaks on all copper alloy sample targets. However, polished surfaces principally lead to higher ion intensities for both additives on all types of material. Comparing two regions of certain roughness (Table 3), the highest drop in ion intensity for both additives was seen when nickel bronze was used as target material. Bronze yielded a decrease of around 30% for both additives. For steel and brass sample targets, the signal intensity for ETA declined significantly more for considered target roughness regimes than

for OA additive. For aluminum samples, similar roughness was not obtained in the polishing process. Maximum ionization intensities of analytes on the gold-covered target are significantly higher than for the other materials and reach 30.8 and 15.3×10^4 cts, for ETA and OA, respectively.

Surface parameters of the target are essential for the ion yield in MALDI-mass spectrometric experiments. The achievable ion sensitivity is strongly dependent on the homogeneity of the sample distribution and the crystallization behavior of matrix and analyte ions. Except for aluminum, for each material, the smoothest sample targets resulted in the highest ion sensitivity. There, the polished surface supplied the most homogeneous distribution of initial nuclei for crystallization. Rougher and furrowed target surfaces, such as the ground samples, lead to fewer and also larger crystals. As a result, this disadvantageous distribution and orientation of sample/matrix crystals can cause less effective interaction between incoming laser energy and analyte crystals.^{15,20}

Subsequently, the possibility of additive identification inside tribologically worn surfaces using m-AP-MALDI was determined. Pin-on-disc SRV-tribotests were carried out with 1.6 kN, and CHCA-matrix was applied onto the surface and dried. M-AP-MALDI analysis of the plain surface outside the wear track showed no signs of the presence of both additives. This indicates that the cleaning procedure was harsh enough for molecules only physically bonded to the surface of the specimen via adsorption. Additional measurements were carried out also on the steel disc's surfaces which were ground to roughnesses (R_a of $0.065 \mu\text{m}$) similar to the wear track's surface roughness (R_a of $0.058 \mu\text{m}$). Additive solutions were applied onto the surface and kept for 1 h. After rinsing of the surfaces with ethanol, no signals of additives could be detected anymore using m-AP-MALDI. For this reason, rinsing was considered a method to sufficiently clean rough steel surfaces from loosely adhering additives.

Though no additives were detected outside the wear tracks, inside the wear track, definite evidence of additive-containing tribolayers was found. Surface roughness inside the wear tracks was significantly increased compared to the polished and original steel surface (Figure 6). The original SRV-disc's surface roughness R_a was at $0.036 \mu\text{m}$. Inside, the wear track roughness increased to $0.058 \mu\text{m}$, which is significantly higher than polished steel surfaces and is a possible reason for low ion intensity of additive peaks detected after the SRV-tribotests.

However, on account of the use of an Orbitrap detector with the modified atmospheric pressure-matrix assisted laser desorption/ionization-mass spectrometry (m-AP-MALDI-MS) system and its high mass resolution, both FM additives yielded significant peak intensity for definite identification despite high roughness values of the steel surface. Mass spectra of both additives are given in Figure 7. Main peaks of polyethoxylated tallow amines appear at m/z 330.34 (C16:0) and m/z 356.35 (C18:1). The oleamide peak was detected at m/z 282.28. Even though matrix peaks lead to complex spectra, the resolution capabilities of Orbitrap detection allowed one to filter for additive peaks with known m/z values but low ion intensities. Tallow amines were clearly differentiable from matrix peaks (Figure 7a), whereas Orbitrap resolution capabilities were important for identification of oleamide molecular ions at m/z 282.28 due to the close proximity of the matrix molecular ion peak at m/z 282.08 (Figure 7b). In general, both used additives could be identified inside the wear track via m-AP-MALDI well above the detection limit with the use of the newly built target holders for components of SRV-tribotests.

During the tribotest, the entire disc was covered in additivated oil and was thoroughly cleaned after the test. Thus, additive molecules, present after the test and subsequent sample cleaning, which were detected inside the wear tracks, are not only physisorbed but also most probably arise from tribolayers partially chemically bound to the specimen surface. Compared to measurements on unstressed surfaces before the tribo-experiment relatively low sensitivity was achieved. This suggests only thin layers of both friction modifiers to be bound onto the surface, whereas larger amounts of additives were used up in the tribo-contact or remained in the oil, which was rinsed from the surface. Degradation products of both friction modifiers were not detected via AP-MALDI due to general low ion intensities.

ESI. In this work, electrospray ionization with an Orbitrap mass spectrometer was used for the direct analysis of residual lubricant of a tribosurface. The collision induced dissociation of precursor ions (m/z) results in characteristic fragmentation ions that allow elucidation of chemical structures and confirmation on the presence of certain compounds.

In the reference lubricant mixture, i.e., both FM additives in base oil before tribotesting, all protonated molecular ions of the additives were identified in positive ion mode. High accuracy Orbitrap-MS yielded m/z 282.28 for oleic acid amide FM additive and m/z 302.30, m/z 316.32, m/z 330.34, m/z 346.33, m/z 356.35, m/z 358.37, m/z 372.35, and m/z 400.38 for corresponding structures of the polyethoxylated tallow amine with different lengths of saturated and unsaturated alkyl chains.²¹ The identities of the structure of additives were confirmed via CID-fragmentation of the corresponding precursor ions.

Total ion count (TIC) mass spectra of the lubricant reference sample and the residual lubricant after the SRV-test were compared in order to find products of degradation reactions of the additives occurring during the tribological experiment. Detected degradation products of the polyethoxylated tallow amines without ethoxylated species were found for example at m/z 130.16 (C8), m/z 144.17 (C9), m/z 158.19 (C10), m/z 172.21 (C11), and m/z 186.22 (C12) for molecular ions of saturated alkyl amines. Various analogous amines were detected at m/z values 2 and 4 units lower for unsaturated amines with one and two double bonds, respectively. Additional reaction products were found in steps of 14.02 mass units (CH_2) up to m/z 270.31 (C18). A peak of low ion intensity at m/z 132.14 was identified as diethoxylated ethylene amine ($\text{C}_6\text{H}_{14}\text{O}_2\text{N}^+$). Degradation products of ETA are given in Figure 8.

Detected ions at m/z 133.10, m/z 135.12, m/z 137.13, m/z 139.11, and m/z 142.12 in the lubricant sample after the SRV-test are identified in a low abundance as degradation product ions from oleic acid amide (Figure 9). Ions with m/z 133.10, m/z 135.12, and m/z 137.13 represent the loss of octyl acid amide with unsaturated carbon chains of different chain length. On the other hand, the molecular ion observed at m/z 139.11 ($\text{C}_9\text{H}_{15}\text{O}^+$) is formed by loss of ammonium and an alkylene group (C9) from oleic acid amide. Degradation product ion octyl amide is detected at m/z 142.12. It can be concluded that the degradation of oleic acid amide during tribotesting occurred predominantly in the region of the double bond.

An overview of various degradation products of both FM additives detected via ESI-MS in residual lubricant after tribotesting is given in Table 4. Structures of the reaction products were confirmed by CID-fragmentation. None of these degradation products were found in ESI-MS of unused reference lubricant fluids before the tribotest.

TOF-SIMS. TOF-SIMS measurements were used as a supporting method to m-AP-MALDI to prove the existence of tribolayers using a complementary ionization method with higher lateral resolution.^{38–40} Mass spectra of wear tracks with additional measurements of reference surface regions in several millimeters distance to the worn area were compared regarding characteristic signals of the lubricant additives and their fragments. Furthermore, the spectra were compared to previous results of the AP-MALDI and ESI-MS analysis.

Molecular ions were detected inside the wear track but were not found on the unloaded reference surface including m/z 281.30 and m/z 282.30 (protonated) for OA as well as m/z 255.28 for an amide with differing alkyl chain length (C16, palmitamide). Detected ions at m/z 330.33, m/z 343.65, m/z 357.65, and m/z 358.65 (protonated) result from ETA of varying carbon chain lengths (C16/C17/C18) (cf. Table 4). All molecular ions showed significant signal-to-noise ratio. Interestingly, of all the detected additive peaks, the highest intensities were found at m/z 281.32 and m/z 282.30, which are referred to oleamide ($\text{C}_{18}\text{H}_{35}\text{NO}^+$) as well as its protonated species ($\text{C}_{18}\text{H}_{35}\text{NO} + \text{H}^+$), respectively. Thus, contrary to m-AP-MALDI- and ESI-MS results, TOF-SIMS investigations yielded higher signal intensities for oleamide ions than for ethoxylated tallow amines. Images of summed up scans show the surface distribution of the recorded analytes inside the measured area of the wear track. Figure 10 shows the ion distribution as the sum of TIC for each friction modifier with equally distributed signals within the worn surface.

In Figure 11, three linear regions of higher stressed areas are visible. Within this more severely worn surface, increased intensities of the unprotonated oleic acid amide of m/z 281.32 ($\text{C}_{18}\text{H}_{35}\text{NO}^+$) in heavily loaded wear tracks were yielded. This significant increase in signal intensity is attributed to a high applied load in the pronounced area and subsequent formation of higher density tribolayers than in adjacent less stressed regions.

CONCLUSION

For this work, we adapted the AP-MALDI ionization chamber to be able to vary the shape of the target specimens for surface analysis. A base oil mixture with two friction modifier additives was applied on different target materials, which are widely used in industrial applications. Both additives could well be identified on all surfaces. However, copper containing compounds yielded significantly lower ion intensities. Increased roughness of sample targets also yielded lower ion sensitivity. The best results were obtained on smooth steel samples and the inert gold-covered reference target.

The surface roughness has a significant effect on matrix crystallization. M-AP-MALDI-MS of tribolayers within the wear tracks after the SRV-tribotests with the lubricant mixture lead to definite identification of both components. Furthermore, newly adapted target holders were applied in the ionization chamber to analyze pin and disc from the tribotest. Orbitrap resolution capabilities lead to definite identification even for low intensity additive peaks.

Through m-AP-MALDI analysis, using the novel target holders, worn surfaces of tribologically stressed materials become readily accessible for analysis of lubricant residue composition and additive behavior. Without further effort, the adapted system of the target holders can be used for failure and surface analysis directly on samples of real field applications. Despite commonly increased roughness of wear tracks using suitable databases, AP-MALDI-MS measurements can become a quick method to

directly investigate additive containing tribolayers and lubricant residues.

ESI and TOF-SIMS measurements helped to further elucidate tribolayers and degradation fragments of used additives on loaded surfaces. The identification of product ions from oleic acid amine and polyethoxylated tallow amines indicates degradation of both additives during the SRV-test. The ability of ESI-Orbitrap-MS and TOF-SIMS to detect and provide the important information about tribolayers and degradation products of additives complements findings of m-AP-MALDI. This is of practical interest for better understanding of the tribological degradation process of lubricants and additive components on tribostressed surfaces.

■ ASSOCIATED CONTENT

● Supporting Information

The Supporting Information is available free of charge on the ACS Publications website at DOI: [10.1021/acs.analchem.5b02793](https://doi.org/10.1021/acs.analchem.5b02793).

CID-spectra of N-containing additives and degradation products thereof after SRV-tribotests measured via ESI-MS (PDF)

■ AUTHOR INFORMATION

Corresponding Author

*E-mail: widder@ac2t.at.

Notes

The authors declare no competing financial interest.

■ ACKNOWLEDGMENTS

The work presented was funded by the Austrian COMET Programme (Project XTribology, no. 849109) and the ERDF, as well as the province of Lower Austria (Onlab project), and carried out at the “Excellence Centre of Tribology” (AC2T research GmbH).

■ REFERENCES

- (1) Laiko, V. V.; Baldwin, M. A.; Burlingame, A. L. *Anal. Chem.* **2000**, *72*, 652–657.
- (2) Laiko, V. V.; Moyer, S. C.; Cotter, R. J. *Anal. Chem.* **2000**, *72*, 5239–5243.
- (3) Laiko, V. V.; Burlingame, A. L. *Proceedings of the 47th ASM Conference on Mass Spectrometry and Allied Topics*, Dallas, TX, June 13–17, 1999.
- (4) Moyer, S. C.; Cotter, R. J. *Anal. Chem.* **2002**, *74*, 468A–476 A.
- (5) Miller, C. A.; Yi, D.; Perkins, P. D. *Rapid Commun. Mass Spectrom.* **2003**, *17*, 860–868.
- (6) Moyer, S. C.; Marzilli, L. A.; Woods, A. S.; Laiko, V. V.; Doroshenko, V. M.; Cotter, R. J. *Int. J. Mass Spectrom.* **2003**, *226*, 133–150.
- (7) Schneider, B. B.; Lock, C.; Covey, T. R. *J. Am. Soc. Mass Spectrom.* **2005**, *16*, 176–182.
- (8) Laiko, V. V.; Taranenko, N. I.; Berkout, V. D.; Yakshin, M. A.; Prasad, C. R.; Lee, H. S.; Doroshenko, V. M. *J. Am. Soc. Mass Spectrom.* **2002**, *13*, 354–361.
- (9) McLean, J. A.; Russell, W. K.; Russell, D. H. *Anal. Chem.* **2003**, *75*, 648–654.
- (10) Von Seggern, C. E.; Gardner, B. D.; Cotter, R. J. *Anal. Chem.* **2004**, *76*, 5887–5893.
- (11) Madonna, A. J.; Voorhees, K. J.; Taranenko, N. I.; Laiko, V. V.; Doroshenko, V. M. *Anal. Chem.* **2003**, *75*, 1628–1637.
- (12) Moyer, S. C.; Von Seggern, C. E.; Cotter, R. J. *J. Am. Soc. Mass Spectrom.* **2003**, *14*, 581–592.

- (13) Taranenko, N. I.; Doroshenko, V. M.; Shukla, A. K.; Shukla, M. M. *Am. Lab.* **2004**, *36*, 34–38.
- (14) Pittenauer, E.; Zehl, M.; Belgacem, O.; Raptakis, E.; Mistrik, R.; Allmaier, G. *J. Mass Spectrom.* **2006**, *41*, 421–447.
- (15) Pittenauer, E.; Kassler, A.; Haubner, R.; Allmaier, G. *J. Proteomics* **2011**, *74*, 975–981.
- (16) Shrivastava, K.; Wu, H. F. *Anal. Chem.* **2008**, *80*, 2583–2589.
- (17) Shrivastava, K.; Wu, H. F. *J. Mass Spectrom.* **2007**, *42*, 1637–1644.
- (18) Shrivastava, K.; Wu, H. F. *Anal. Chim. Acta* **2008**, *628*, 198–203.
- (19) Hanton, S. D.; Parees, D. M.; Zweigenbaum, J. *J. Am. Soc. Mass Spectrom.* **2006**, *17*, 453–458.
- (20) Kassler, A.; Pittenauer, E.; Dörr, N.; Allmaier, G. *Rapid Commun. Mass Spectrom.* **2009**, *23*, 3917–3927.
- (21) Widder, L.; Brenner, J.; Hutter, H. *Eur. Mass Spectrom.* **2014**, *20*, 299–305.
- (22) Papay, A. G. *Lubr. Eng.* **1983**, *39*, 419–426.
- (23) So, H.; Hu, C. C. *ASTM Spec. Technol. Publ.* **2001**, *1404*, 125–139.
- (24) Anghel, V.; Bovington, C.; Spikes, H. A. *Lubr. Sci.* **1999**, *11*, 313–335.
- (25) Spikes, H. A. *Lubr. Sci.* **2002**, *14*, 147–167.
- (26) Widder, L.; Grafl, A.; Lebel, A.; Tomastik, C.; Brenner, J. *Tribol. Schmierungstech.* **2011**, *58*, 11–15.
- (27) Holmberg, K.; Andersson, P.; Erdemir, A. *Tribol. Int.* **2012**, *47*, 221–234.
- (28) Tartakovsky, L.; Gutman, M.; Mosyak, A. Energy efficiency of road vehicles – trends and challenges. In *Energy Efficiency: Methods, Limitations and Challenges*; Nova Science Publishers: New York, 2012; pp 63–90.
- (29) Chu, S.; Majumdar, A. *Nature* **2012**, *488*, 294–303.
- (30) Kenbeck, D.; Bunemann, T. Organic Friction Modifiers. In *Lubricant Additives: Chemistry and Applications*, 2nd ed.; Rudnick, L. R., Ed.; CRC Press: Boca Raton, 2009; p 195–212.
- (31) Braun, J. Additives. In *Lubricants and Lubrication*, 2nd ed.; Mang, T., Dresel, W., Eds.; Wiley-VCH: Weinheim, 2007; p 88–118.
- (32) Basu, S. Friction Modifiers. In *Encyclopedia of Lubricants and Lubrication*; Mang, T., Ed.; Springer: Weinheim, 2014; p 700–707.
- (33) Gabler, C.; Pittenauer, E.; Dörr, N.; Allmaier, G. *Anal. Chem.* **2012**, *84*, 10708–10714.
- (34) Tan, P. V.; Laiko, V. V.; Doroshenko, V. M. *Anal. Chem.* **2004**, *76*, 2462–2469.
- (35) Garrett, T. J.; Prieto-Conaway, M. C.; Kovtoun, V.; Bui, H.; Izgarian, N.; Stafford, G.; Yost, R. A. *Int. J. Mass Spectrom.* **2007**, *260*, 166–176.
- (36) de Hoffmann, E.; Stroobant, V. *Mass Spectrometry – Principles and Application*, 3rd ed.; Wiley: Chichester, 2007; p 243.
- (37) Esser, E.; Keil, C.; Braun, D.; Montag, P.; Pasch, H. *Polymer* **2000**, *41*, 4039–4046.
- (38) Gunst, U.; Zabel, W. R.; Poll, G.; Arlinghaus, H. F. *Surf. Interface Anal.* **2004**, *36*, 1231–1235.
- (39) Carlsson, P.; Bexell, U.; Olsson, M. *Wear* **2001**, *251*, 1075–1084.
- (40) Gunst, U.; Zabel, W. R.; Valle, N.; Migeon, H. N.; Poll, G.; Arlinghaus, H. F. *Tribol. Int.* **2010**, *43*, 1005–1011.

12 Conclusions and Outlook

It has been shown that a combination of various analytical techniques can result in broad understanding of the present condition of a given tribosystem. While substantial amounts of information are generated certain analytical methods are focused on special aspects and other topics can be left neglected. To contribute to a deepened comprehension of the determination of the chemical structure of constituents of such tribofilms an additional examination by means of atmospheric pressure-matrix assisted laser desorption/ionization was undertaken. Thus, also the identification of originally used additive composition was aimed to become accessible, which can be essential to aid understanding processes of energy dissipation and surface wear occurrences.

The possibility of identification of both, ethoxylated tallow amines and oleic acid amide friction modifier additives with Orbitrap high mass resolution directly from oil blends without the use of any separation techniques prior to the measurements is a significant step towards the simplification of lubricant analysis. Furthermore, strong dependence of signal intensities on the used material and surface roughness was observed in analytical results. Their influence on matrix crystallization strongly influences the results. Hence, the preferences for certain material parameters was established. The additional identification of used additives in boundary tribofilms achieved through tribological experiments using newly adapted sample holders opens new doors towards analytical feasibilities of original stressed sample surfaces in a simple way. Aided by supplementary use ofToF-SIMS and ESI-MS measurements, further elucidation of tribofilms and degradation products of applied friction modifiers complemented previous findings. The degradation of both additives could thus be displayed.

The achieved development could prepare the grounds for failure and stressed surface analysis directly on targets from real field applications for a better comprehension of lubricant and additive degradation processes on tribostressed surfaces. The AP-MALDI measurements including the utilization of ToF-SIMS and ESI-MS are a quick method for future investigations of boundary tribofilms and additive residues. However, the application of these techniques on genuine field samples requires further experiments on a more broad spectrum of lubricant additive molecules. Future applications may also include simultaneous online analytical assessments of an engaged surface concurrent to ongoing tribometric experiments to correlate friction and wear parameters to additive degradation processes.

Curriculum vitae

Lukas Widder

BORN: March 7th, 1982
in Oberpullendorf, Austria
ADDRESS: Franz Ermes-Gasse 4
7210 Mattersburg
Austria
PHONE: +43 664 543 7474
E-MAIL: lwidder@yahoo.com

Education

JUNE 2019 TECHNICAL CHEMISTRY, PH.D. DEGREE

Doctoral Program (Dr. techn.), Thesis title: "A novel approach to characterization of industrial lubricant additives in boundary surface tribofilms by atmospheric pressure matrix assisted laser desorption/ionization." Institute of Chemical Technologies and Analytics, Faculty of Chemistry, Technische Universität Wien, Austria

AUGUST 2013 SUSTAINABLE ENERGY SYSTEMS, MASTER'S DEGREE

Diploma Program (Dipl.-Ing.), Thesis title: "Prosumer, Wirtschaftlichkeit eines losen Microgrids." University of Applied Sciences Burgenland, Campus Pinkafeld, Austria.

JUNE 2008 TECHNICAL CHEMISTRY DEGREE, MASTER'S DEGREE

Diploma Program (Dipl.-Ing.), Thesis title: "TOF-SIMS investigations of metal impurities in silicon." Institute of Chemical Technologies and Analytics, Faculty of Chemistry, Technische Universität Wien, Austria

JULY 2000 HIGH SCHOOL DIPLOMA

Bundesgymnasium Mattersburg, Mattersburg, Burgenland, Austria

Professional experience

OCTOBER 2008 to present RESEARCH ASSOCIATE at AC2T research GmbH
Viktor Kaplan-Straße 2/C
2700 Wiener Neustadt
Austria

List of Publications

Publications in peer reviewed journals

1. **Widder, L.**, Nevosad, A., Reichmann, F., & Adam, K. (2019). Development of testing method for assessment of release agent effectiveness in high temperature forming processes. *Trans. Tech. Publications*. (article in press).
2. **Widder, L.**, Nevosad, A., Reichmann, F., & Adam, K. (2018). Improvement of friction behavior and wear resistance in high temperature applications through release agents. *Tribologie und Schmierungstechnik*, 65(6), 21-24.
3. **Widder, L.**, Leroch, S., Kirchgaßner, M., & Varga, M. (2018). Finite Elemente-Simulation als Werkzeug für ein spannungsgünstiges Design von Hochdruck-Rollenpressen in der Zementindustrie. *BHM Berg- und Hüttenmännische Monatshefte*, 1-7.
4. **Widder, L.**, Varga, M., Adam, K., & Kuttner, A. (2017). Development of Impact Energy Distribution of Various Abrasives during Cyclic Impact/Abrasion Testing. In *Solid State Phenomena* (Vol. 267, pp. 234-242). Trans Tech Publications.
5. Rojacz, H., Birkelbach, F., **Widder, L.**, & Varga, M. (2017). Scale adhesion, scratch and fracture behaviour of different oxides formed on iron based alloys at 700° C. *Wear*, 380, 126-136.
6. Rojacz, H., Neacşu, I. A., **Widder, L.**, Varga, M., & Heiss, J. (2016). Thermal effects on wear and material degradation of slag pots operating in steel production. *Wear*, 350, 35-45.
7. Varga, M., **Widder, L.**, Griesinger, M., Adam, K., & Badisch, E. (2016). Wear progress and mechanisms in high temperature sieves. *Engineering Failure Analysis*, 61, 46-53.
8. **Widder, L.**, Ristic, A., Brenner, F., Brenner, J., & Hutter, H. (2015). Modified-Atmospheric Pressure-Matrix Assisted Laser Desorption/Ionization Identification of Friction Modifier Additives Oleamide and Ethoxylated Tallow Amines on Varied Metal Target Materials and Tribologically Stressed Steel Surfaces. *Analytical chemistry*, 87(22), 11375-11382.
9. **Widder, L.**, Brenner, J., & Hutter, H. (2014). Atmospheric pressure matrix-assisted laser desorption/ionization mass spectrometry of friction modifier additives analyzed directly from base oil solutions. *European Journal of Mass Spectrometry*, 20(4), 299-305.
10. **Widder, L.**, Grafl, A., Lebel, A., Tomastik, C., & Brenner, J. (2011). Triboanalysis of hypoid gear components in drive trains. *Tribologie und Schmierungstechnik*, 58(2), 11-15.

Conference contributions

1. **Widder, L.**, Nevosad, A., Reichmann, F., & Adam, K. (2019). *Development of testing method for assessment of release agent effectiveness in high temperature forming processes*. Modern Materials and Manufacturing 2019, host of 27th International Baltic Conference on Materials Engineering, Tallinn, (EST), April 23rd-26th. 2019.
2. **Widder, L.**, Leroch, S., Kirchgaßner, M., Trenk, M., Edelhauser, T., Varga, M. (2017). *Optimization of layer design in high-pressure grinding rolls through finite element simulati-*

- ons of equivalent and residual stresses*, 42. ÖTG-Symposium 2017: Tribology in Industry and Research: New Tasks – Innovative Solutions, Österreichische Tribologische Gesellschaft (ÖTG), Wiener Neustadt (AUT), November 22nd 2017.
3. **Widder, L.**, Varga, M., Adam, K., Kuttner, A.: *Development of impact energy distribution of various abrasives during continuous impact/abrasion testing*, 26th International Baltic Conference on Materials Engineering, Kaunas (LIT), October 26-27th 2017.
 4. **Widder, L.**, Varga, M., Kirchmayer, R., Griesinger, M., Kirchgaßner, M., Adam, K. *Optimierung des Heißsiebes in der Sinteranlage*, Österreichische Tribologische Gesellschaft (ÖTG), ÖTG-Symposium 2016, Linz (AUT), November 23rd, 2016. Poster.
 5. Varga, M., **Widder, L.**, Griesinger, M., Adam, K., Badisch, E. *Hochtemperatur-Tribologie und Verschleiß in der Sinteranlage*, Österreichische Tribologische Gesellschaft (ÖTG), ÖTG-Symposium 2016, Linz (AUT), November 23rd, 2016. Poster.
 6. Rojacz, H., Varga, M., **Widder, L.**, Neacsu, I.A. *Optimierung des Schlackekübels im Stahlwerk*, Österreichische Tribologische Gesellschaft (ÖTG), ÖTG-Symposium 2016, Linz (AUT), November 23rd, 2016. Poster.
 7. Kirchgaßner M., Kirchmayer R., Adam K., Varga M., **Widder L.**: *Gesteigerte Produktivität beim Klassieren durch maßgeschneiderte Hochleistungsschichten*, Österreichische Tribologische Gesellschaft (ÖTG), ÖTG-Symposium 2016, Linz (AUT), November 23rd, 2016.
 8. **Widder, L.**, Varga, M., Kirchgaßner, M., Badisch, E.: *Combined impact/abrasive wear performance of carbide-reinforced hardfacings*, 39. ÖTG-Symposium 2014: Tribologie in Industrie und Forschung / Werkstoffe, Konstruktion und Technologie, Österreichische Tribologische Gesellschaft (ÖTG), Leoben (AUT), November 26th 2014.
 9. Varga M., **Widder L.**, Kirchmayer R., Adam K., Badisch E.: *Experimental simulation of abrasive wear of hot sieves*, International conference on abrasive processes (ICAP) 2014, Cambridge (GB), September 8th-10th 2014.
 10. Brenner J., Dörr N., Gabler C., **Widder L.**: *Comprehensive characterisation of tribologically stressed surfaces*, 19th International Colloquium Tribology: Industrial and Automotive Lubrication, Technische Akademie Esslingen (TAE) 2014, Ostfildern (DE), January, 21st-23rd 2014.
 11. Gabler C., Brenner J., **Widder L.**, Dörr N.: *Ionic liquid in the tribocontact - impact of cations*, 15th European conference on applications of surface and interface analysis (ECASIA) 2013, Sardinien (IT), October 13th-18th 2013.
 12. Grafl A., Lebel A., **Widder L.**, Franek F.: *Triboanalysis of hypoid gear components over operation time*, Production and Failures of Gear Wheels and Gear Boxes, Slovak Society of Tribology, Trnava (SK), April 26-27th 2012, <http://www.intertribo.sk>
 13. **Widder L.**, Grafl A., Lebel A.: *Triboanalysis of system components in drive trains*, Proceedings, 35. ÖTG-Symposium 2010: Competitive Advantages through Tribo-Innovation – Controlling Friction and Wear by Surface and Lubrication Engineering, Österreichische Tribologische Gesellschaft (ÖTG), Dornbirn (AUT), November 18th 2010.